Characterization of A Carbon Fiber Sheet Molding Compound for Compression Molding Simulation

Yining Jiang

Department of Mechanical Engineering

McGill University, Montreal

A thesis submitted to McGill University in partial fulfillment of the requirements for the degree of Master of Science

August 16th, 2021

"The best view comes after the hardest climb."

I dedicate this work to my mom and dad.

ACKNOWLEDGEMENTS

First and foremost, I would like to express my sincerest gratitude to my supervisor Prof. Larry Lessard for his help, support and mentorship throughout this project. I will forever be grateful to Prof. Lessard for giving me the opportunity to do this project, which leads me to where I am today. I would also like to express the deepest appreciation to my co-supervisor Dr. François Lebel, whose vast invaluable expertise in composite materials, enthusiasm in research and sophisticated methods in problem solving, have inspired me to become a better researcher and engineer. Without his patient teaching, guidance and persistent help, the completion of this work would not have been possible.

Second, I would like to thank the partner of this project Centre technologique en aérospatiale (CTA) for their support and guidance at every step of this research. I would especially like to acknowledge the continuous help and rich advice from my supervisor at CTA Philippe Murray. Besides, a special thanks to Luc Pelletier and Hugo Dubreuil who helped to turn ideas into reality and provided me with great technical support. I also wish to thank Dr. Thierry Klotz, Jeremy Elsek-Valois, Daniel Gareau, Carl Ouellet, Michel Barrette and Julien Roy for their helps regarding experimental and technical issues. Thanks to George Dabbaghian for sample preparation.

Third, I would like to thank the industrial partner Magna International Inc., not only for their financial support, but also for their advice and assistance throughout this project. Notably, thanks to Dr. Ranjit Pachha and Zongxun Wang whose guidance and feedback on material characterization were vital. I also wish to thank Mitacs for their financial support.

In addition, I wish to express my great appreciation to all the members of the excellent Structures and Composite Materials Laboratory, especially Prof. Pascal Hubert and Dr. Adam Smith for their precious scientific advice and guidance on flow-compaction testing. I also thank Lucie Riffard for her long-term help with experiments and lab equipment. The support and friendships of my fellows: Zhengshu Yan, Sidharth Sarojini Narayana, Leonardo Barcenas Gomez and Farnaz Mazaheri Karvandian, have been invaluable, for which I am extremely thankful.

Away from work, some special words of gratitude go to my dear friends Zian Zhang and Yulin Chen, who have always been the major source of emotional support when things would get a bit discouraging. I would like to thank them for always being there for me.

At last, I am forever indebted to my parents for their unconditional love and support throughout my life. I wish to thank them for always believing in me and letting me chase my dreams whatever they may be. My journey in Canada would not have been possible if not for them and I dedicate this work to them.

ABSTRACT

Carbon fiber reinforced sheet molding compound (CF-SMC) is a ready-to-mold prepreg material made from chopped carbon fibers combined with a thermosetting resin system. Compression molding of CF-SMCs is a promising process to deliver lightweight and high-volume composite parts for the automotive industry. During compression molding, a stack of CF-SMC prepreg sheets, called a charge, is placed inside a pre-heated tooling cavity. As the tooling is closed under high pressure, the charge is squeezed and forced to flow and fill the volume of the cavity. The tooling is then kept closed until the material is fully cured.

A few technical aspects complicate the production of high-quality SMC parts using compression molding. Defining a robust and optimized processing window for a new part geometry and a given CF-SMC system can be challenging since the thermosetting resin system of CF-SMC depends nonlinearly on molding temperature, pressure and cavity closing rate [1]. Hence, the selection of an appropriate set of process parameters is not intuitive, which could lead to various undesired mold-filling scenarios and questionable part qualities. Besides, randomly oriented carbon fibers in the CF-SMC inherently pose a great challenge to material flow predictions during molding trials. Nowadays, process and tooling design to manufacture SMC parts with the required features are still relying on costly and labor-intensive trial-and-error molding practices. Therefore, virtual manufacturing of SMC parts through physics-based simulations is favored since it has the potential to replace the traditional trial-and-error approach, shorten the early process development stage and mitigate the associated technical risks [2]. Proper material characterization and modeling of CF-SMC prepreg system are the fundamental building blocks of accurate and realistic compression molding process simulations.

This thesis first presents an integrated material characterization roadmap for a CF-SMC prepreg and its corresponding thermosetting resin system. The carbon fibers used in this CF-SMC are about 25.4mm long. The main chemical species of this resin system are vinyl ester primary backbone, styrene reactive diluent and isocyanate thickening agent.

Thermokinetics behavior of the neat resin is studied and characterized using differential scanning calorimetry (DSC Q2000 from TA Instruments) through temperature scanning and isothermal experiments. A cure kinetics model is developed using Advanced Kinetics and Technology Solutions-Thermokinetics (AKTS-TK) software. The model generation process is based on the differential isoconversional method of Friedman [3], where activation energy and pre-exponential factor are functions of the extent of reaction. Isothermal model predictions are compared with experimental data from isothermal DSC runs and they have shown good agreement.

Relative viscosity evolution and gel time of the neat resin and the CF-SMC prepreg are measured using a rheometer (MCR302 from Anton Paar) with parallel plate configuration under isothermal and dynamic testing conditions. Parallel plates with a diameter of 25 mm are used with resin samples, while plates with a diameter of 50mm are used with prepreg samples to accommodate the length of fibers. Gelation models for both systems, the neat resin and the CF-SMC prepreg, are proposed.

A flow-compaction testing fixture is developed to study the CF-SMC prepreg flow under several testing conditions, namely at different temperatures and mold closure rates, based on the work of Smith and Hubert [4]. The test fixture is mounted on an MTS Landmark servohydraulic testing system. The cavity gap thickness is monitored and controlled by a high-precision LVDT, mounted closely to the testing fixture, throughout the characterization trials. One flush-mounted pressure sensor is also used to track pressure changes in the mold cavity. Compression load during the SMC charge molding is acquired by the MTS 100kN load cell and TestSuite TW Elite software. The length, width and thickness of each SMC prepreg specimens before and after their compression trials are measured to obtain the corresponding strain. Correlations with these sample attributes are studied to better understand the material flow characteristics during compression molding.

Then the material models developed in this work are implemented into a commercial software package Autodesk Moldflow 2021 through Solver Application Programming Interface (API). A simulation of CF-SMC compression molding process is developed using Moldflow software. The experimental data obtained from flow-compaction testing trials is ultimately used to validate the simulation.

ABRÉGÉ

Le matériau composite de moulage en feuille renforcé de fibres de carbone (CF-SMC) est un matériau préimprégné prêt à mouler composé de fibres de carbone coupées combinées avec un système de résine thermodurcissable. Le moulage par compression des CF-SMC est un processus prometteur pour fournir des pièces composites légères et de grand volume pour l'industrie automobile. Lors du moulage par compression, une pile de feuilles de préimprégné CF-SMC, appelée charge, est placée à l'intérieur d'une cavité d'outillage préchauffée. Lorsque l'outillage est fermé sous haute pression, la charge est comprimée et forcée de s'écouler et de remplir le volume de la cavité. L'outillage est ensuite maintenu fermé jusqu'à ce que le matériau soit complètement durci.

Quelques aspects techniques compliquent la production de pièces SMC de haute qualité par moulage par compression. Définir une fenêtre de traitement robuste et optimisée pour une nouvelle géométrie de pièce et un système CF-SMC donné peut être difficile car le système de résine thermodurcissable de CF-SMC dépend de manière non linéaire de la température de moulage, de la pression et du taux de fermeture de la cavité [1]. Par conséquent, la sélection d'un ensemble approprié de paramètres de processus n'est pas intuitive, ce qui pourrait conduire à divers scénarios de remplissage de moule et qualités de pièce indésirables. En outre, les fibres de carbone orientées de manière aléatoire dans le CF-SMC posent intrinsèquement un grand défi aux prévisions de flux de matériaux lors des essais de moulage. De nos jours, la conception des processus et de l'outillage pour fabriquer des pièces SMC avec les caractéristiques requises repose toujours sur des pratiques de moulage par essais et erreurs coûteuses et exigeantes en main-d'œuvre. Par conséquent, la fabrication virtuelle de pièces SMC par le biais de simulations basées sur la physique est privilégiée car elle a le potentiel de remplacer l'approche traditionnelle d'essais et d'erreurs, de raccourcir la première étape de développement du processus et d'atténuer les risques techniques associés [2]. La caractérisation et la modélisation appropriées des matériaux du système préimprégné CF-SMC sont les éléments fondamentaux des simulations de processus de moulage par compression précises et réalistes.

Cette thèse présente d'abord une feuille de route intégrée de caractérisation des matériaux pour un préimprégné CF-SMC et son système de résine thermodurcissable correspondant. Les fibres de carbone utilisées dans ce CF-SMC mesurent environ 25 mm de long. Les principales espèces chimiques de ce système de résine sont la base primaire d'ester vinylique, le diluant réactif au styrène et l'agent épaississant isocyanate.

Le comportement thermocinétique de la résine pure est étudié et caractérisé en utilisant la calorimétrie différentielle à balayage (DSC Q2000 TA Instruments) par le biais d'un balayage de température et d'expériences isothermes. Un modèle de cinétique de guérison est développé à l'aide du logiciel Advanced Kinetics and Technology Solutions-Thermokinetics (AKTS-TK). Le processus de génération de modèle est basé sur la méthode d'isoconversion différentielle de Friedman [3], où l'énergie d'activation et le facteur pré-exponentiel sont fonction de l'étendue de la réaction. Les prédictions du modèle isotherme sont comparées aux données expérimentales d'essais DSC isothermes et elles ont montré une bonne concordance.

L'évolution de la viscosité relative et le temps de gel de la résine pure et du préimprégné CF-SMC sont mesurés à l'aide d'un rhéomètre (MCR302 Anton Paar) avec une configuration de plaques parallèles dans des conditions d'essai isothermes et dynamiques. Des plaques parallèles d'un diamètre de 25 mm sont utilisées avec des échantillons de résine, tandis que des plaques d'un diamètre de 50 mm sont utilisées avec des échantillons préimprégnés pour s'adapter à la longueur des fibres. Des modèles de gélification pour les deux systèmes, la résine pure et le préimprégné CF-SMC, sont proposés.

Un banc d'essai de compactage par écoulement est développé pour étudier l'écoulement du préimprégné CF-SMC dans plusieurs conditions d'essai, à savoir à différentes températures et vitesses de fermeture du moule, sur la base des travaux de Smith et Hubert [4]. Le montage d'essai est monté sur un système d'essai servohydraulique MTS Landmark. L'épaisseur de l'espace de la cavité est surveillée et contrôlée par un LVDT de haute précision, monté à proximité du montage d'essai, tout au long des essais de caractérisation. Un capteur de pression encastré est également utilisé pour suivre les changements de pression dans la cavité du moule. La charge de compression pendant le moulage par charge SMC est acquise par la cellule de charge MTS 100kN et le logiciel TestSuite TW Elite. La

longueur, la largeur et l'épaisseur de chaque échantillon de préimprégné SMC avant et après leurs essais de compression sont mesurées pour obtenir la déformation correspondante. Les corrélations avec ces attributs de l'échantillon sont étudiées pour mieux comprendre les caractéristiques d'écoulement du matériau pendant le moulage par compression.

Ensuite, les modèles de matériaux développés dans ce travail sont implémentés dans un logiciel commercial Autodesk Moldflow via Solver Application Programming Interface (API). Une simulation du processus de moulage par compression CF-SMC est développée à l'aide du logiciel Moldflow. Les données expérimentales obtenues à partir des essais d'essais de compactage à l'écoulement sont finalement utilisées pour valider la simulation.

Table of Contents

List of Figures

List of Tables

Chapter 1. Introduction

To address climate change, Canada aims to reduce its greenhouse gas emissions by 30 Mt every year by 2030 [5]. The transportation industry is responsible for 30% of Canada's total greenhouse gas emissions [6]. It is expected by the government that automobile manufacturers find solutions to reduce fuel consumption of their vehicles so that the new vehicles will consume up to 50% less fuel than 2008 vehicles by 2025 [5].

Reduction of vehicle weight plays a significant role in reducing fuel consumption. Every 100 kg weight saving reduces fuel consumption by an average of 0.40 L/100 km for cars, and 0.49 L/100 km for light trucks [7].

One of the weight reduction strategies is to use lighter materials for interior and exterior automotive parts. However, the material performance which ensures the vehicle safety should not be compromised. Addressing a balance between vehicle performance and light weight should be the priority for automotive manufacturers.

Sheet molding compound (SMC) is a kind of fiber-reinforced polymer (FRP), which has drawn considerable attention from car manufacturers and suppliers to replace conventional automotive materials for its high strength-to-mass ratio, high stiffness and excellent corrosion resistance. Its stiffness and strength are comparable to metals but it has much lower density than metals.

1.1 Sheet Molding Compound (SMC)

Sheet molding compound (SMC) is a ready-to-mold fiber-reinforced thermosetting polymer product, which is also called SMC prepreg (pre-impregnated sheet). It is produced in an uncured sheet form between 1 mm and 3 mm thick. Fiber materials are embedded within a thermosetting matrix to mechanically increase the strength and elasticity of the composites.

The matrix of SMC is usually composed of a thermosetting resin (typically unsaturated polyester, vinyl ester and epoxy), fillers (such as calcium carbonate, alumina) and other additives [8].

Polyesters and vinyl esters are the most commonly used thermosetting resins for SMC in automotive industry due to their shorter curing times and lower costs compared to epoxy resins [9]. However, epoxy resins are more commonly seen in advanced applications such as aerospace industry, because of their higher moisture resistance and better mechanical properties [10].

Fillers and additives are added to the neat resin to improve the material performance or to ease the processing of the material [11]. Fillers such as calcium carbonate and alumina could increase some of the final physical or mechanical properties of the SMC such as density, conductivity and ultimate strength. They could also reduce the fabrication cost. The initiation of the resin curing reaction requires an initiator which is able to induce free radicals in the resin at high temperatures. Peroxyesters and peroxyketals are frequently-used initiators in SMC formulations [12]. As a counterpart, inhibitors are added to slow the early curing process before the SMC is consumed, for example, during the mixing of the resin and the shelf life. Before molding, SMC is subjected to several handling operations such as cutting, folding and placement in the mold. Such manipulations would not be possible if the SMC matrix is a liquid-like paste. Adding thickening agents significantly increases the viscosity of the SMC matrix, which allows easier handling of the SMC sheets before molding process [8]. Thickening agents such as magnesium oxide (MgO) and isocyanate are often seen in SMC formulations.

Commonly used fibrous reinforcements for SMC compounds are glass fiber, carbon fiber and plant-based fibers. The fiber length varies from 25mm to 50mm and those discontinuous fibers are usually randomly distributed within the resin paste. The mass fraction of the fibrous reinforcement ranges between 10% and 65%.

How is sheet molding compound made?

SMC can be manufactured in-house or by compounders to meet particular performance requirements such as tensile strength and Class A surface finish [11]. Manufacturing of

sheet molding compounds is a continuous in-line process. The material is sheathed both top and bottom with a polyethylene or nylon plastic film to prevent auto-adhesion and contamination. The SMC matrix is spread uniformly onto the bottom film. Chopped fibers are randomly distributed onto the matrix. The top film is applied, and the sandwich is then rolled into a pre-determined thickness. The sheet is then allowed to mature for 48-72 hours. SMCs are usually produced in thin uncured and thickened sheets between 1mm and 3mm thick that can be handled easily.

1.2 Compression Molding of SMC

SMC is commonly processed through compression molding in the automotive industry [8]. Upon molding, SMC sheets are cut into certain geometry and are stacked together, forming a laminate. This stack of SMC (also called a charge) is then placed on a heated mold which is mounted on a hydraulic or mechanical press. As the tooling is closed under high pressure, the SMC charge is squeezed and forced to flow and fill the cavity of the mold, which is called the mold filling stage. The mold is then kept closed until the material has reached a high extent of degree-of-cure, which is known as the curing stage. At last, the part is demolded and goes through the finishing operations such as trimming and polishing.

Several technical aspects complicate the production of high-quality SMC parts by compression molding. First, because of the normal thickness irregularity of compounded sheets, it is hard to determine the initial geometrical shapes and position of the SMC charge that will produce a geometrically defect-free final part. Second, defining a robust and optimized molding procedure in terms of molding temperature, pressure and mold closure rate can be challenging. During mold filling stage, material flow mechanisms are closely related to the rheology of SMC, which is strongly coupled and depending nonlinearly on the processing conditions [1]. During curing stage, kinetics of the cure reaction is also dependent on the processing parameters and is very complicated due to the complex composition of the thermosetting resin system. Furthermore, randomly oriented fibers in the SMC inherently pose great challenge to material flow predictions during moulding. Hence, the selection of an appropriate set of process parameters is not intuitive, which could lead to various undesired mold-filling scenarios and part qualities.

At present, the trial-and-error approach is still commonly used by many automotive manufacturers to develop compression molding processes. Due to the challenges stated in the previous paragraph, this approach inevitably consists of numerous trials with different processing conditions until the desired characteristics of the part are obtained. Evidently, this method is time-consuming, labor-intensive and costly.

Therefore, virtual manufacturing of SMC parts through physics-based simulations is favored since it has a great potential to replace the traditional trial-and-error approach, shorten the early process development stage and mitigate the associated technical risks [2].

Proper material characterization and modeling of SMC prepreg system are the fundamental building blocks of an accurate and realistic compression moulding process simulation. Among the multitude of phenomena occurring during compression molding, several material behaviors of SMC are of great importance for process development: thermokinetics behavior, gelation point and flow mechanism.

Thermokinetics behavior of SMC determines the relationship between time, temperature and degree-of-cure. During compression molding, the mold keeps closed until the SMC reaches a certain extent of cure. Predicting SMC charge's degree-of-cure at a certain time under a certain temperature is one of the crucial factors to determine the process time and temperature. Therefore, characterization of SMC thermokinetics is necessary.

Gelation of SMC is another important phenomenon that occurs during compression molding. It is an irreversible reaction in which the polymer transforms from a viscous liquid into a cross-linked gel. Gelation is the incipient formation of a cross-linked network, and it is the most distinguishing characteristic of a thermoset. At gelation point, known as gel point (GP), the average value of the molecular weight reaches maximum, usually assumed to be infinite [13]. During the molding process, the SMC flow must completely fill the mold cavity before it reaches the gel point since it is not able to flow after that. Therefore, the gel point needs to be determined for the selection of the process parameters.

SMC exhibits a complicated flow mechanism due to the nature of its complex thermoset paste, high fiber content, random fiber orientation and relative long fiber length (compared to the sheet thickness). With inappropriate process parameters, undesired SMC flow

drastically affects the final properties of the parts. As a result, it is critical to describe the flow behavior of SMC in order to determine, for example, the mold closure velocity, the mold temperature and the mold closure force, to name a few.

The main goal of the present research is to perform an integrated material characterization roadmap for an SMC prepreg and to develop a simulation of compression molding using a commercial software package. To achieve this objective, the present work is organized as follows:

1) First, a literature review of SMC material characterizations is presented in Chapter 2.
2) In Chapter 3, thermokinetics behavior of the resin system of the SMC is studied and characterized. A cure kinetics model is developed based on the experimental data. Gel point and viscosity evolution of both the resin paste and the SMC prepreg are measured. Gelation model and viscosity model were proposed.
3) In Chapter 4, a flow-compaction testing fixture is developed to study the SMC flow mechanism under several testing conditions, namely at different temperatures, mold closure rates and compression forces.
4) In Chapter 5, the material models developed in previous chapters are implemented into a commercial software package to build a simulation of SMC compression molding process.

Chapter 2. Literature Review

This chapter contains a concise literature review on the characterization of thermoset resins and SMC.

2.1 Kinetics of Thermoset Cure Reaction

Cure reaction of a thermosetting resin is a chemical process where molecules of monomers or prepolymers are cross-linked together to form polymer networks, which is known as polymerization. The curing process produces the toughening or hardening of a polymer material. Degree-of-cure (DOC) is a numerical representation of how far the chemical curing reaction (crosslinking process) has advanced. It starts from 0 (at the beginning of the reaction) and grows until 1 (at the completion of the reaction).

Kinetics of a thermoset cure reaction can be defined as developing mathematical relationships between time, temperature and degree-of-cure. In the process of SMC compression molding, the mold stays closed until the SMC resin system fully cures. A good understanding of SMC cure kinetics is very important to optimize the process in terms of process time, process temperature and energy consumed, which ultimately affect both the cost and the quality of the final part.

A full kinetic analysis of cure reaction could be separated into three major steps: (1) experimental collection of data; (2) computation of kinetic parameters using the experimental data; (3) prediction of the cure progress for required temperature profiles using determined kinetic parameters.

2.1.1 Experimental Characterization

One of the most widely used experimental methods to study cure kinetics is thermal analysis by differential scanning calorimeter (DSC) through isothermal or dynamic tests [14-20]. DSC measures the difference in the amount of heat necessary to increase the temperature of a material sample compared to a reference, the later being an empty sample

pan strictly identical to the one encapsulating the studied material. When the material goes through a physical change due to chemical reactions, it will take more or less heat to keep the temperature increasing at the same rate as the reference. The thermoset cure reaction is an exothermic process, thus DSC measures the heat that flows out of the material as a function of temperature. For thermosetting resins, DSC provides valuable information on glass transition temperature, onset of cure (observed as an exothermic event), heat of cure (integration of the area under the exothermic peak), maximum rate of cure (the exothermic peak), completion of cure (indicated when DSC response returns to baseline behavior) and degree-of-cure.

In DSC thermal analysis, it is generally assumed that the rate of the chemical cure reaction ($\frac{d\alpha}{dt}$) is proportional to the rate of heat evolution ($\frac{dH}{dt}$), which is described as follows [21, 22]:

$$\frac{\mathrm{d}\alpha}{\mathrm{dt}} = \frac{1}{\mathrm{H_T}} \frac{\mathrm{dH}}{\mathrm{dt}} \tag{2.1}$$

where H_T is the total enthalpy of the cure reaction.

Another fundamental assumption for the application of standard DSC to thermoset cure analysis is that the total heat flow detected during the process is identical to the heat evolved by the cure reaction, which assumes that no other enthalpic events occur. Therefore, the total heat of cure reaction (H_T) is obtained from integrating the enclosed area under the scanning heat flow thermogram. An example of the total enthalpy of the cure reaction of a thermosetting resin during DSC thermal analysis is shown in Figure 2.1.

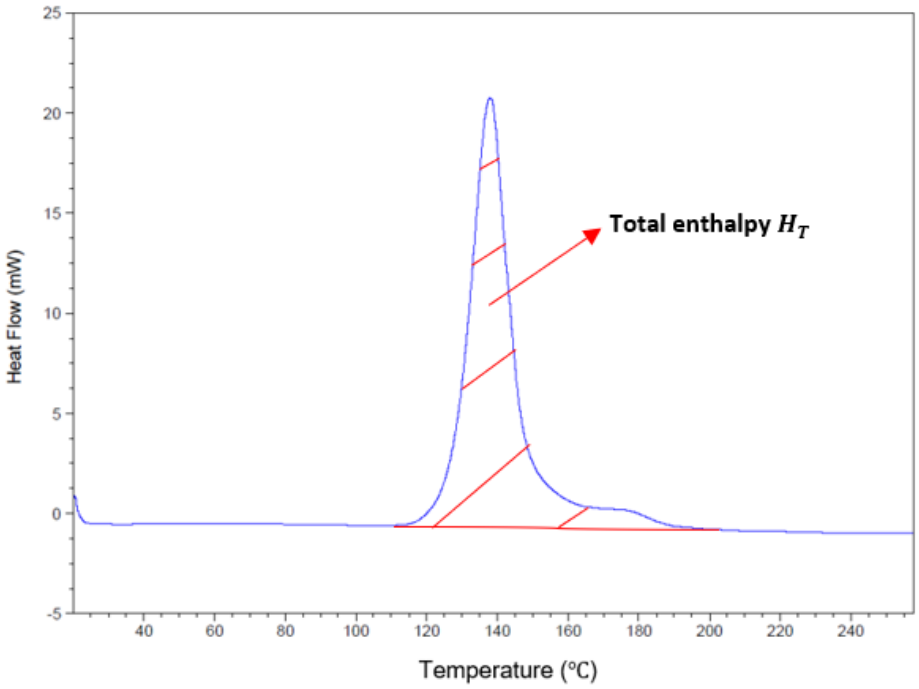

Figure 2.1 Example of the total enthalpy of a cure reaction

In DSC measurements, the conversion or the degree-of-cure α ranges from 0 (completely uncured) to 1 (fully cured). The degree-of-cure at time t, α_t, is defined as [22]:

$$\alpha_t = \frac{H_t}{H_T} = \frac{1}{H_T}\int_0^t \left(\frac{dH}{dt}\right) dt \tag{2.2}$$

where H_t is the amount of heat liberated from the reaction up to time t and H_T is the total enthalpy of the reaction.

2.1.2 Standard Cure Kinetics Models

Once the heat flow of the resin during the cure reaction has been examined by the DSC, it is important to find a cure kinetics model that can describe the cure behavior. A variety of kinetics reaction models have been developed to relate reaction rate to temperature and extent of reaction progress degree-of-cure. Phenomenological reaction models are the most commonly used models to describe thermoset cure reactions. The kinetic parameters of the cure reaction can be obtained by fitting the data obtained from the DSC measurements to the phenomenological reaction models.

Generally, cure kinetics models can describe cure reaction rate as the convolution of two functional forms having respectively temperature and extent of cure progress dependency. This can be written as follows, for the reaction rate equation and the Arrhenius equation respectively:

$$\frac{d\alpha}{dt} = k(T)f(\alpha) \tag{2.3}$$

$$k(T) = A \exp\left(\frac{-E}{RT}\right) \tag{2.4}$$

where

α = conversion or degree of cure (unitless)

$\frac{d\alpha}{dt}$ = rate of conversion (1/s)

k = rate constant with Arrhenius temperature dependency

$f(\alpha)$ = reaction model

A = pre-exponential factor (1/s)

E = activation energy (kJ/mol)

R = universal gas constant = 8.314 J/mol/K

T = absolute temperature in Kelvin (K)

Combining the two equations together, the rate of reaction can be described as:

$$\frac{d\alpha}{dt} = A \exp\left(\frac{-E}{RT}\right) f(\alpha) \tag{2.5}$$

Many studies have been conducted on the thermoset cure kinetics and a variety of reaction models have been proposed to adequately describe the cure behavior of thermosets, some of which are presented in Table 2-1.

Table 2-1 Typical cure kinetics models

Model	**Reaction Rate ($\frac{d\alpha}{dt}$)**
nth Order	$k\ (1-\alpha)^n$
Power Law	$k\ n\ \alpha^{(1-\frac{1}{n})}$

Autocatalytic (Ng [23])	$k\,\alpha^m\,(1-\alpha)^n$
Autocatalytic (Kamal et al. [24])	$(k_1 + k_2\alpha^m)\,(1-\alpha)^n$

The nth order rate equation is a simplest model which assumes that one master curve could represent the overall cure reaction kinetics [22]. In the equation, n is a reaction order which is calculated to best fit the experimental data [14]. α is the conversion of the reactants and (1- α) represents the concentration of reactants which varies from 1 at the beginning of the reaction to 0 at the end of the reaction. This model has been utilized by many researchers to describe the cure behaviors of different kinds of resin systems, including Lee and Macosko [25], Rojas et al. [26], Adabbo et al. [27] and Reboredo et al. [28]. However, under isothermal condition, the nth order kinetics model is not applicable for autocatalytic cure processes as it is a decelerating model which predicts the maximum reaction rate at time = 0 (Figure 2.2) and it is not the case for autocatalytic reaction.

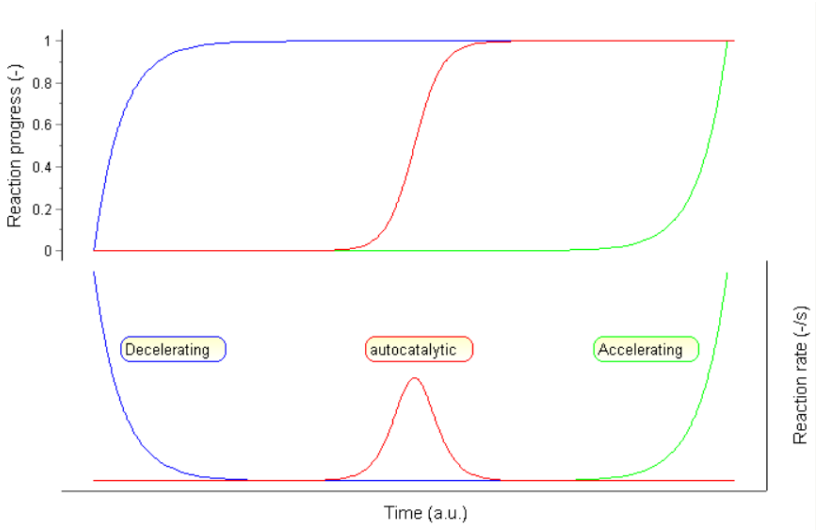

Figure 2.2. Reaction profiles of decelerating, autocatalytic and accelerating models [29]

Prout and Tompkins [30] developed a kinetics model for autocatalytic processes, which is:

$$\frac{d\alpha}{dt} = k\alpha(1-\alpha) \tag{2.6}$$

This equation clearly shows that the reaction rate depends on not only the amount of reactant left $(1-\alpha)$ but also the amount of product formed (α), which is known as autocatalysis.

A more general expression was proposed by Ng [23]:

$$\frac{d\alpha}{dt} = k\alpha^m(1-\alpha)^n \tag{2.7}$$

where m and n are reaction orders to be determined by experimental data.

All the three models introduced above use a single rate constant k for the whole cure process. However, several different events could take place simultaneously during the process, leading to a very complex kinetics of cure.

Kamal et al. [24, 31] proposed an autocatalytic model for isothermal cure data, which involves two rate constants and it has shown good agreement with the experimental DSC data of epoxy and unsaturated polyester systems:

$$\frac{d\alpha}{dt} = (k_1 + k_2\alpha^m)(1-\alpha)^n \tag{2.8}$$

where k_1 and k_2 are rate constants with Arrhenius temperature dependency, m and n are constants to be determined by experimental data. This equation has been extensively used by researchers to successfully represent cure kinetics of thermosetting resins and molding compounds including unsaturated polyesters and epoxies (Progelhof and Throne [32], Dutta and Ryan [33], Pusatcioglu et al. [34], Lin et al. [35], Gebart [36], to name a few).

2.1.3 Differential Isoconversional Methods of Cure Kinetics

Being different from the kinetics models mentioned in the previous section, the isoconversional method does not assume a specific form of reaction model $f(\alpha)$, and additionally does not assume the constancy of pre-exponential factor A and activation energy E throughout the reaction [29].

Isoconversional methods of cure kinetics make use of the isoconversional principle, which states that at a constant extent of conversion/degree-of-cure, the reaction rate is only a

function of temperature [37]. This can be easily yielded by taking the logarithmic derivative of the reaction rate (Eq. 2.3) at a certain extent of conversion α, which is:

$$\left[\frac{dln\left(\frac{d\alpha}{dt}\right)}{d\frac{1}{T}}\right]_{\alpha} = \left[\frac{dln\left(k(T)\right)}{d\frac{1}{T}}\right]_{\alpha} + \left[\frac{dln\left(f(\alpha)\right)}{d\frac{1}{T}}\right]_{\alpha} \tag{2.9}$$

where α is the extent of conversion, which can be determined from TGA runs as a fractional mass loss or from DSC runs as a fractional heat flow, t is the time, T is the temperature, $k(T)$ is the rate with Arrhenius temperature dependency, and $f(\alpha)$ is the reaction model. Since at a certain extent of conversion, α = constant, and $f(\alpha)$ is also constant, the second term in the right side of Eq. 2.9 equals to zero, which yields:

$$\left[\frac{dln\left(\frac{d\alpha}{dt}\right)}{d\frac{1}{T}}\right]_{\alpha} = -\frac{E(\alpha)}{R} \tag{2.10}$$

This equation shows that the isoconversional values of the activation energy $E(\alpha)$ can be evaluated from the temperature dependence of the isoconversional reaction rate $\frac{d\alpha}{dt}$, without assuming any specific form of reaction model $f(\alpha)$ [37]. Therefore, isoconversional methods are often called "model-free" methods [38].

Isoconversional methods can be divided into two categories: differential and integral. This review will mainly focus on the differential isoconversional method.

The most popular representative of differential isoconversional method is the method of Friedman [3]. The method is based on the inter-comparison of experiments that are performed at different heating rates. In the work of Friedman, fiberglass-reinforced resin was studied through temperature scanning experiments with linear heating rates of 50, 100, 180, and 360 °C/hr. Since the activation energy E and pre-exponential factor A are changing correspondingly to the conversion α according to the isoconversional principle, Eq. 2.5 can be written as:

$$\left(\frac{d\alpha}{dt}\right)_{\alpha,i} = A_{\alpha} \exp\left(\frac{-E_{\alpha}}{RT_{\alpha,i}}\right) f(\alpha)$$

where the index i denotes the number of experiments with different temperature heating rates [38].

Friedman [3] proposed to apply the logarithm of both sides of the equation, which gives:

$$\ln\left(\frac{d\alpha}{dt}\right)_{\alpha,i} = \ln[A_\alpha f(\alpha)] - \frac{E_\alpha}{RT_{\alpha,i}} = \ln[A'_\alpha] - \frac{E_\alpha}{RT_{\alpha,i}} \qquad (2.12)$$

Let $A'_\alpha = A_\alpha f(\alpha)$ and A'_α is named as modified pre-exponential factor.

At any selected value of α (from 0 to 1), plot of $\ln(\frac{d\alpha}{dt})$ versus $\frac{1}{T}$ shows a straight line with the slope equal to $-\frac{E_\alpha}{R}$ and intercept equal to $\ln A'_\alpha$. Therefore, the values of isoconversional kinetic parameters: activation energy E_α and modified pre-exponential A'_α can be evaluated at any conversion α.

Prediction of material kinetic behavior is one of the most important practical purposes of kinetic analysis [38]. Studies have shown that isoconversional kinetic analysis method is reliable to predict the curing kinetics of various resins at an arbitrary temperature program [39]. Vyazovkin and Sbirrazzuoli [40, 41] obtained the set of isoconversional kinetic parameters of epoxy from nonisothermal experiments with different heating rates using DSC. The nonisothermal data was utilized to predict the epoxy curing kinetics under isothermal conditions. The isoconversional predictions have shown great agreement with the experimental measurements and was found to be more accurate than the predictions obtained by other methods. Privalko et al. [42] studied the crosslinking kinetics of hexamethylene diisocyanate-epoxy resin by DSC and found that the isoconversional approach describes quantitatively the reaction kinetics over the entire range of conversions. Wang et al. [43] utilized isoconversional kinetics method to model and predict the cure kinetics of commercial phenol-formaldehde resin and reported that isothermal cure is well predicted with this method, showing good agreement with experimental isothermal runs. Salla et al. [44] studied the curing kinetics of unsaturated polyester resin crosslinked with styrene using DSC and applied the isoconversional methodology to the non-isothermal data. Other researchers (He et al. [45], Li et al. [46], Vazquez et al. [47], to name a few) have also provided numerous examples of successful kinetic predictions obtained by applying the isoconversional approach to the curing kinetics of various resins.

2.2 Gelation and Viscosity of Thermosets

Gelation is a phenomenon of thermosetting system which occurs during the curing process. Viscosity is a physical parameter which measures a material's internal flow resistance. The viscosity changes are usually significant during the polymer processing, especially for thermoset polymers. For example, before the curing reaction, the viscosity is high due to lack of thermal mobility of chains. At the beginning of the reaction, the viscosity drops due to the increase of thermal motion. However, the thermoset becomes more and more viscous during the reaction, which is caused by the crosslinking of the molecules. At one point, the reacting system finally forms a macro-network and results in a rapid approach toward infinite viscosity. This rheological event is typically called gelation or gel point [48]. A thermoset loses its ability to flow and is no longer processable above the gel point, and therefore gelation defines the upper limit of the material processing window from a mold filling standpoint. That is why the determination of gel point is very important for the manufacturing process development.

Several experimental techniques can be used for rheological study, typically oscillatory rheometer (also known as rotational dynamic analyser (RDA)), press rheometer, capillary rheometer, viscometer, dielectric analyser, dynamic mechanical analyser (DMA) and thermomechanical analyser (TMA). In RDA and DMA experiments, the complex viscosity (η^*), storage modulus (G'), loss modulus (G''), displacement (angular or linear), strain and normal force are usually measured or computed as a function of temperature and/or time.

A number of criteria are used to determine the gel point from these experimental procedures.

(1) Point where the loss factor $tan\delta = G''/G'$ is independent of frequency [49-51].
(2) Point where the relative viscosity $\eta_r = \eta/\eta_o$ (where η is the instantaneous viscosity and η_o is the initial viscosity) is equal to 10^4 or 10^3 [52, 53].
(3) Point where G' equals to G'', or the point where the loss factor $tan\delta = 1$ [13, 54, 55].
(4) Intersection point of the two linear parts of the log G'' curve [56-58].
(5) Point where the loss factor $tan\delta$ is maximum [59-61].
(6) Onset point of the rapid viscosity increase [48].

(7) Onset point of the rapid normal force drop [13].

However, the gel points determined by these criteria for the same material might be different. For example, the gel points defined by the criterion where G' equals to G'' were found to be earlier than those measured by the criterion where η_r is equal to 10^4 or 10^3 for unsaturated polyester resins [48]. In addition, some of the criteria are not applicable for fiber reinforced prepreg materials. For example, prepreg materials have a high viscosity and the changes in the viscosity are usually not as notable as the one for neat resins [62]. Therefore, the sixth criterion: onset point of rapid viscosity increase is usually hard to define and thus not suitable for them. Besides, for some fiber reinforced polymers or polymers with additives and charges, G' is always bigger than G'' during the rheological experiment [62]. There is no cross-over point of G' and G'' so the third criterion might not be applicable either.

Hence, the gel point determination criteria need to be chosen carefully for the studied material, according to the actual experimental data and its ultimate application.

Chapter 3. Material Characterization

3.1 Materials

The materials studied in this work are carbon fiber reinforced SMC (CF-SMC) prepreg sheets, neat resin which is used to produce this SMC prepreg and resin extracted from the SMC prepreg. Throughout this thesis, those materials are referred to as CF-SMC prepreg, neat resin and extracted resin, respectively.

The CF-SMC and the neat resin are provided by the industrial partner of this research: Magna International Inc. The CF-SMC was manufactured in-house by Magna. The main chemical species of the neat resin system are vinyl ester primary backbone, styrene reactive diluent and isocyanate thickening agent. At the request of the industrial partner, the exact percentages of those components stay confidential in this thesis. The carbon fibers used in this SMC are about 25 mm long. During the pre-pregging process of this SMC sheet, an inhibitor was added to the material system to extent its shelf life in cold storage prior being ready for its thermal processing. It means that the CF-SMC prepreg contains this inhibitor, while the neat resin does not. The impact of this inhibitor on the cure kinetics behavior and the rheological behavior is unclear and needs to be studied.

Using SMC prepregs to study cure kinetics by differential scanning calorimetry (DSC) is challenging, as they often feature non-uniform spatial distribution of resin mass content and chemical composition which promote significant variations in measured cure profile. Besides, the presence of fibers complicates the measurement of rheological behavior by parallel plate rheometry. For these reasons, a resin extraction technique was developed to obtain resin from the SMC prepreg, while mitigating thermal ageing and cure progress of the extracted resin, in order to study the impact of inhibitor through comparing the characterization results of the neat resin and the extracted resin. Another benefit of resin extraction is that the influence of the carbon fibers on the cure kinetics and rheology can also be isolated and studied by comparing the material properties of the CF-SMC and the extracted resin.

Resin extraction technique is described as follows. (1) Cut the CF-SMC prepregs into squares and stack them between two release films. (2) Preheat hydraulic Wabash press to 50°C. (3) Place the stack onto the press platen. (4) Close the press slowly to increase the force by small incremental steps of one ton-force over an hour and squeeze out only resin by percolation flow from the CF-SMC prepreg. (5) Open the press and scrape the extracted resin into a glass container.

3.2 Cure Kinetics

The curing behavior of neat resin, CF-SMC and extracted resin were studied using differential scanning calorimetry (DSC) through temperature scanning and isothermal experiments. A cure kinetics model was developed for neat resin and extracted resin, respectively, using Advanced Kinetics and Technology Solutions-Thermokinetics (AKTS-TK) software. The model generation process was based on the differential isoconversional method of Friedman [3], where activation energy and pre-exponential factor are functions of the extent of reaction, which have been introduced in section 2.1.3 in Chapter 2. Isothermal model predictions were compared with experimental data from isothermal DSC runs and they have shown good agreement.

3.2.1 Cure Kinetics of Neat Resin

This section introduces an experimental method for studying the curing behavior of the neat resin and presents a cure kinetics model that is developed based on the temperature scanning experimental data. Isothermal experimental data is used to validate the predictive capability of this model.

3.2.1.1 Experimental Method

The cure kinetics of the neat resin was studied using a Q2000 DSC from TA Instruments. The instrument was calibrated for temperature, enthalpy and heat capacity using appropriate standard reference materials. Both dynamic and isothermal scans were carried out to track the heat flow of the neat resin under different time-temperature profiles. The

experiments were all carried out under a constant purging gas of nitrogen of 50 mL/min, which creates an inert and dry atmosphere in the measurement cell. The nitrogen atmosphere also eliminates air oxidation of the samples at high temperatures. Prior to each DSC run, a small amount of sample was weighed accurately by a balance and sealed into a Tzero aluminum hermetic DSC pan, using a DSC sample press. Subsequently, the samples were down selected and the corresponding weights of these samples ranged from 4 mg to 7 mg in order to minimize heat flow variations arising from sample preparation variability. The sample pan was then transferred to the DSC autosampler with a pair of tweezers. The autosampler would automatically load the sample into the measurement cell next to the reference pan. Once the autosampler loads the pan and the cell cover is in place, the controller takes over and runs preprogrammed dynamic or isothermal experiments on the sample. The methods of experiments were programmed through TA Thermal Advantage software.

For the dynamic DSC measurements, the DSC cell was subsequently heated at a constant rate of 0.5, 1, 2, 4, 8, 10, 20 and 40 °C/min over a temperature range of 20 °C to 260 °C. One repetition test was performed for each testing condition. DSC measures the heat flow out of the samples during these runs. An example of dynamic DSC experiment result is shown in Figure 3.1. As expected, the DSC cure of the neat resin is characterized by a broad exothermic peak. In addition, the curve has a small second bump at the end of the reaction which is observed for every experiment. The dynamic experimental data is used to develop the cure kinetics model in section 3.2.1.2.

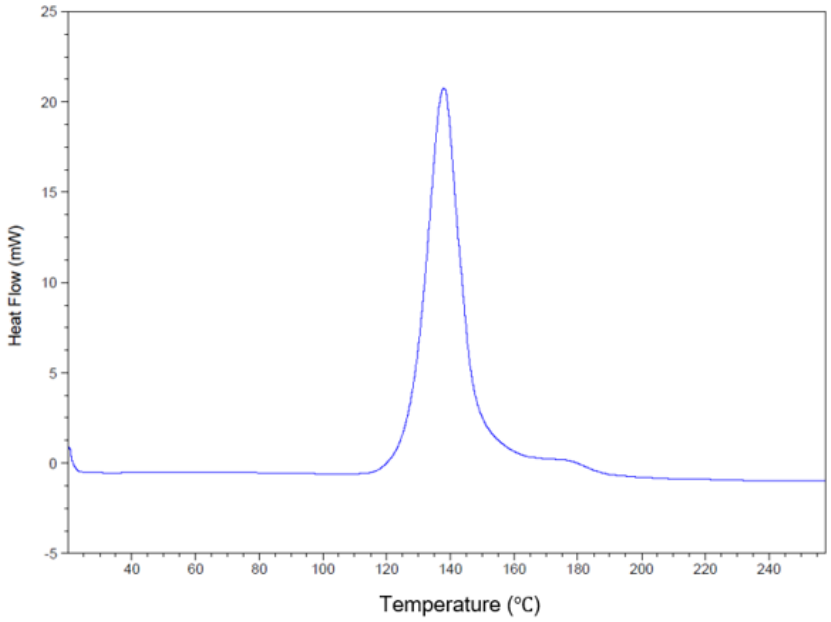

Figure 3.1 Dynamic scan from 20°C to 260°C with heating rate of 8°C/min for the neat resin

Isothermal DSC measurements were carried out at 130 °C on the neat resin as well and two repetitions were performed. The curing behavior of the neat resin under isothermal condition at 130 °C will be predicted by the cure kinetics model. The isothermal experimental data is used to validate the prediction accuracy of the model.

3.2.1.2 Cure Kinetics Model

Advanced Kinetics and Technology Solutions-Thermokinetics (AKTS-TK) software is used to facilitate the kinetic analysis and to determine the kinetic parameters (activation energy E and pre-exponential factor A) based on the measurements performed by DSC. After the collection of all experimental dynamic DSC data sets representing a broad range of heating rates (0.5, 1, 2, 4, 8, 10, 20 and 40 °C/min), these data sets were imported into AKTS-TK for model training purpose.

Since the total enthalpy (H_T) is obtained from integrating the enclosed area under the scanning heat flow thermogram, the construction of a correct baseline is a crucial procedure in avoiding introduction of systematic errors during reaction kinetics model elaboration

from the DSC data. Generally, the application of the straight-line form for the baseline is incorrect. The recorded signal results not only from the heat of the reaction but is additionally affected by the change of the specific heat and its temperature dependence of the reactants and products during the progress of the reaction. AKTS-TK uses the tangential area-proportional baseline because of its correction possibilities and degrees of freedom for baseline shape optimization. It is created at $\alpha_t = 0$ and at $\alpha_t = 1$ by the appropriate tangents at the beginning or the end of the measured DSC signal. It allows compensation of not only changes in the value of specific heat of the reactant and product, but also of changes in their temperature dependency. Two baselines were constructed using two sets of data (0.5 °C/min and 40 °C/min) manually and the "automatic baseline" function of the software, thus automatically constructed the baselines for the remaining sets of data. Baselines were improved by manual adjustment and also by the "optimize baseline" function of the software.

The total enthalpy (H_T) of each test, which is the enclosed area between the heat flow thermogram and the baseline, is then calculated by the software. As an example, the construction of total enthalpy of the dynamic experiment with heating rate of 8°C/min is shown in Figure 3.2.

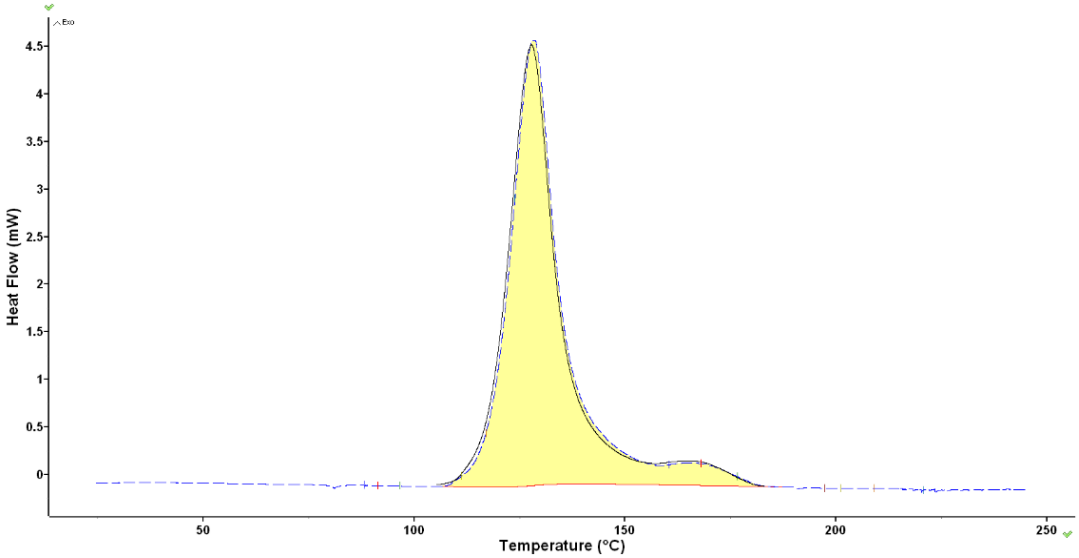

Figure 3.2 Red line: baseline; Yellow area: total enthalpy

Next, the "kinetics" function of the software applies a differential isoconversional analysis based on all of the dynamic experimental data. Isoconversional method of Friedman is used

to develop a cure kinetic model for the neat resin, namely, to establish a mutual mathematics relationship between the reaction rate $\frac{\mathrm{d}\alpha}{\mathrm{dt}}$, the reaction progress α, and the temperature.

As reviewed in section 2.1.3, the differential isoconversional method of Friedman can be written as:

$$\ln\left(\frac{d\alpha}{dt}\right)_{\alpha,i} = \ln[A'_{\alpha}] - \frac{E_{\alpha}}{RT_{\alpha,i}} \tag{3.1}$$

where A'_{α} is modified pre-exponential factor, E_{α} is activation energy and they are both functions of the reaction progress α, R is universal gas constant which equals to 8.314 J/mol/K, T is temperature in units of Kelvin.

The model parameters A'_{α} and E_{α} need to be obtained using the experimental data.

At any selected value of α (from 0 to 1), plot of $\ln(\frac{d\alpha}{dt})$ versus $\frac{1}{T}$ shows a straight line with the slope equal to $-\frac{E_{\alpha}}{R}$ and intercept equal to $\ln[A'_{\alpha}]$. In more details, E_{α} and A'_{α} are calculated by the software with the following steps. First, plot $\ln(\frac{d\alpha}{dt})$ versus reciprocal temperature for all the dynamic DSC experimental data. Find the point where reaction progress α = 0.99 (example value) on each dataset and connect the points to form a straight line, which is shown as the first line from the left in Figure 3.3. The slope of the line equals to $-\frac{E_{\alpha}}{R}$ and the intercept equals to $\ln[A'_{\alpha}]$. Therefore, E_{α} and A'_{α} can be calculated at α = 0.99. Repeat this step for all the α (from 0 to 1). As a result, the values of isoconversional kinetic parameters: activation energy E_{α} and modified pre-exponential factor A'_{α} can be calculated at any conversion α.

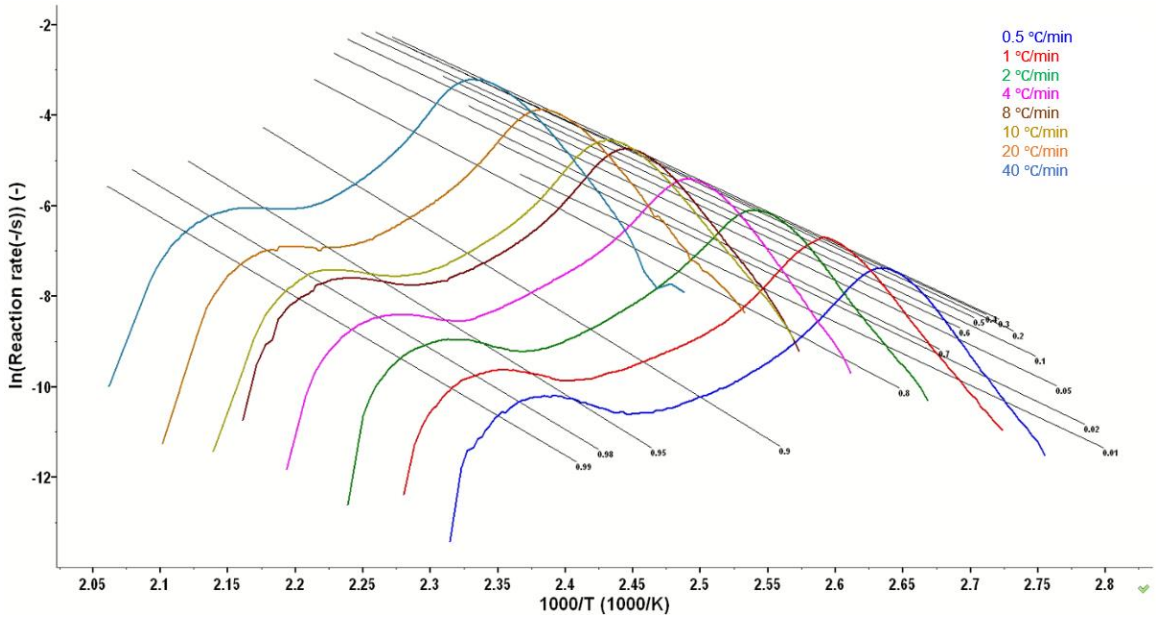

Figure 3.3 Plot of $ln(\frac{d\alpha}{dt})$ versus reciprocal temperature of each dynamic DSC experimental data for the neat resin

Therefore, a triplet lookup table for activation energy E_α and modified pre-exponential factor A'_α, which are dependent on reaction progress α can be developed. Since the step of α is small, the complete lookup table contains numerous entries and it was not put here in the thesis in its integral version. A schematic version is presented in Figure 3.4.

Reaction Progress α [-]	Activation Energy E_α [kJ/mol]	Modified Pre-exponential Factor A'_α [ln(1/s)]
1.08E-06	15136.4071	28.1883
2.00E-06	15136.2826	28.1884
3.00E-06	15136.1471	28.1885
4.00E-06	15136.0114	28.1886
⋮	⋮	⋮
1.00E+00	11605.1914	13.6702

Figure 3.4 Lookup table for activation energy E_α and modified pre-exponential factor A'_α

The corresponding values of E_α and A'_α to α can also be represented in a graph, as shown in Figure 3.5.

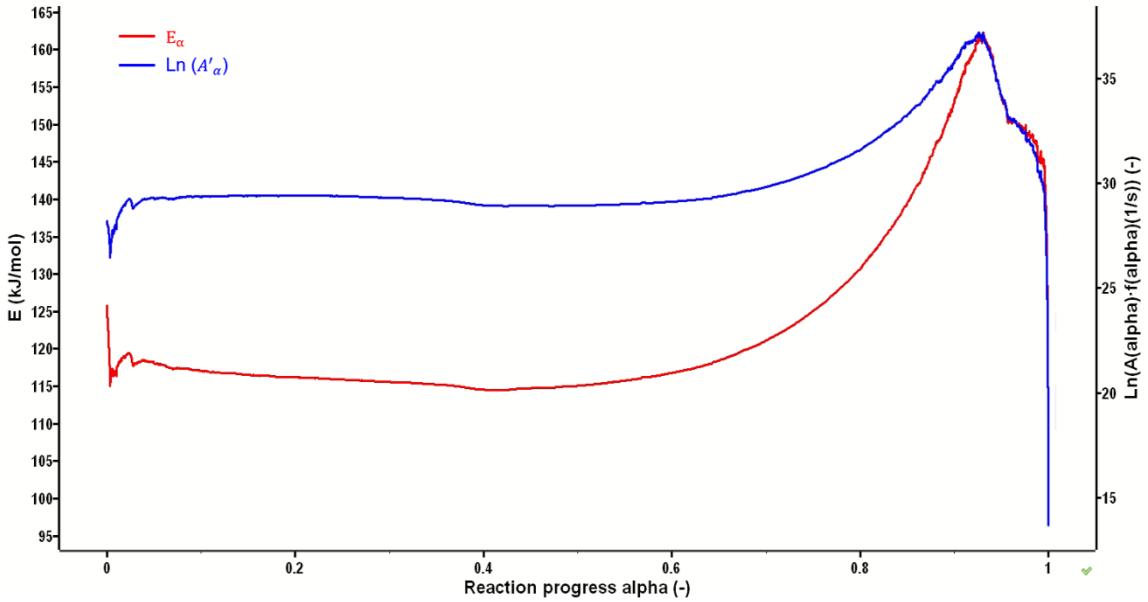

Figure 3.5 E_α and A'_α as a function of α for the neat resin

After obtaining the E_α and A'_α, the reaction rate can be modeled using the following equations:

$$\ln\left(\frac{d\alpha}{dt}\right)_{\alpha,i} = \ln[A'_\alpha] - \frac{E_\alpha}{RT_{\alpha,i}} \tag{3.2}$$

$$\frac{d\alpha}{dt} = A'_\alpha \exp\left(-\frac{E_\alpha}{RT_{\alpha,i}}\right) \tag{3.3}$$

The reaction progress α is then computed automatically by the software based on the simulation of $\frac{d\alpha}{dt}$.

Then, the accuracy of the model is validated by comparing the simulated reaction rate and reaction progress to the experimental data.

The reaction rate ($\frac{d\alpha}{dt}$) of each experiment was computed, based on the following equation:

$$\frac{\mathrm{d}\alpha}{\mathrm{dt}} = \frac{1}{\mathrm{H_T}}\frac{\mathrm{dH}}{\mathrm{dt}} \tag{3.4}$$

where H_T is the total enthalpy of the cure reaction, $\frac{dH}{dt}$ is the rate of heat evolution.

The experimental reaction rate curves are plotted against the model, as shown in Figure 3.6.

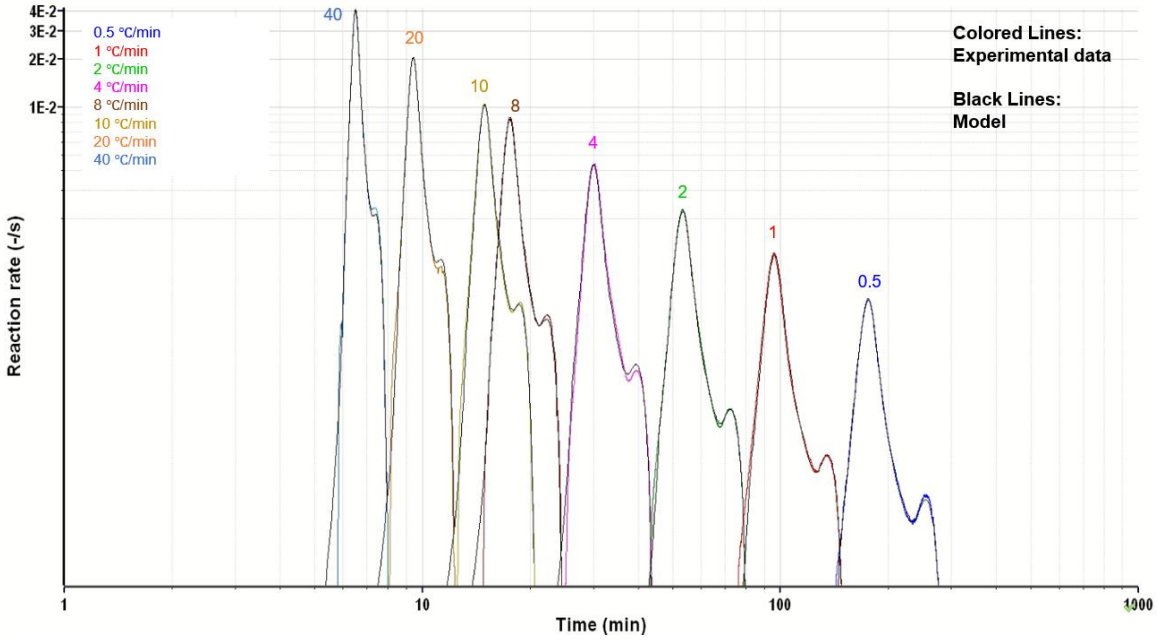

Figure 3.6 Measured and modeled reaction rate curves for the neat resin

The reaction progress (from 0 at the beginning to 1 at the end) of each experiment was calculated, based on the following equation, which is also described in section 2.1.1:

$$\alpha_t = \frac{H_t}{H_T} = \frac{1}{H_T} \int_0^t \left(\frac{dH}{dt}\right) dt \tag{3.5}$$

where H_t is the amount of heat flow up to time t and H_T is the total enthalpy of the reaction.

The measured reaction progress curves are plotted against the modeled reaction progress curves, which is shown in Figure 3.7.

The average correlation coefficient R is equal to 0.99921, which indicates a great match between the model and the experimental data. Therefore, the model can adequately describe the curing of the neat resin.

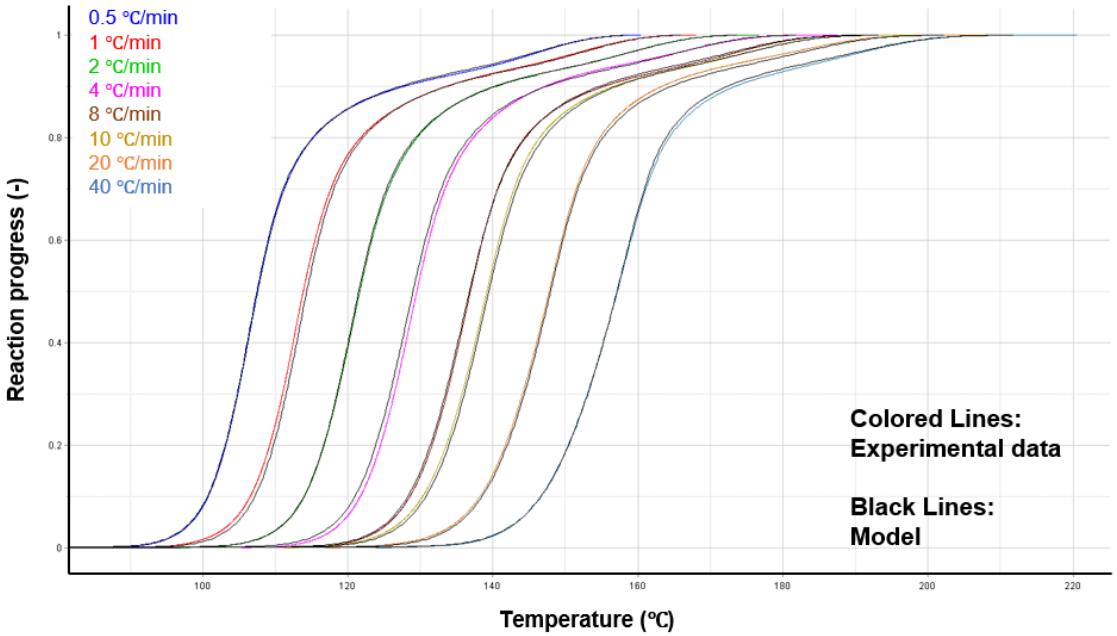

Figure 3.7 Measured and modeled reaction progress curves for the neat resin

Using this differential isoconversional model, predictions of reaction rate and reaction progress can also be developed for any temperature profile.

The reaction rate of the neat resin under isothermal condition at 110°C, 120°C, 130°C, 140°C, 150°C and 160°C is predicted by the model, which could be seen in Figure 3.8.

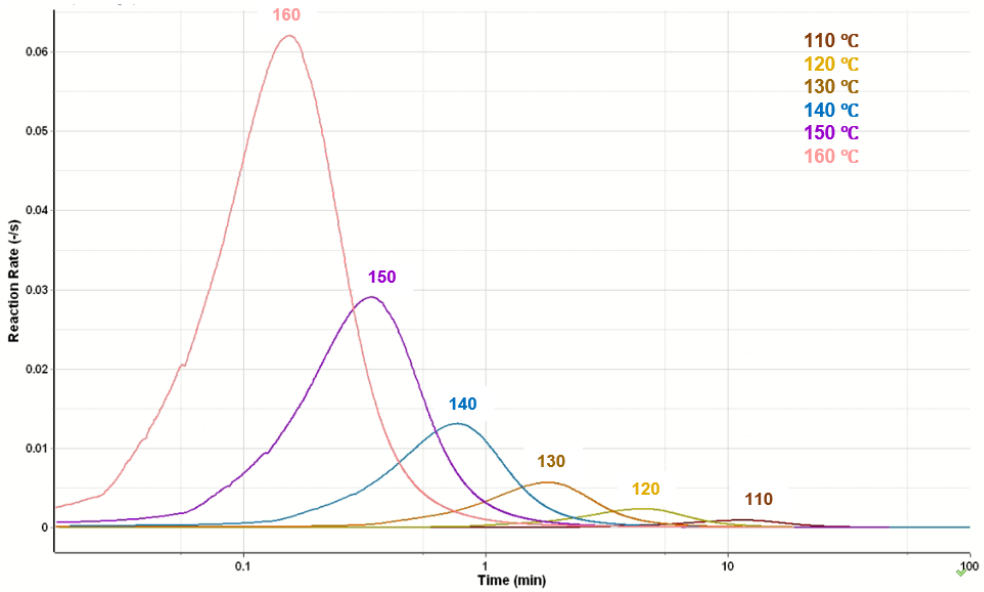

Figure 3.8 Predicted reaction rate curves for the neat resin under isothermal condition

The prediction accuracy of the model needs to be validated.

Isothermal DSC measurements were carried out at 130°C on the neat resin. This experimental data is used for model validation and testing purpose. The measured reaction rate is plotted against the predicted reaction rate. The coefficient of determination R^2 is equal to 0.98, which indicates a good fit between experimental data and model prediction.

Therefore, the cure kinetics model is validated to be adequate to predict the curing behavior of the neat resin at any temperature profile.

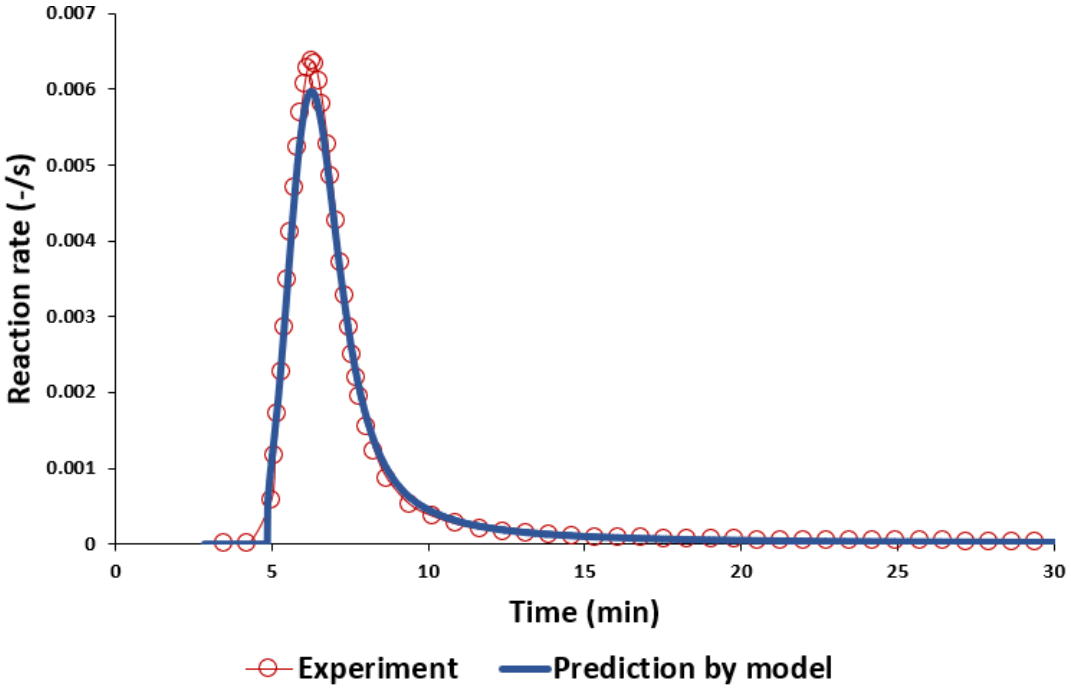

Figure 3.9 Measured and predicted reaction rate curves for the neat resin at 130°C

3.2.2 Cure Kinetics of Extracted Resin

As described in section 3.1, the extracted resin and the CF-SMC prepreg contain an inhibitor, while the neat resin does not. The impact of this inhibitor on the cure kinetics behavior can be studied by comparing the curing behavior of the neat resin and the extracted resin. Therefore, the thermal analysis methodology based on DSC used to

characterize the cure kinetics of neat resin was again leveraged to study the curing behavior of the extracted resin.

3.2.2.1 Experimental Method

The cure kinetics of the extracted resin was studied using a DSC 250 from TA Instruments. The instrument was calibrated for temperature, enthalpy and heat capacity using appropriate standard reference materials. The sample preparation method is the same as the DSC experiments of the neat resin in the previous section.

Dynamic DSC measurements with heating rates of 0.5, 1, 2, 4, 8, 10, 20 and 40 °C/min over a temperature range of 20 °C to 250 °C were carried out to track the heat flow of the extracted resin. The experimental data of the dynamic tests are used to develop the cure kinetics model of the extracted resin, using AKTS-TK software.

Isothermal scans at 105, 110, 115, 120, 125 °C were also performed to track the evolution of the resin cure under different isothermal temperatures.

One repetition test was performed for each testing condition. DSC measures the heat flow out of the sample during the experiments. An example of the dynamic DSC experiment result is shown in Figure 3.10. The same as the neat resin, the heat flow of the extracted resin curing is characterized by a broad exothermic peak. In a similar way as the neat resin, there is a small second peak of heat flow at the end of the reaction which is observed for every dynamic experiment. The temperature scanning experimental data is used to develop the cure kinetics model in the following section.

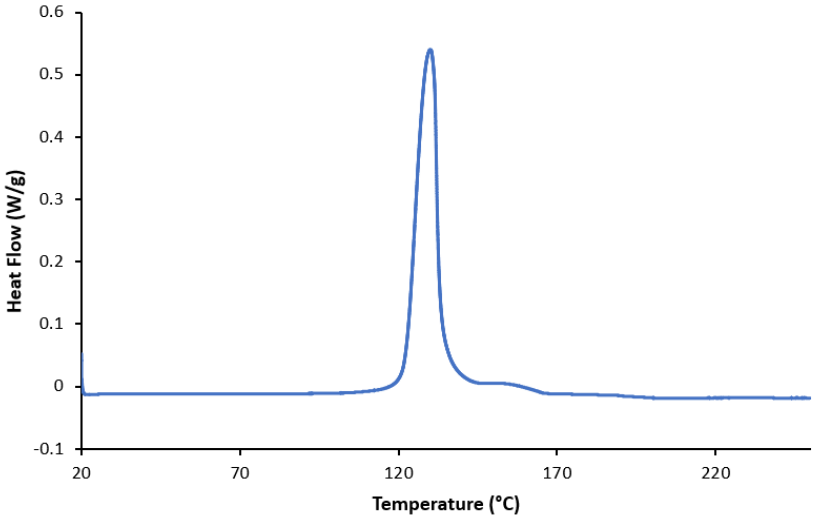

Figure 3.10 Dynamic scan from 20°C to 250°C with heating rate of 1°C/min for the extracted resin

3.2.2.2 Cure Kinetics Model

After the collection of all experimental dynamic DSC data, the temperature scanning experiment data with different heating rates (0.5, 1, 2, 4, 8, 10, 20 and 40 °C/min) was imported into AKTS-TK software.

Baseline for each test result needs to be constructed to obtain the total enthalpy of each test. The first two baselines (for the datasets with the heating rates of 0.5 °C/min and 40 °C/min) were constructed manually and then the "automatic baseline" function of the software automatically constructed the baselines for the remaining sets of data.

The total enthalpy (H_T) of each test, which is the enclosed area between the heat flow thermogram and the baseline, is then calculated by the software. As an example, the construction of total enthalpy of the dynamic experiment with heating rate of 1°C/min is shown in Figure 3.11. The yellow area represents the total enthalpy of the curing process.

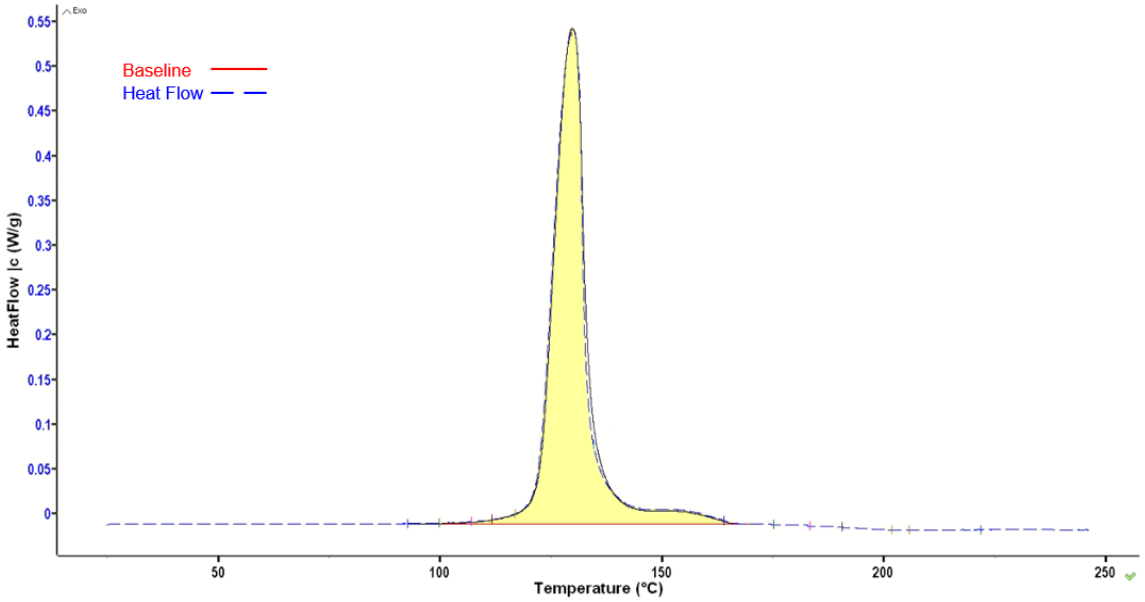

Figure 3.11 Yellow area: the total enthalpy of the dynamic experiment with heating rate of 1°C/min for the extracted resin

Then, a differential isoconversional analysis is carried out based on all of the dynamic experimental data. Isoconversional method of Friedman is applied to develop a cure kinetic model for the extracted resin, in the same way as for the neat resin in the previous section.

The isoconversional kinetic parameters: modified pre-exponential factor A'_α and activation energy E_α can be calculated by plotting $\ln(\frac{d\alpha}{dt})$ versus $\frac{1}{T}$. At any fixed value of reaction progress α, the dependence of $\ln(\frac{d\alpha}{dt})$ on $\frac{1}{T}$ shows a straight line with the slope equal to $-\frac{E_\alpha}{R}$ and intercept equal to $\ln[A'_\alpha]$. Straight lines at some picked value of α are shown in Figure 3.12. E_α and A'_α can be calculated from the slope and the intercept separately. Activation energy E_α and modified pre-exponential factor A'_α as a function of reaction progress α are presented in Figure 3.13.

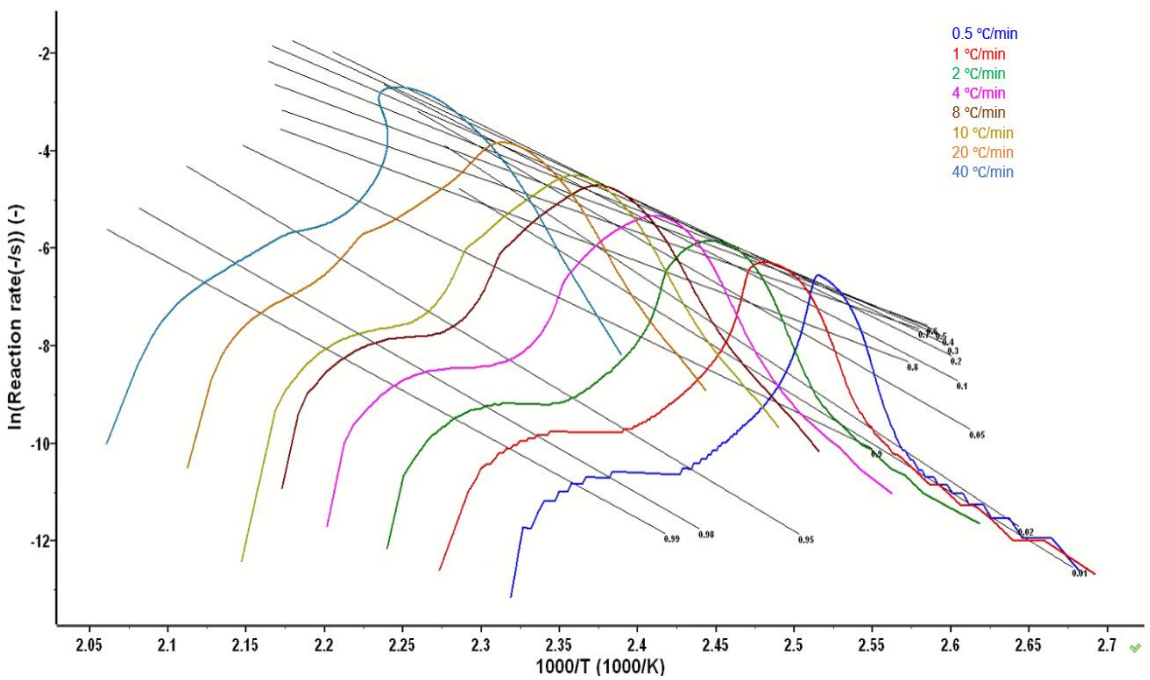

Figure 3.12 Plot of $ln(\frac{d\alpha}{dt})$ versus reciprocal temperature of each dynamic DSC experimental data for the extracted resin

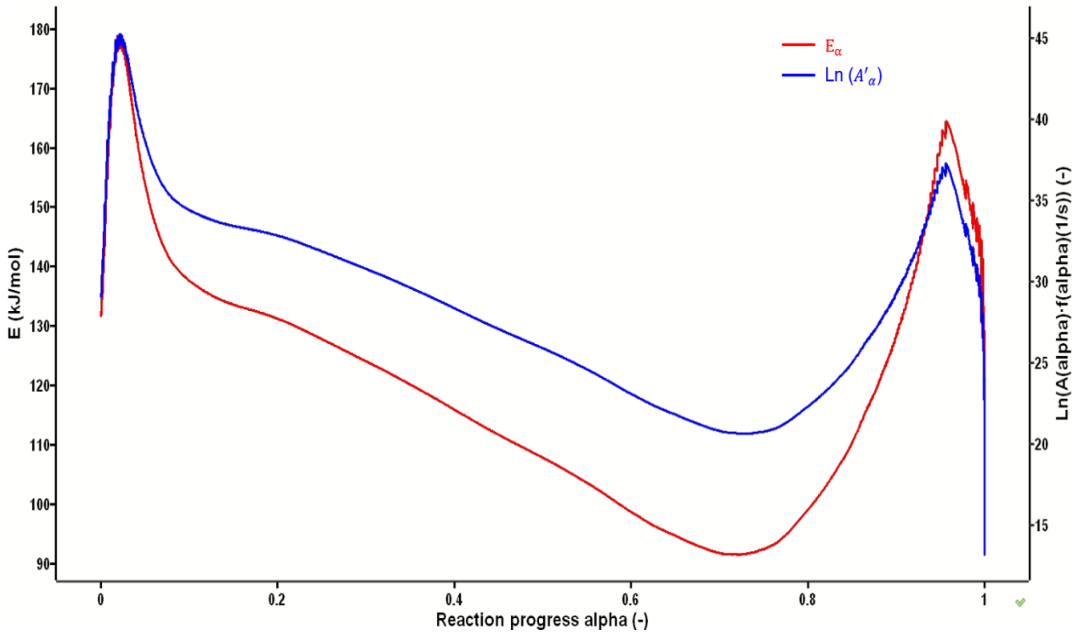

Figure 3.13 Activation energy E_α and modified pre-exponential factor A'_α as a function of reaction progress α for the extracted resin

The dependence of E_α and A'_α on the reaction extent α can then be applied for accurate simulation of the reaction rate $\frac{d\alpha}{dt}$ as described in 3.2.1.2, using the following equation:

$$\frac{d\alpha}{dt} = A'_{\alpha} \exp\left(-\frac{E_{\alpha}}{RT_{\alpha,i}}\right) \tag{3.6}$$

The simulated reaction rate curves are plotted against the experimental reaction rate curves for the dynamic test conditions of the extracted resin, which is presented in Figure 3.14.

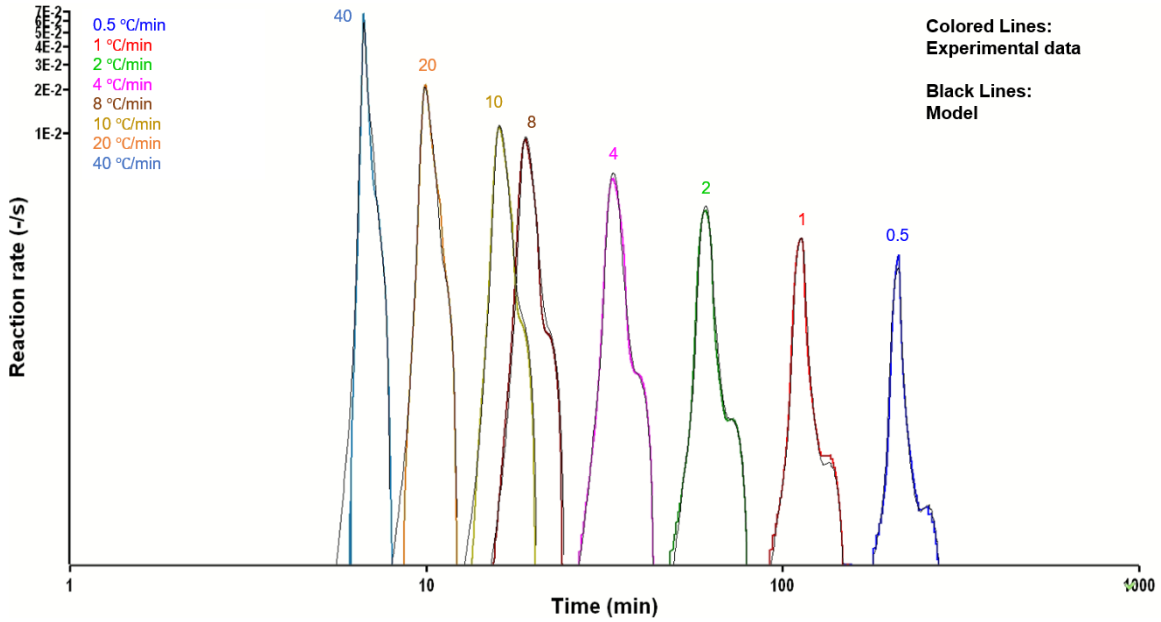

Figure 3.14 Measured and modeled reaction rate curves for the extracted resin

The reaction progress α is then computed based on the reaction rate $\frac{d\alpha}{dt}$. The modeled reaction rate curves are plotted against the experimental data, as shown in Figure 3.15.

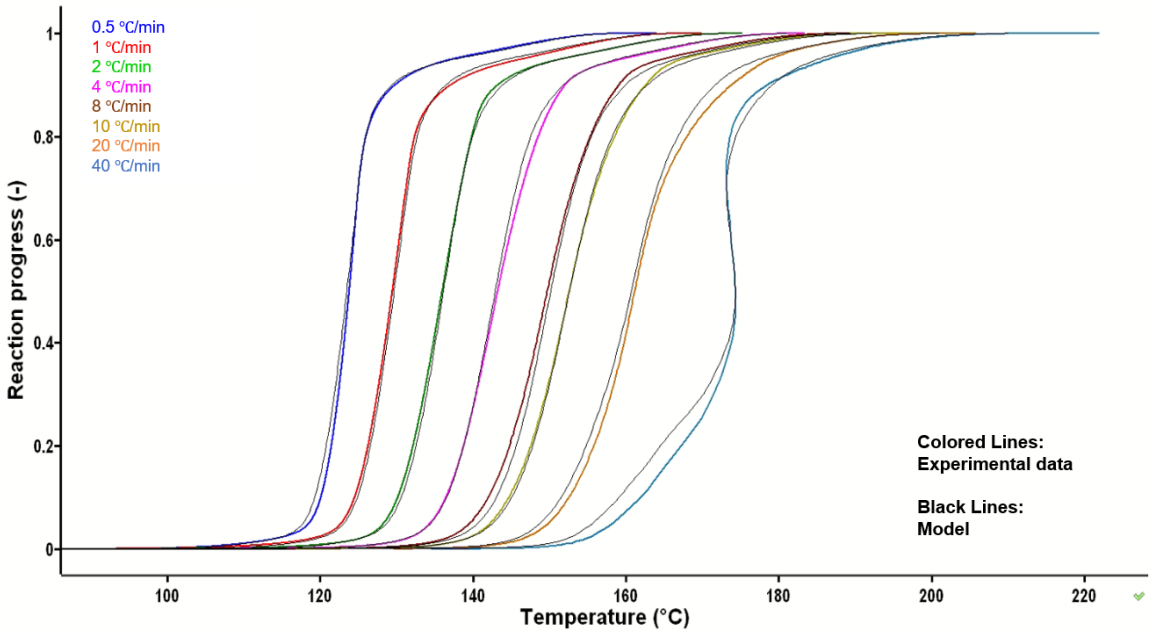

Figure 3.15 Measured and modeled reaction progress curves for the extracted resin

The average correlation coefficient R is equal to 0.99426 for both the reaction rate and the reaction progress, which means that the model prediction is very close to the experimental data. Therefore, the model is appropriate to describe the curing behavior of the extracted resin.

The reaction rates of the extracted resin under isothermal condition at 110°C, 120°C, 130°C, 140°C, 150°C and 160°C are also predicted by the model, which is shown in Figure 3.16.

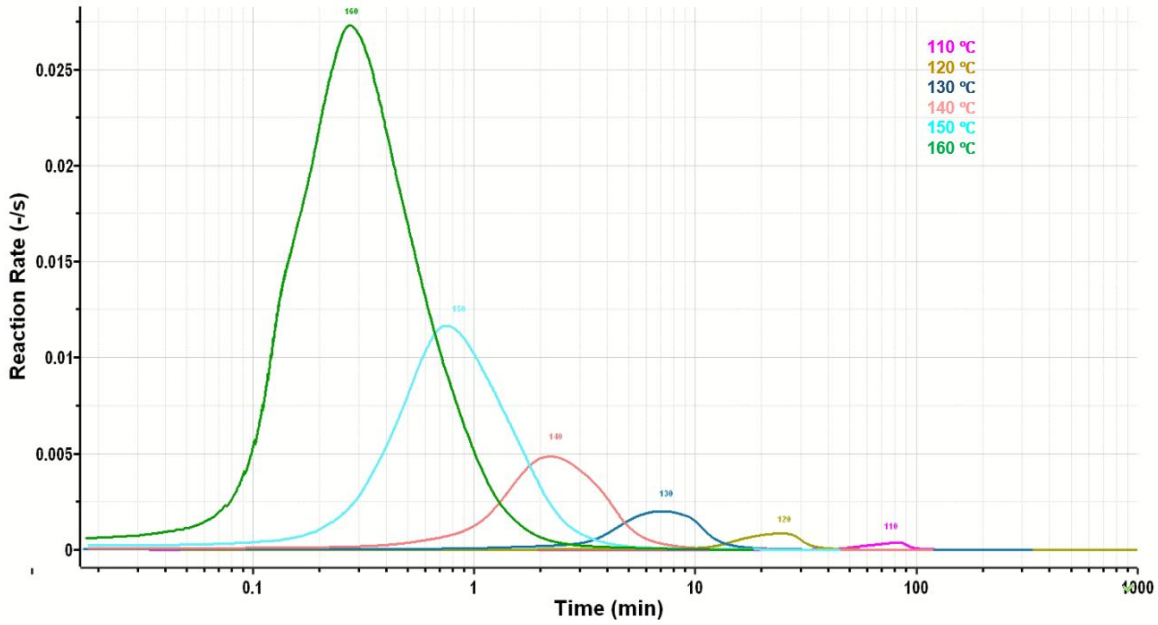

Figure 3.16 Predicted reaction rate curves for the extracted resin under isothermal condition

3.2.3 Cure Kinetics of CF-SMC

In order to study the influence of the carbon fibers on the cure kinetics of the material, the curing behavior of the CF-SMC prepreg needs to be compared to the curing of the extracted resin. Therefore, the curing behavior of the CF-SMC prepreg was also studied by DSC. This section reveals that large variations were observed in the heat of cure of the samples from experiment to experiment, which is expected due to the fact that the resin mass fractions are different in the samples. As a result, the generated cure kinetics model is not accurate enough to describe the curing behavior of the CF-SMC prepreg.

3.2.3.1 Experimental Method

The cure kinetics of CF-SMC prepreg was studied using a DSC 250 from TA Instruments. Dynamic experiments with heating rate of 0.5, 1, 2, 8, 10, 20 and 40 °C/min over a temperature range of 20°C to 260°C were carried out. One repetition test was performed for each testing condition.

3.2.3.2 Cure Kinetics Model

The dynamic experimental data is imported into AKTS-TK software for analysis. The analyzing method is still the differential isoconversional method of Friedman, the same as the one for the neat resin and the extracted resin. Therefore, it is not repeated here and only the results are shown as followed.

The kinetics parameters E_α and A'_α as a function of reaction progress α are presented in Figure 3.17.

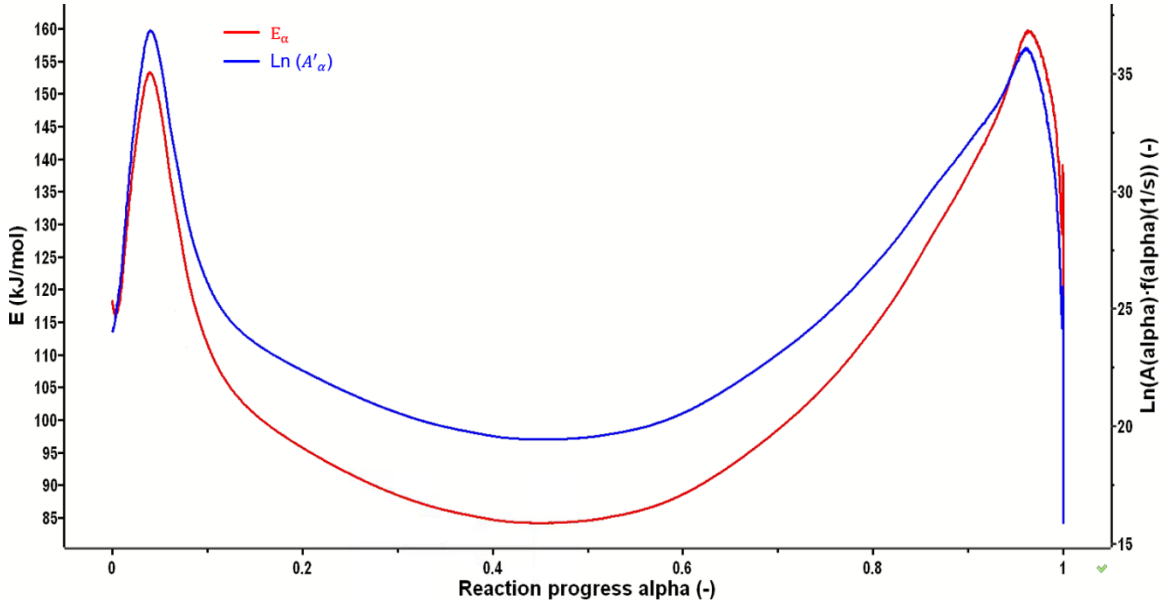

Figure 3.17 Activation energy E_α and modified pre-exponential factor A'_α as a function of reaction progress α for the CF-SMC prepreg

Figure 3.18 shows the modeled reaction rate plotted against the experimental reaction rate under different temperature scanning conditions for the CF-SMC prepreg.

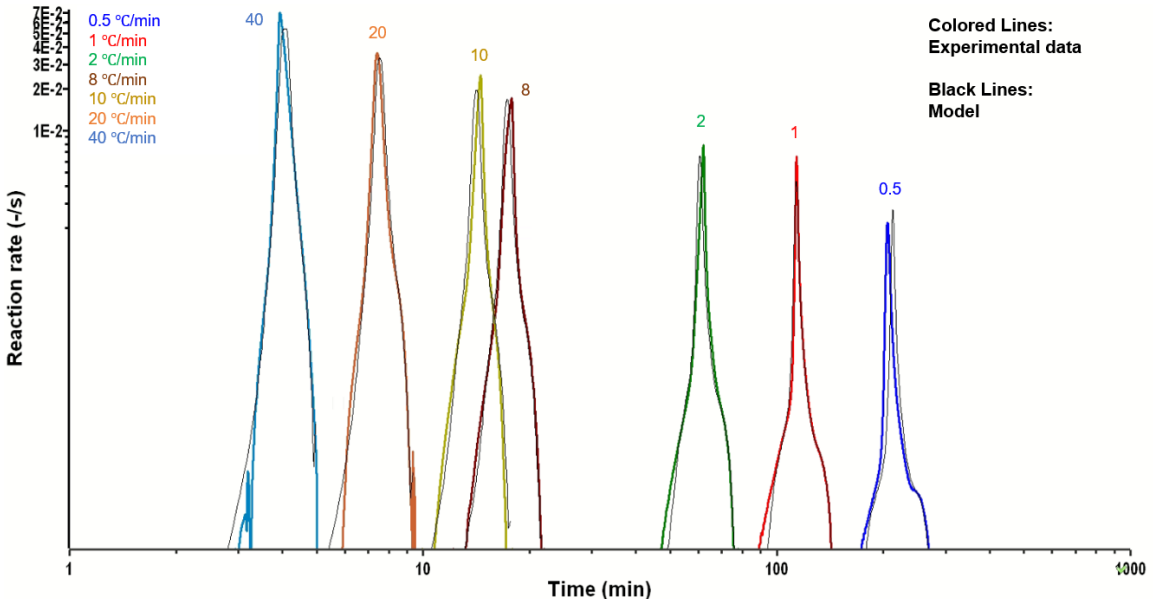

Figure 3.18 Measured and modeled reaction rate curves for the CF-SMC prepreg

The simulated reaction progress is plotted against the experimental data for the different heating rates in Figure 3.19.

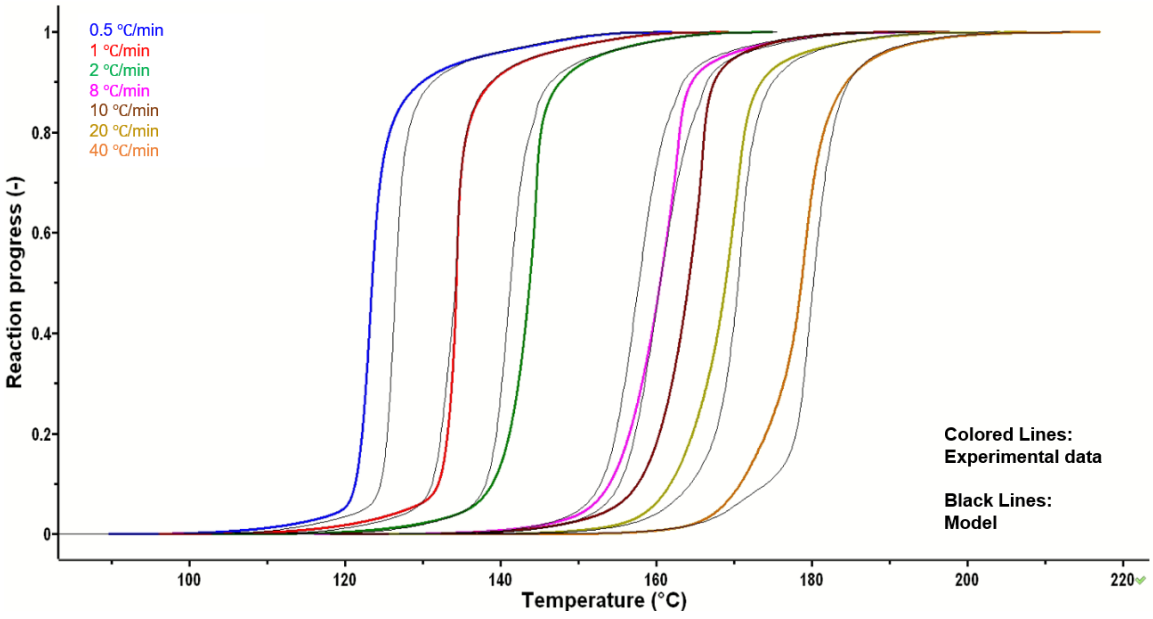

Figure 3.19 Measured and modeled reaction progress curves for the CF-SMC prepreg

It is obvious that the model does not coincide with the experimental data very well. For both the reaction rate and the reaction progress curves, the average correlation coefficient

R is equal to 0.97401, which is less than 0.99, meaning this is not a good fit. Hence, the analysis failed to generate an accurate model from the experimental data for the CF-SMC prepreg.

This failure is not caused by the isoconversional method itself. However, it is caused by the nature of the CF-SMC material. The carbon fibers in this prepreg are randomly oriented and positioned. Therefore, the CF-SMC samples used for the DSC tests contain different resin mass contents and variation in terms of chemical composition across prepreg roll width, which promotes spatial variations in the measured heat of cure. Figure 3.20 shows the reaction heat of each dynamic test. The average reaction heat is 170.623 J/g, however, the standard deviation of the reaction heats determined at all heating rates exceeds 10%. This influences the course of reaction progress - temperature dependence and results in improper kinetic data during the analysis. It is the main reason why no accurate model can be generated from this set of experimental data.

Figure 3.20 The reaction heats determined at all heating rates for the CF-SMC prepreg

3.2.4 Comparison and Conclusion

The curing behavior of the neat resin is compared to the curing behavior of the extracted resin, with the purpose of studying the influence of the inhibitor (which is present in the extracted resin and CF-SMC) on the cure kinetics.

In order to study the impact of the carbon fibers on the cure kinetics, the curing behavior of the extracted resin is compared to the one of the CF-SMC.

Values of the total enthalpy, for the neat resin, extracted resin and CF-SMC, at different heating rates are summarized in Table 3-1.

Table 3-1 The total enthalpy as a function of heating rate

Heating Rate (°C/min)	Neat Resin (J/g)	Extracted Resin (J/g)	CF-SMC (J/g)
0.5	283.81	307.59	199.16
1	272.75	297.32	197.70
2	256.52	307.77	153.08
8	266.19	319.58	159.97
10	297.67	321.91	146.47
20	271.53	309.17	172.59
40	270.08	301.30	165.39
		Average	
	275.54	307.70	170.62

The time required to reach the reaction rate peak (time_p) at every heating rate for the neat resin, extracted resin and CF-SMC is summarized in Figure 3.21. As expected, the time required to reach the peak is found to decrease with increasing heating rate for all the three materials.

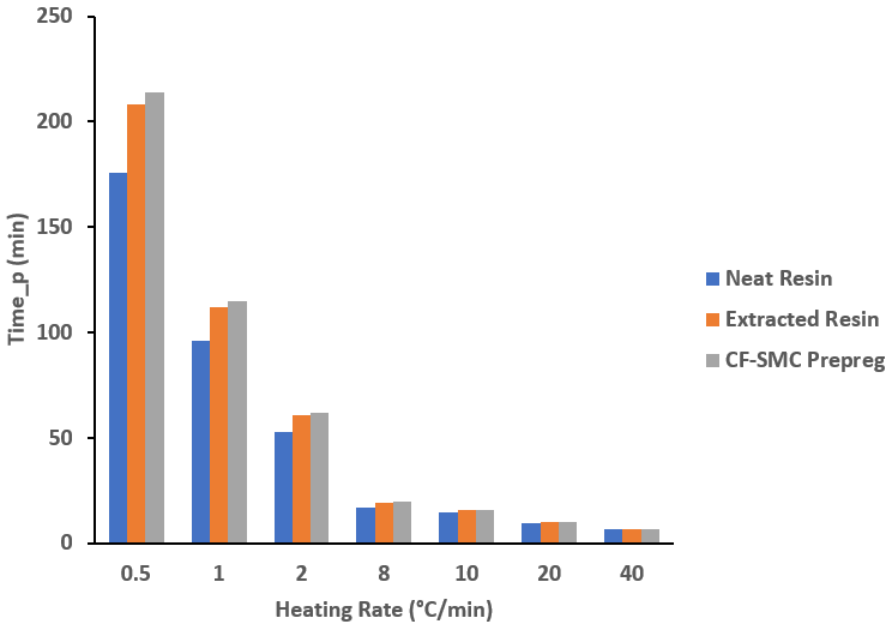

Figure 3.21 Time required to reach reaction rate peak at different heating rates for neat resin, extracted resin and CF-SMC prepreg

Influence of the inhibitor:

As is shown in Table 3-1, the total enthalpy of the extracted resin is about 11% higher than the neat resin. The reason for it will be studied in future work.

It is clear to see from Figure 3.21 that at a given heating rate, it takes longer for the extracted resin to reach the reaction rate peak than the neat resin and the difference is more obvious at lower heating rates. Inhibitor is used to prevent measurable and undesirable resin ageing and curing prior to its planned thermal processing. They act as cure inhibitor by trapping the first free radicals of the resin, until they are consumed. That could be the reason why it takes longer for the extracted resin to cure than the neat resin.

Influence of the carbon fibers:

From Table 3-1, it could be seen that the total enthalpy of curing reaction of the CF-SMC is around 44% less than the extracted resin. It appears that the carbon fibers act as a heat sink, which reduces the total exotherm.

Figure 3.21 shows that it takes a little longer for the CF-SMC to cure, compared to the extracted resin and the difference is also bigger at lower heating rates, namely less than 10°

C/min. It is possible that the presence of carbon fibers plays a role in restricting the molecular mobility of the reactive species, thus decreasing the overall number of chemical reactions.

Recommendations for compression molding process:

Since no accurate cure kinetics model was generated for the CF-SMC prepreg, the model for extracted resin is used instead in the compression molding simulation in Chapter 5.

The cure kinetics model also provides useful information for the compression molding process parameters. The reaction progress at different isothermal temperatures are predicted by the model, which is shown in Figure 3.22. During compression molding process, the material needs to reach a high degree of cure (about 0.9) in the mold. As could be seen in Figure 3.22, at a lower isothermal temperature (below 120°C), it takes more than 30 minutes for the reaction progress to reach 0.9, which is not applicable for high-volume automotive manufacturing. At a higher temperature (above 150°C), it takes less than 2 minutes to reach 0.9 degree of cure. This is too fast and unrealistic for real-life operations. At 140°C, it takes about 4 minutes for the degree of cure to reach 0.9, which is a suitable time frame for SMC compression molding process. Therefore, molding temperature around 140°C is recommended for this CF-SMC in automotive applications.

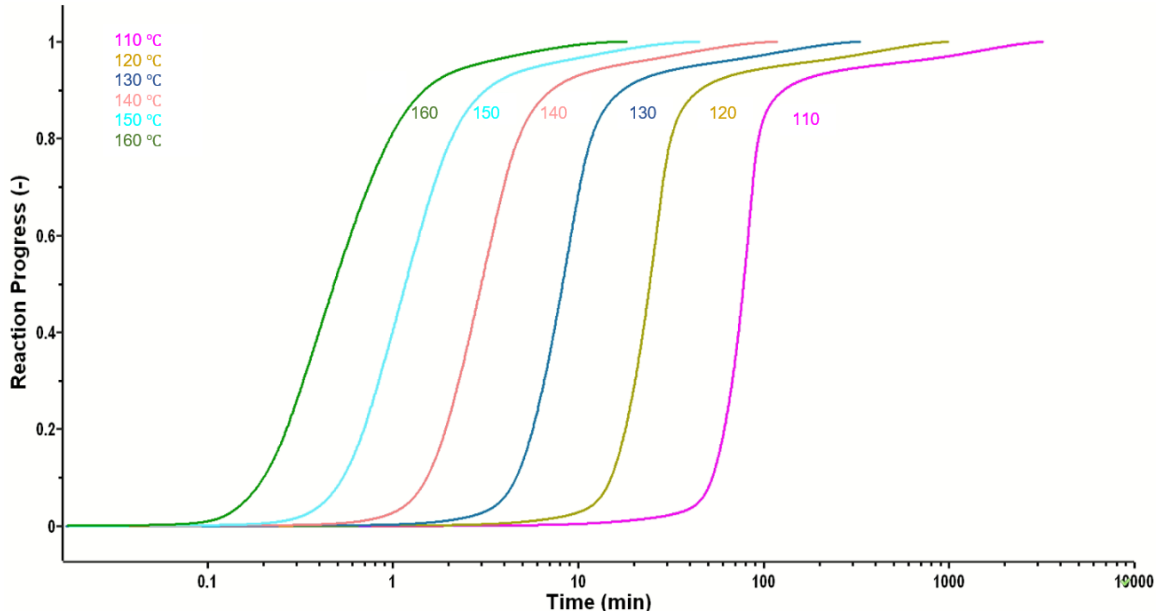

Figure 3.22 Prediction of reaction progress at different isothermal temperatures

3.3 Gelation and Viscosity

From a manufacturing standpoint, the knowledge of the resin gelation timing (gel point) is of crucial importance. During the SMC compression molding process, the material must completely fill the mold before the gel point since it is not able to flow after this irreversible event.

This section studies the gelation and viscosity of the neat resin, extracted resin and CF-SMC prepreg, using a rheometer. The influences of the inhibitor and the fibers on the gelation and viscosity are also studied. This section also proposes a simple gelation model and a viscosity model for the extracted resin. Comparison of the models with experimental data shows good agreement. The cure kinetics and the viscosity/gelation models are uncoupled and they can be used and implemented independently to simulate the flow-compression stage and the curing stage of these material systems.

3.3.1 Experimental Method

An Anton Paar MCR302 rheometer with convection temperature device (CTD) is used to study the gelation and viscosity of the neat resin, extracted resin and CF-SMC prepreg, with parallel plate fixture. The CTD is used to control the experiment temperatures. Parallel plates with diameter of 25 mm are used for the neat resin and the extracted resin. Since the fiber length is about 25.4 mm (>25 mm diameter), parallel plates with diameter of 50 mm are used for the CF-SMC in order to accommodate the length of the fibers and have a sample size bigger than its minimum representative elementary volume.

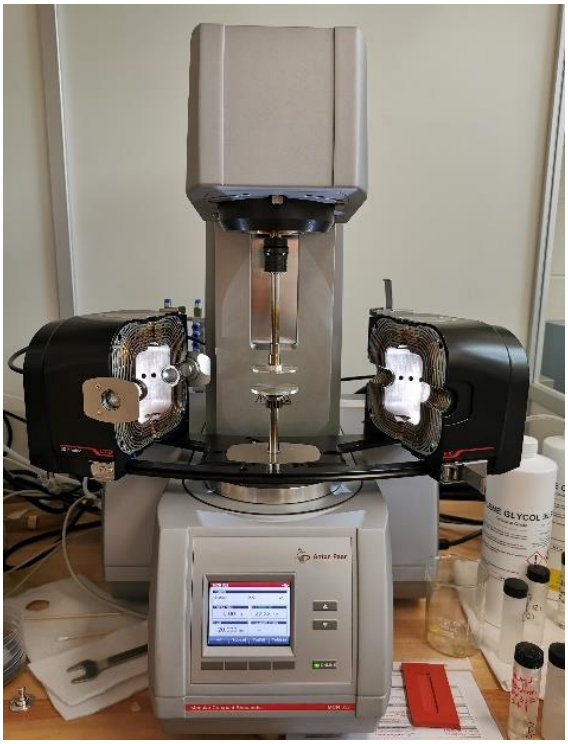

Figure 3.23 Anton Paar MCR 302 with parallel plates fixture

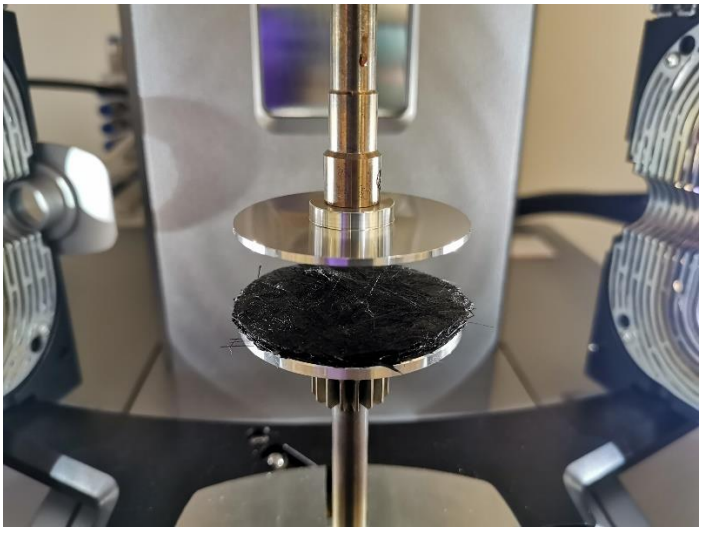

Figure 3.24 Loading CF-SMC prepreg onto the plate

Before experiments, samples are taken out of the freezer 30 minutes earlier to get thawed. The bottles of the two resins/the bag of the CF-SMC are not opened until the materials are totally thawed to avoid moisture contamination from lab environment.

Dynamic scans with heating rates of 3°C/min, 2°C/min, 1°C/min, starting from 25°C were conducted for all the three material systems. Isothermal tests at 80, 82.5, 85, 87.5, 90°C were carried out for the neat resin. Isothermal tests ranging from 85°C to 100°C were performed for the extracted resin. The isothermal tests under 85°C were not performed for the extracted resin because it takes too long for the extracted resin to gel at these temperatures, unlike the neat resin. Isothermal scans ranging from 70°C to 120°C were conducted for the CF-SMC prepreg in order to find their corresponding gel points.

Preliminary method development tests - strain sweep tests were performed to study the linear viscoelastic range (LVE range), for the purpose of choosing a proper strain amplitude for each material system. From the strain sweep test results, it is found that strain amplitude of 5% is suitable for the neat resin and the extracted resin. However, strain amplitude of 0.2% is rather appropriate for the CF-SMC prepreg as a result of the presence of stiff carbon fibers.

Therefore, dynamic and isothermal scans were performed at 5% strain amplitude and 10rad/s frequency to track the evolution of viscosity for the neat resin and the extracted resin. Dynamic and isothermal scans with strain amplitude of 0.2% and frequency of 6.28rad/s (1Hz) were carried out for the CF-SMC. One repetition test was performed for each testing condition.

3.3.2 Experimental Results

Dynamic Experiments:

Dynamic scans with heating rates of 3°C/min, 2°C/min and 1°C/min were carried out for the neat resin, extracted resin and CF-SMC prepreg.

The gel point determination criteria need to be studied and chosen for each material system.

For the neat resin, the storage modulus G' is always bigger than the loss modulus G'' after stabilization during the temperature scanning test, as can be seen in Figure 3.25. Therefore, the cross-over point of G' and G'' [54] cannot be used as the criterion to determine the gel

point in this case. However, the complex viscosity builds up sharply around 30 minutes in the graph. Hence, the rapid relative increase in viscosity could qualify as a "processing" gel point for this material system, namely a state under which the polymer cannot flow anymore for all practical purpose. [48]

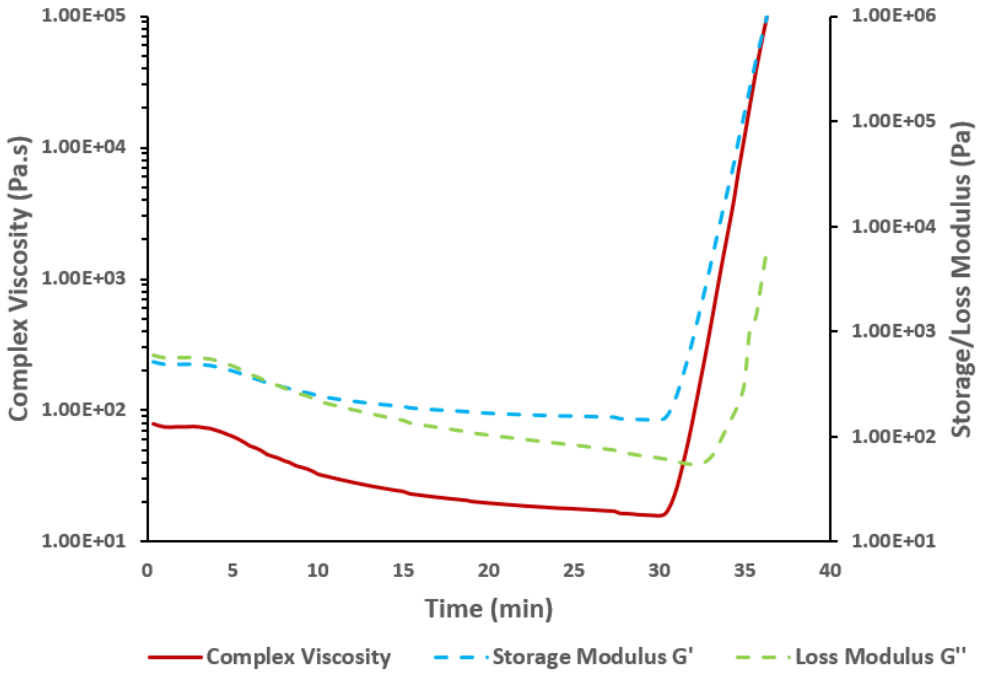

Figure 3.25 Dynamic scan with heating rate of 3°C/min for the neat resin

In terms of the extracted resin, the storage modulus G' is smaller than the loss modulus G'' at the beginning, which is shown in Figure 3.26. However, at one point, G' becomes larger than G''. Therefore, the cross-over point of G' and G'' is used as the indication of gelation for the extracted resin. The cross-over point appears to coincide with the sharp build-up of the complex viscosity, thus the rapid relative increase in viscosity would again be an appropriate criterion in this context.

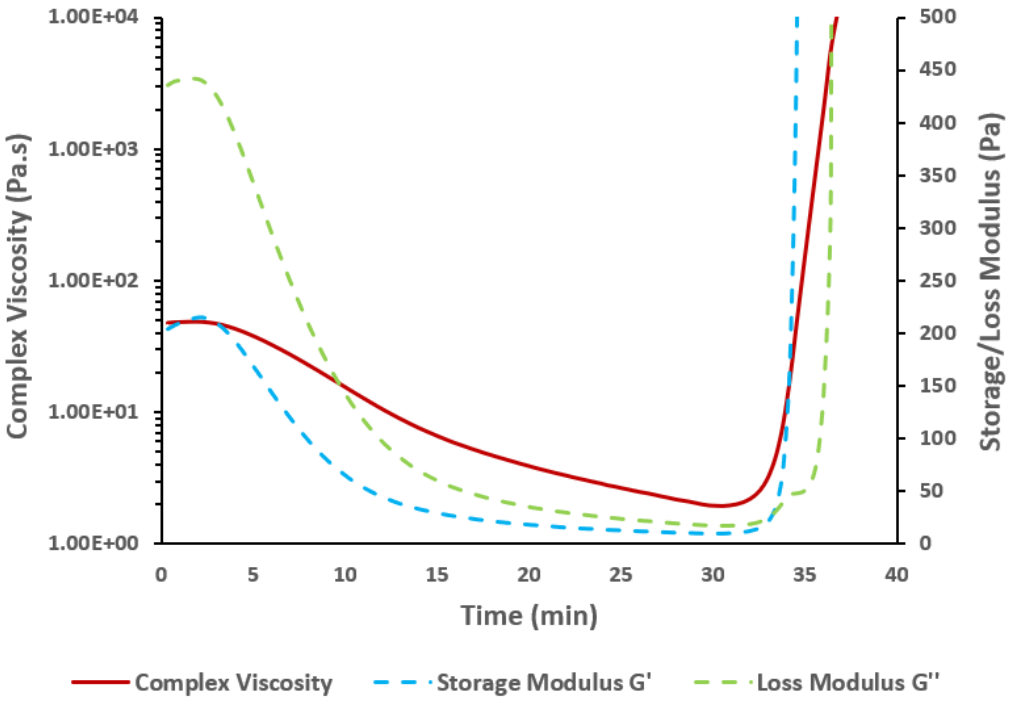

Figure 3.26 Dynamic scan with heating rate of 3°C/min for the extracted resin

For the CF-SMC prepreg, the sharp increase in complex viscosity is used to determine the gel point since G' is always bigger than G'' throughout the test, as shown in Figure 3.27.

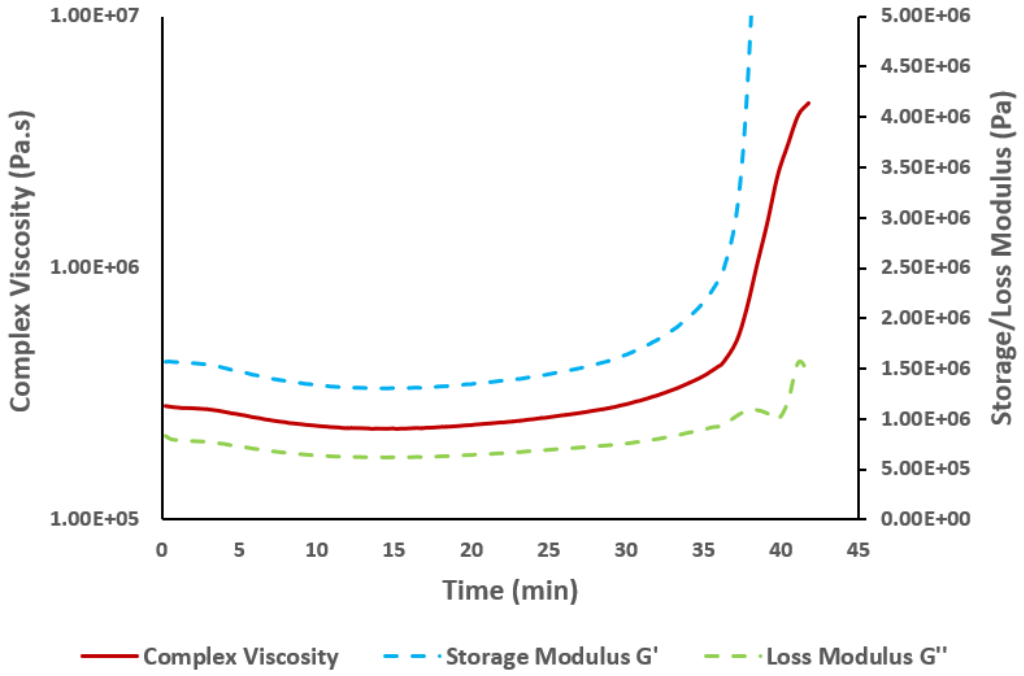

Figure 3.27 Dynamic scan with heating rate of 3°C/min for the CF-SMC prepreg

All the dynamic scanning test results for the neat resin, extracted resin and CF-SMC prepreg are summarized in Figure 3.28. The initial complex viscosities of the neat resin and the extracted resin are close to each other, which is around 80 Pa·s. The initial complex viscosity of the CF-SMC is much bigger than the two resins (which is about 2E+05 Pa·s) because of the presence of the stiff carbon fibers. For all three material systems, the viscosity drops at the beginning of the test due to the increase in thermal mobility of chains, and it builds up rapidly at gelation and subsequently.

It can be seen from Figure 3.28 that a higher heating rate results in an earlier gelation for all three material systems.

Under the same heating rate condition, it takes longer for the extracted resin to gel than the neat resin, comparing their viscosity curves. Since the only difference between the two resin systems is the presence of inhibitor in the extracted resin with respect to the neat resin, it arises logically that the presence of the inhibitor delays the resin gelation.

The complex viscosity curve of the CF-SMC is compared to the curve of the extracted resin, in an attempt to study the influence of the carbon fibers on the gelation. At the same heating rate, the gel point of the CF-SMC appears later than the extracted resin, which indicates that the fibers play a role in delaying the gelation. Besides, the impact of delaying is more and more obvious as the heating rate decreases. The specific reason why the carbon fibers have this impact on the gelation is still unknown and needs to be studied in future work.

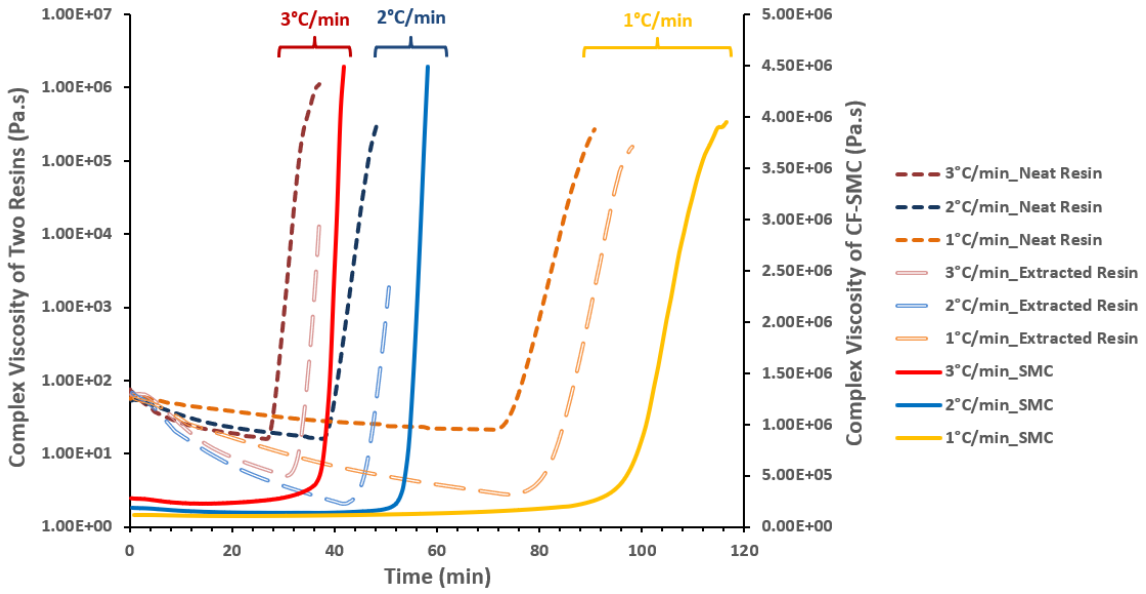

Figure 3.28 Summary of the dynamic scans for the neat resin, extracted resin and CF-SMC prepreg

Isothermal Experiments:

Isothermal scans were performed for the neat resin, extracted resin and CF-SMC prepreg.

The gel point determination criteria are the same for the neat resin and the extracted resin. To be specific, the rapid relative increase in viscosity is seen as the gel point for the neat resin while the cross-over point of G' and G'' is used for the extracted resin.

However, it was difficult to determine the gel point of the CF-SMC under isothermal conditions. Figure 3.29 shows two examples of the isothermal tests which were carried out on the CF-SMC prepreg. As can be seen from the figure, the viscosity change throughout

the experiment is not as pronounced as the one in dynamic test. There is no sharp viscosity build up which could be seen as the indication of gelation. Besides, G' curve is always above G'' curve so the cross-over point of G' and G'' cannot be used.

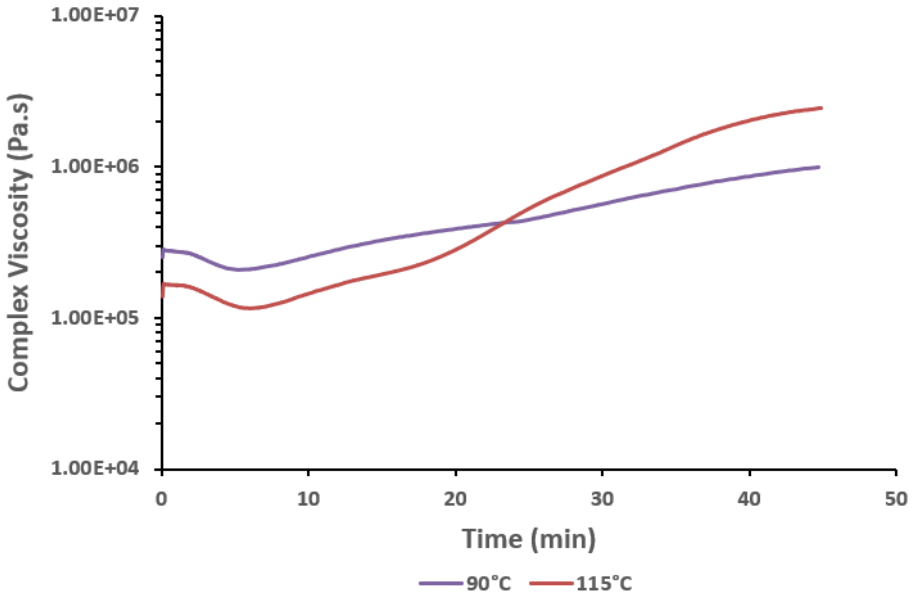

Figure 3.29 Isothermal tests at 90°C and 115°C for the CF-SMC prepreg

Another testing method (still using the same rheometer) is utilized in an effort to determine the gel point of CF-SMC, which are multiwave tests. A compound waveform allows the sample to be exposed simultaneously to multiple frequencies. Gel point can be determined as the point where the loss factor $tan\delta = G''/G'$ is independent of frequency [49, 51]. Multiwave tests at 105, 110, 115, 120°C isothermal conditions were performed for the CF-SMC. Three to four repetitions were carried out at each temperature condition.

Only one good result was obtained from all the multiwave experiments, which is shown in Figure 3.30. Loss factors $tan\delta$ at three different frequencies are plotted versus time. The intersection of the three curves is the point where $tan\delta$ is independent of frequency, which is the gel point. However, no consistent results could be obtained from the repetition tests. In addition, no good result was acquired at the other isothermal temperatures. Therefore, the author failed to obtain the gel points of the CF-SMC under isothermal conditions unfortunately.

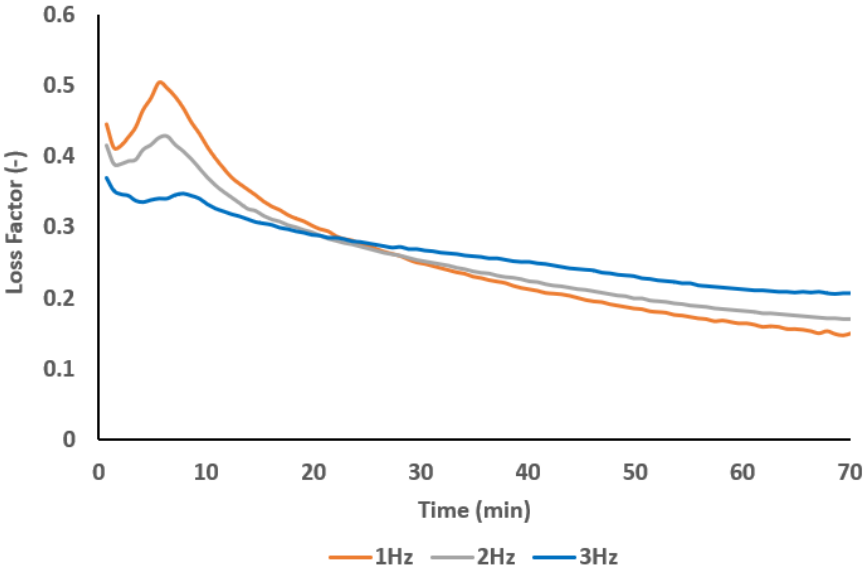

Figure 3.30 Multiwave test at 105°C for the CF-SMC

The gel times of the neat resin and the extracted resin under isothermal conditions are summarized in Table 3-2.

Table 3-2 Gel times of the neat resin and extracted resin under isothermal condition

Isothermal Temperature (°C)	Neat Resin Gel Time (min)	Extracted Resin Gel Time (min)
80	85.3	N/A
82.5	63.8	N/A
85	44.8	99.5
87.5	27.5	75.4
90	21.5	55.5
92.5	N/A	41.2
95	N/A	31.2

As is shown in the table, a small change of 2.5°C in isothermal temperature can cause a big change in the gel time for both resins. Therefore, the gel time of the resins is highly sensitive to temperature.

Comparing the gel times of the two resins at 85, 87.5 and 90°C, it is obvious that it takes much longer for the extracted resin to gel than the neat resin. It is indicated that the inhibitor in the extracted resin has a huge impact on the gel time and it leads to a much slower gelation. This is expected to some extent since inhibitor is used by the manufacturers to extent shelf life in cold storage and prevent early ageing and curing prior to its planned thermal processing.

3.3.3 Gelation Model and Viscosity Model

Since the gel time of the CF-SMC could not be consistently obtained from the experiments as described in the previous section, gelation model and viscosity model are developed for the extracted resin instead, to represent the rheology of the CF-SMC, which constitutes a more conservative identification of the gel point from a processing standpoint.

The free radical polymerization theory of Yang and Suspene [48] was found to be adequate to describe the gelation profile and viscosity evolution of the extracted resin.

Gel Time Model:

A modified version of the gel time (t_{gel}) model proposed by Yang and Suspene [48] was fit to the gel time data obtained from the isothermal experiments, and is shown in Eq. 3.7:

$$\ln(t_{gel}) = A + B\left(\frac{1}{T_{relative}}\right) \tag{3.7}$$

where A and B are fitting parameters and $T_{relative}$ is a relative temperature with respect to a relevant reference temperature. 90°C is chosen to be the reference temperature (T_{ref}, in Kelvin) and $T_{relative} = \frac{T_{ref}}{T} - 1$.

A = 4.0163 and B = 42.419 can enable the model to fit the experimental data, as is shown in Figure 3.31. The coefficient of determination R^2 is equal to 0.98, which indicates a good agreement between the experimental data and the model prediction.

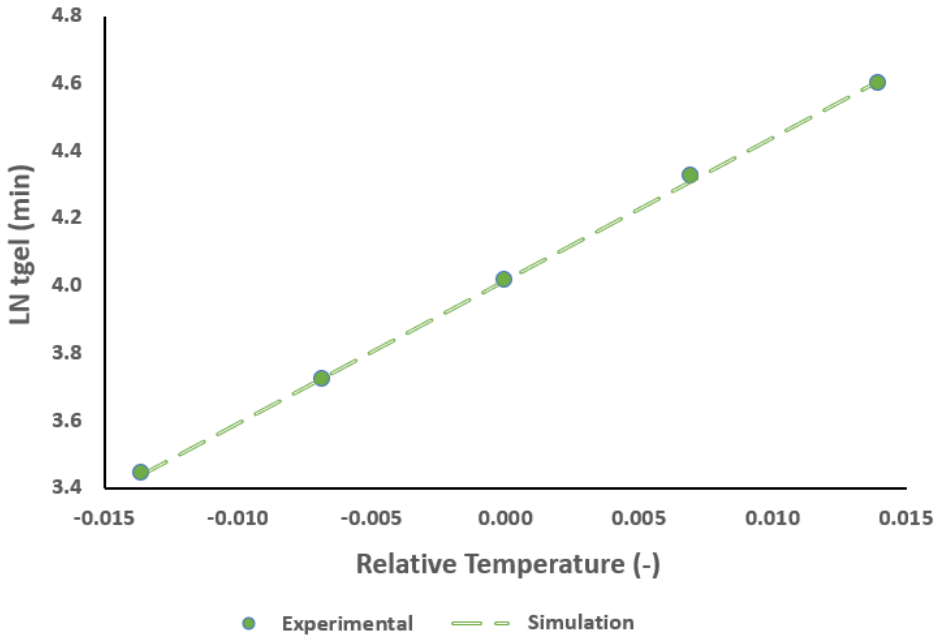

Figure 3.31 Logarithmic gel time versus relative temperature for isothermal scans of the extracted resin

The model is also used to predict the gel time of the extracted resin under dynamic scanning conditions. Comparisons of the prediction results with the experimental data showed good agreement, which can be seen in Figure 3.32.

Therefore, the gel time model is proved to be adequate to predict the gel time of the extracted resin at any temperature profile.

Temperature ramp [°C/min]	Experimental gel time [min]	Gel time prediction by model [min]
3	33.5	34.6
3	33.4	34.2
2	47.1	47.5
2	47.1	47.5
1	85.7	85.7
1	84.8	85.6

Figure 3.32 Measured and predicted gel time for the extracted resin under dynamic conditions

Viscosity Model:

Logarithm form of relative viscosity η_r (instantaneous viscosity/initial viscosity: $\frac{\eta}{\eta_0}$) is plotted versus reduced time (t/t_{gel}), as shown in Figure 3.33. All results are falling on a master curve which can be classified into three straight lines. The relative viscosity can be expressed by three viscosity evolution stages as follows.

(1) When t/t_{gel} ≤ 0.85,

$$\ln \eta_r = 0.0523 + 1.3735 \left(\frac{t}{t_{gel}}\right)$$

(2) When 0.85 < t/t_{gel} ≤1,

$$\ln \eta_r = -2.8594 + 4.798 \left(\frac{t}{t_{gel}}\right)$$

(3) When t/t_{gel} > 1,

$$\ln \eta_r = -5.75 + 7.6648 \left(\frac{t}{t_{gel}}\right)$$

Knowing the initial viscosity of the extracted resin and the simulated gel time from the gel time model, the system viscosity during the process can be predicted by the three equations.

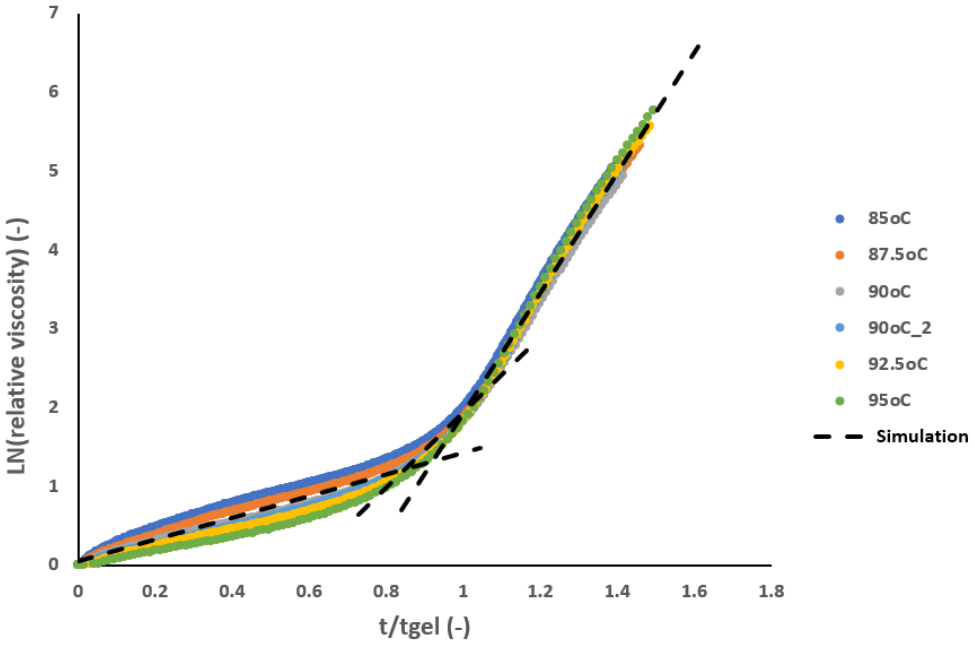

Figure 3.33 Logarithmic relative viscosity versus reduced time for the extracted resin

The experimental viscosity evolution curves are plotted against the model predictions in Figure 3.34. The comparison shows reasonably good agreement, which indicates that the viscosity model works well for the extracted resin.

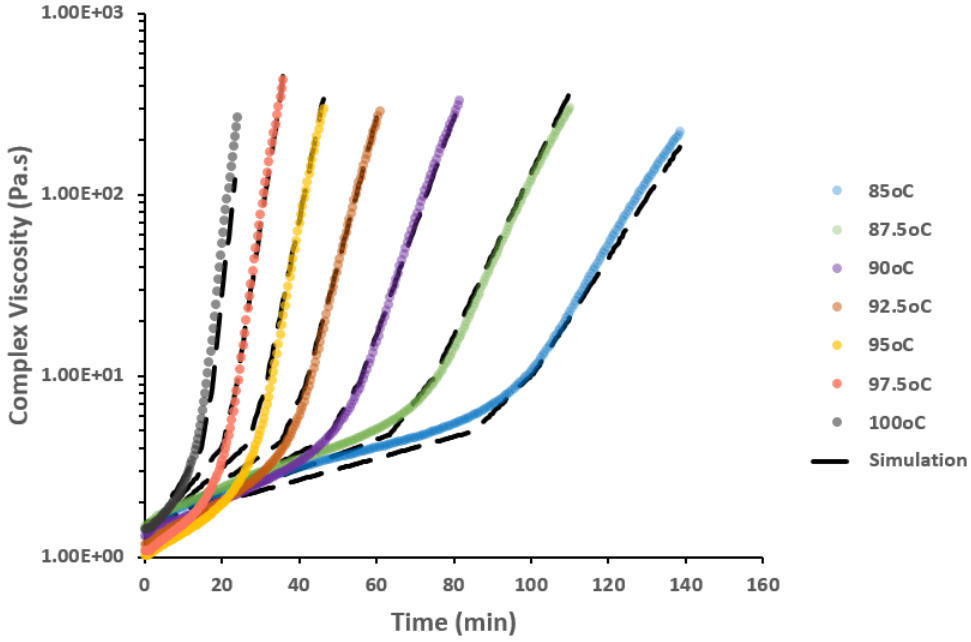

Figure 3.34 Measured and predicted viscosity curves for the extracted resin

3.3.4 Conclusion

Gelation and viscosity of the neat resin, extracted resin and CF-SMC were studied under both dynamic and isothermal temperature conditions using oscillatory rheometry. Gel point determination criteria were defined for each of the material, except that gel point could not be obtained for the CF-SMC under isothermal conditions.

The inhibitor was found to have a huge impact on the gel time, which is delaying the gelation to a great extent.

Gel time model and viscosity model were developed for the extracted resin. Comparisons of the simulation results with the experimental data showed good agreement. Since technical roadblocks appeared when determining consistent gel points for the CF-SMC, no

model can be developed for the CF-SMC. Hence, the models for the extracted resin will be used to represent the gelation and viscosity evolution of the CF-SMC in the compression molding simulation in Chapter 5.

Chapter 4. Flow-Compaction Test

A one-dimensional flow-compaction testing apparatus was designed to study the CF-SMC prepreg flow under several testing conditions, namely at different temperatures and mould closure rates, based on the work of Smith and Hubert [4]. The test fixture was mounted on an MTS Landmark servohydraulic testing system. The length, width and thickness of each SMC prepreg specimens before and after their compression trials were measured. Correlations with these sample attributes are studied to better understand the material flow characteristics during compression moulding.

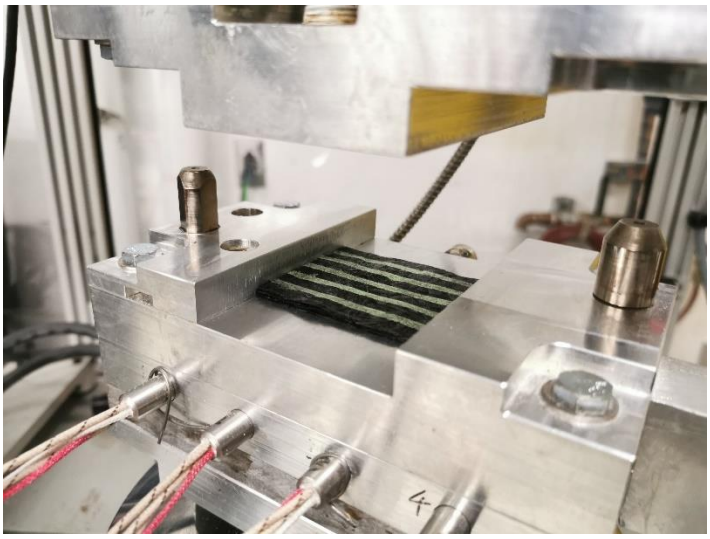

Figure 4.1 One-dimensional flow-compaction test

4.1 Testing Setup

The flow compaction test jig was designed using a computer aided design (CAD) software package – CATIA V5. The whole assembly consists of two main parts: the upper piston part and the bottom molding cavity part which have sliding fit tolerance to prevent material infiltration along the cavity walls. The upper piston part includes a grip plate, an insulation plate, a heating plate and a piston plate (from top to bottom in Figure 4.2). The bottom molding part includes a molding cavity plate, a heating plate, an insulation plate and a grip plate (from top to bottom).

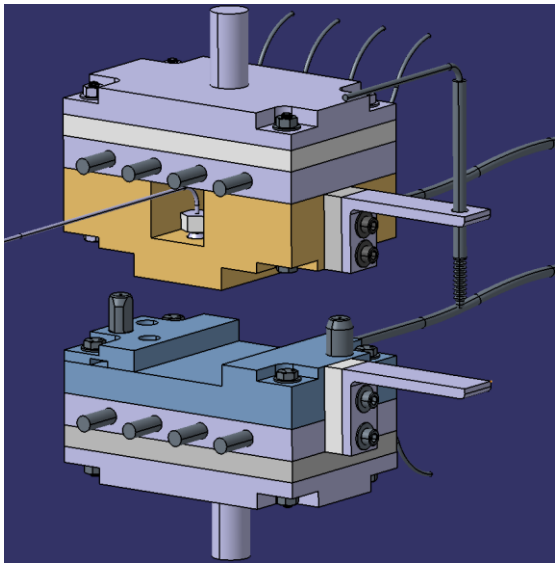

Figure 4.2 CAD of the flow-compaction test jig

The insulation plates are made from mica muscovite for its low heat conductivity, so that it can protect the MTS hydraulic grippers from high temperatures. Aluminum was chosen to be the material of the other parts and the parts were manufactured by a machine shop. The final manufactured test jig is shown in Figure 4.3.

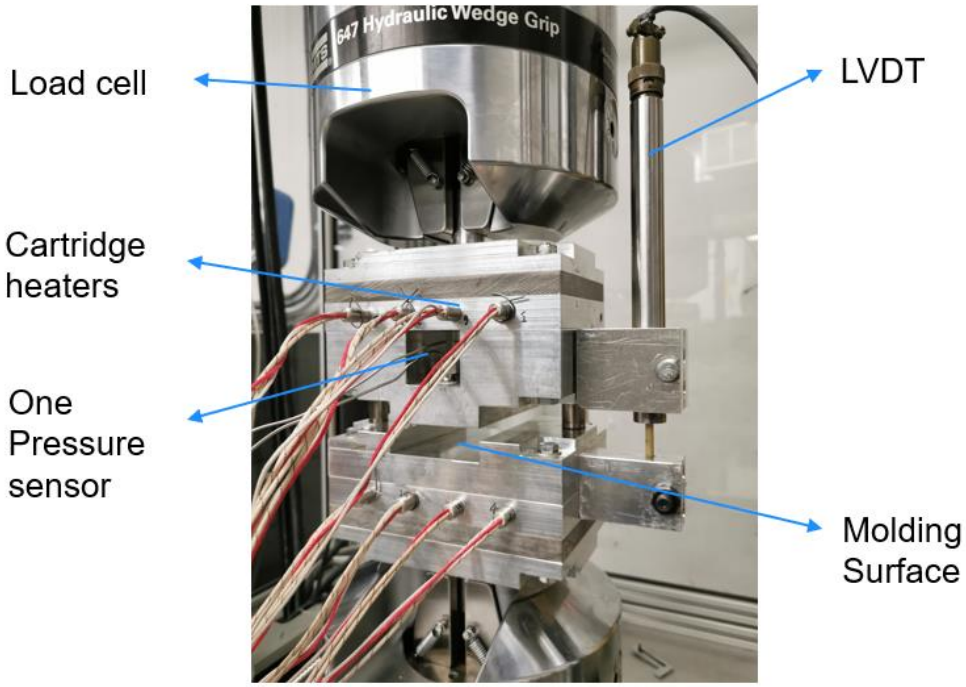

Figure 4.3 Flow-compaction test jig

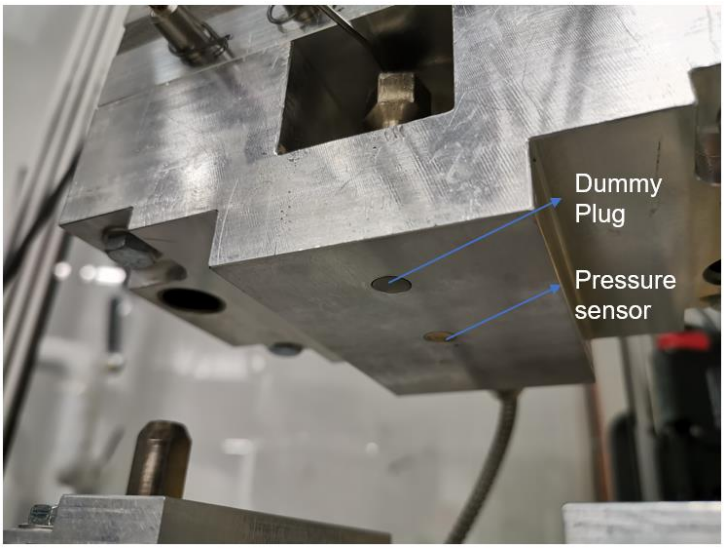

Figure 4.4 Location of the pressure sensor and dummy plug

The test jig consists of the following features:

(1) A 2.5inch (63.5 mm) wide molding area to accommodate the length of the carbon fibers (25.4 mm).

(2) Two dowel pins to assist the alignment of the upper and bottom jig.

(3) 8 cartridge heaters (4 in the top heating plate, 4 in the bottom heating plate) are controlled by two ZESTA temperature controllers to heat up the test jig to desired test temperatures. Two type-J thermocouples (one in the upper piston plate, one in the bottom molding plate) provides feedback temperatures to the ZESTA controllers.

(4) One pressure sensor (from Gefran) which is flush mounted in the piston plate is used to obtain pressure data throughout the flow-compaction test. There is another hole which could be used by a second pressure sensor in future work.

(5) A linear variable differential transformer (LVDT) from Hoskin Scientific LTD. Is installed closely to the test jig to obtain precise displacement data.

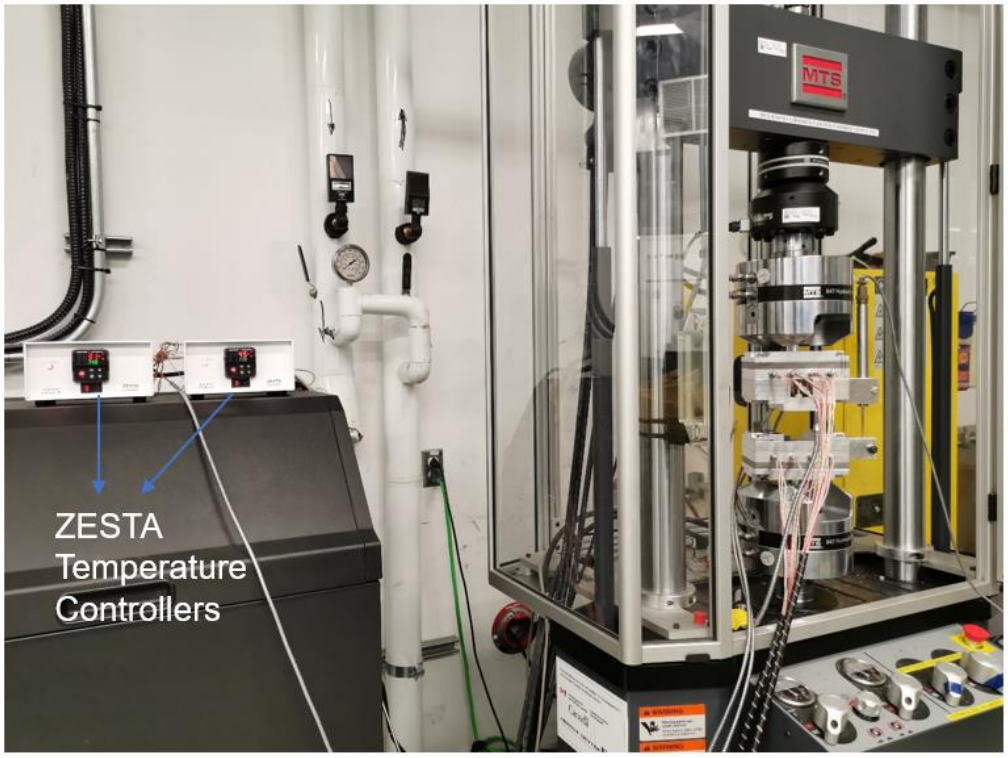

Figure 4.5 The whole setup of the flow-compaction testing apparatus

The test jig is mounted on an MTS 100kN Landmark servohydraulic testing system, as could be seen in Figure 4.5. The MTS system is able to control the displacement rate while measuring the force with the 100kN load cell. However, the LVDT provides more accurate displacement data than the built-in displacement sensor as a result of the thermal expansion and overall compliance of the complete load trail assembly. Therefore, the LVDT is connected to the MTS and get calibrated so that the MTS can precisely control the displacement rate from a sample thickness standpoint using the LVDT.

4.2 Specimen Preconditioning

CF-SMC prepregs were stored in sealed bags in the freezer at -18 °C until needed to preserve the state of the resin and avoid moisture contamination. Thirty minutes before testing, the prepregs were taken out of the freezer and get thawed at room temperature until the sealed bag is free of condensation and no longer cool to the touch.

Specimens were cut to the dimension of 63.5 mm x 50.8 mm. The width of the specimen (63.5 mm) is the same as the width of the molding area so that the flow will be one-dimensional. Since there are a lot of air bulk in the prepregs, every specimen went through a room temperature debulking process. They were placed in a vacuum bag with full vacuum for 10 minutes to remove the air bulk before the test.

The initial thicknesses (9 points across the specimen) after room temperature debulking were measured by a micrometer for every specimen in order to study the impact of the thickness on the flow pattern of the material. The nine areas are shown in Figure 4.6.

Figure 4.6 Thicknesses of the nine areas to be measured

The initial length and width of each specimen were also measured in order to be compared to the final length and width.

A special way to study qualitatively how the material flows spatially during the compression was developed. UV fluorescent powder which are excited under the UV light was spread and pressed onto the surface of the specimen as a flow tracer, using a stencil. Its color contrasts strongly with the prepreg's color and the feasibility of this method was proved by several trials. An example of the specimen with the luminous powder before and after the test is shown in Figure 4.7. As it can be seen from the figure, although the lines of the powder become a little blurry after the test because of the friction between the specimen and the molding surfaces, the tracer lines are still reasonably visible under the UV light and it provides insights on the material flow pattern. Therefore, this method is

retained for the sequel and the powder is applied to every specimen before the test to track the material flow.

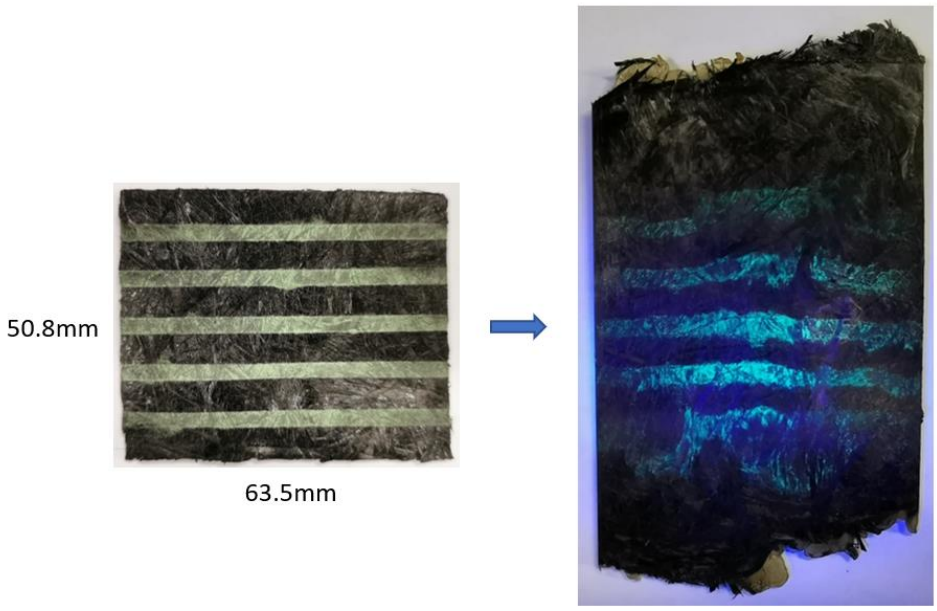

Figure 4.7 Specimen with the luminous powder before and after test

The last step before the test is to take pictures of the specimen so that it can be compared to the after-test specimen.

4.3 Compression Test Procedure

Compression Test Conditions:

Four isothermal temperature: 110°C, 120°C, 130°C and 140°C were chosen based on the results of the cure kinetics study in chapter 3, in order to study the influence of temperature on the flow.

Tests with compression strain rate of 0.6 1/s, 0.7 1/s, 0.8 1/s and 0.9 1/s were performed at each of the isothermal condition. The displacement rate which needs to be input into the MTS controlling software is calculated based on the strain rate. For example, if the average initial thickness of the 9 areas of the specimen is 2 mm and the strain rate is 0.6 1/s, the displacement rate will be the strain rate multiplied by the average initial thickness, which

is 1.2 mm/s. Two repetitions were performed for each testing condition. The relationship between the compression strain rate and the resulting shear strain is studied.

Test Procedure:

A prepared specimen is placed in the channel mold which is preheated to the desired isothermal temperature. The bottom part is risen until the specimen almost touches the upper mold and the position is held constant for a minute to ensure that the specimen reaches the mold temperature. The MTS then applies constant displacement rate loading on the specimen until a compression force of 55kN is reached, at which point it switches to constant force control for the rest of the test.

4.4 Measurement Methodology of In-plane Shear Strain

The final length of each specimen after test needs to be measured for calculating the in-plane shear strain. Since the final specimen has an irregular shape on its two ends (an example is shown in Figure 4.8), it is hard to measure the final length using standard methods, such as a caliper or ruler.

Figure 4.8 Specimen after test

An image processing method through MATLAB is developed to measure the final specimen length (L_f). The general concept of this method is to use pixels to calculate the final length. The detailed procedure is described as follows.

The final specimen is placed next to a sheet with known width and length (63.5 mm x 50.8 mm), and a photo is taken of them from right above, as shown in Figure 4.9. A MATLAB program using photo processing toolbox is developed to convert the photo to greyscale image and then to binary image so that the sheet and the specimen can be easily distinguished from the background. However, due to the reflection on the specimen, some of the specimen pixels are not distinguished from the background in the binary image, as can be seen in Figure 4.10. “Imfill” function is applied to fill all the pixels inside the contour of the specimen.

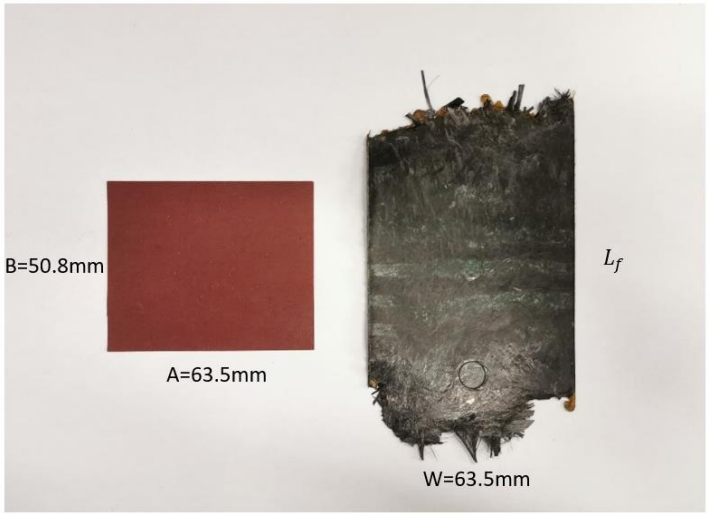

Figure 4.9 A sheet with known size and a specimen after test

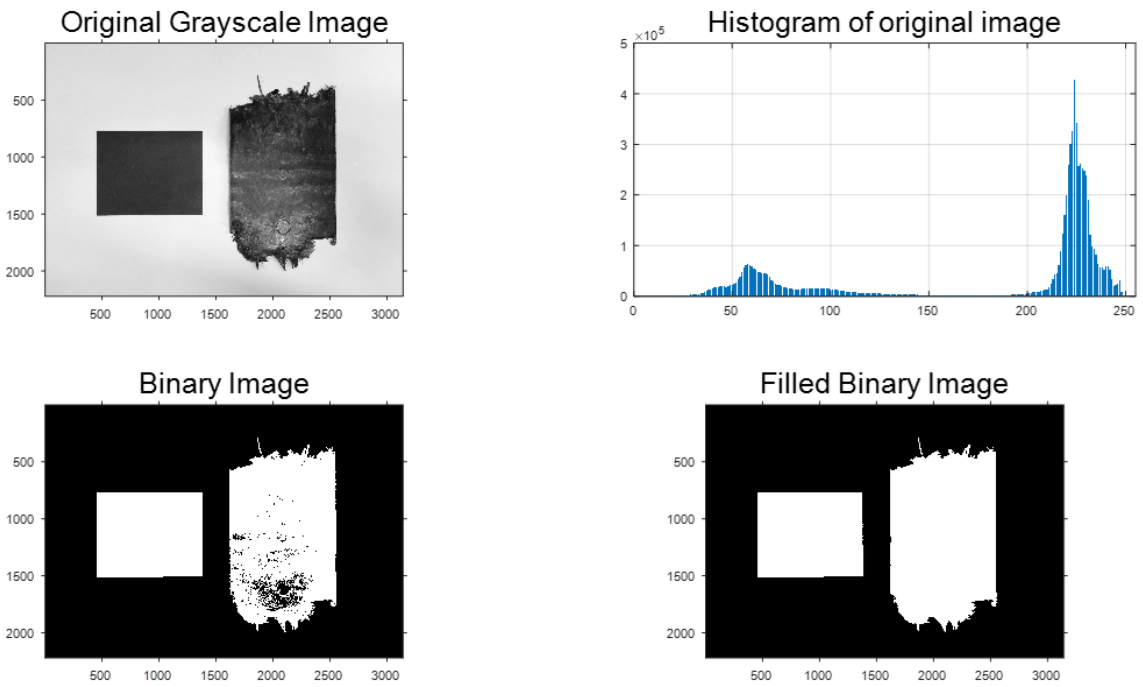

Figure 4.10 Converted images using MATLAB

The program measures the pixels corresponding to the width of the sheet (A=63.5 mm). Thus, the real-life distance of one pixel can be calculated. The area of the specimen in pixels is then measured by the program. It is assumed that there is no flow in the width of the specimen so that the width in pixels of the specimen is the same as the width in pixels of the sheet. Hence, the length in pixels of the specimen can be calculated as

$$length\ in\ pixels = \frac{area\ in\ pixels}{width\ in\ pixels} \tag{4.1}$$

Since the real-life distance of one pixel has been calculated, the final length of the specimen can be calculated using the equation:

$$L_f = length\ in\ pixels\ \times distance\ of\ one\ pixel \tag{4.2}$$

The complete MATLAB codes are provided in APPENDIX A.

The final shear strain of the specimen ($e_x{}^s$) is calculated using the Green strain tensor equation since it includes quadratic terms in addition to the small strain terms, which makes it preferred for large deformations [4]. The equation is shown as follows:

$$e_x{}^s = \frac{1}{2}\left[\left(1 + \frac{L_f - L_0}{L_0}\right)^2 - 1\right] \tag{4.3}$$

where L_0 is the initial length of the specimen.

4.5 Test Results and Discussion

Impact of the compression strain rate and the temperature on the flow:

Tests with four strain rates (0.6, 0.7, 0.8, 0.9 1/s) were carried out at each isothermal temperature (110, 120, 130, 140 °C). Two repetitions were performed for every testing condition. The final specimen lengths were established using the image processing method presented previously and the final in-plane shear strain was calculated using the Green strain tensor equation. The average in-plane shear strain of each testing condition is summarized in Figure 4.11. It shows that among the four strain rates, larger compression strain rates lead to larger final in-plane shear strain, meaning that there is more material flow during the compression. When the compression strain rate is 0.6 1/s, the final in-plane shear strain is small (less than 0.4), which means that there is not much material flow in this condition.

During industrial compression molding of CF-SMC, larger material flow is preferred to fill all the cavity of the mold. Therefore, a strain rate of at least 0.7 1/s is recommended for the automotive application.

In addition, it is also noticed that among the four isothermal temperatures which were tested, the temperature does not appear to have obvious influence on the final shear strain.

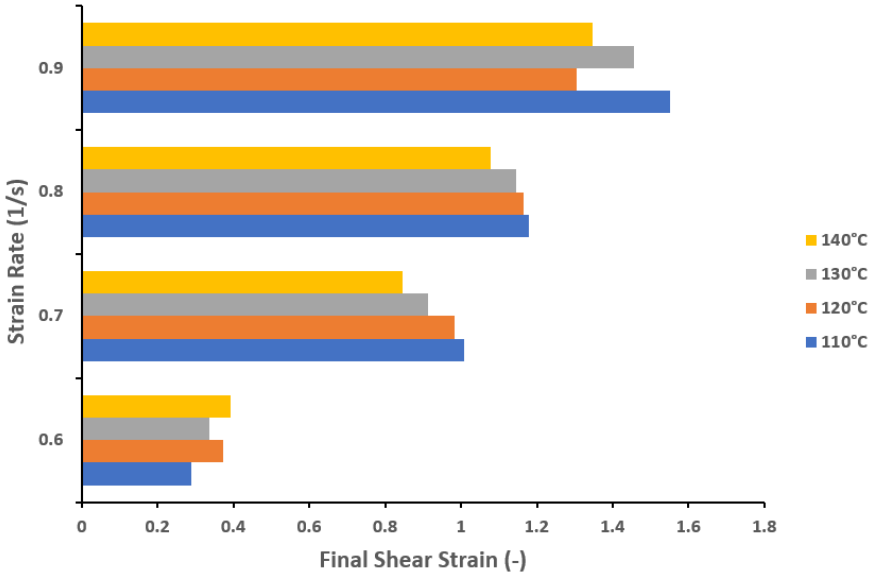

Figure 4.11 Strain rate versus final shear strain under four isothermal conditions

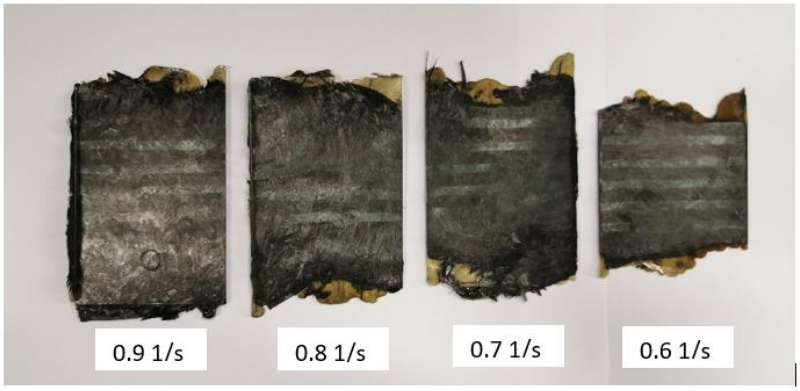

Figure 4.12 Final specimens using different strain rates at 110°C

Impact of the thickness on the flow:

The initial thicknesses of nine locations across the specimens were measured using a micrometer before each test.

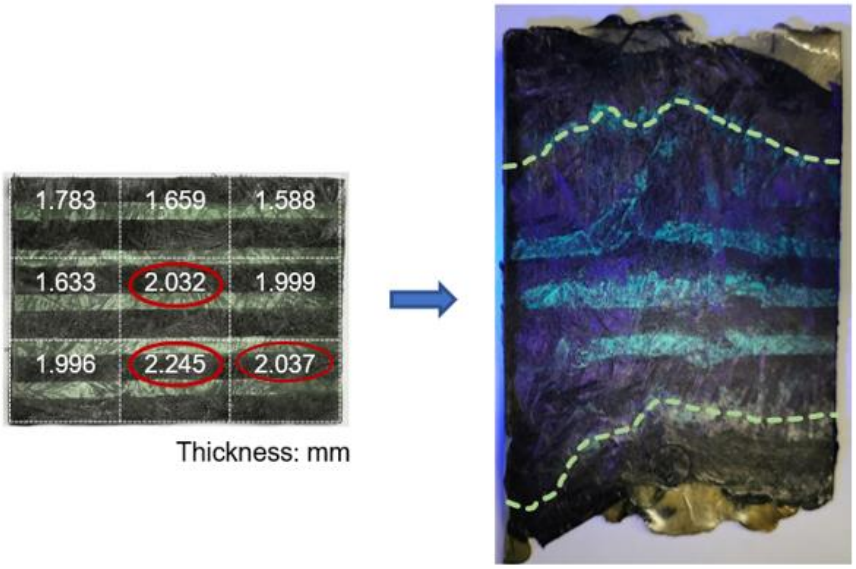

Figure 4.13 Specimen with the luminous powder before and after test

It is observed that the CF-SMC material is preferred to flow to the thinner areas. An example is shown in Figure 4.13. The areas with red circles are the three thickest locations of the specimen. Learning from the tracer lines of the luminous powder under an UV light, it appears that the tracer lines stayed still at those areas, however the material did flow to the thinner areas close to them.

The possible explanation is that the test jig comes in contact with the thickest part of the sample first and it pushes the flow to the thinner areas around them, which causes the trace in the final sample.

Chapter 5. CF-SMC Compression Molding Simulation

Autodesk Moldflow Insight 2021 is used to develop a simulation of CF-SMC compression molding, corresponding to the part geometry and processing conditions as in the flow-compaction test in Chapter 4. The cure kinetics model and viscosity model of the material, which were developed in Chapter 3 are implemented into the software using Moldflow Solver application programming interface (API). The other SMC material properties, such as density values, thermal properties and pressure-volume-temperature (PVT) properties were provided by the industrial partner - Magna International Inc.. The output variables of the simulation are compared with the flow-compaction test results.

5.1 CAD Geometry

For Moldflow simulation, the initial charge and the desired final part after molding need to be modeled. In this simulation, the initial charge with the same size of the specimen in the flow-compaction test (Chapter 4) was modeled using Autodesk Inventor 2020, which is shown as the red part in Figure 5.1. The ideal final part should have the same size as the whole molding area of the flow-compaction test jig, which is shown as the black part in Figure 5.1.

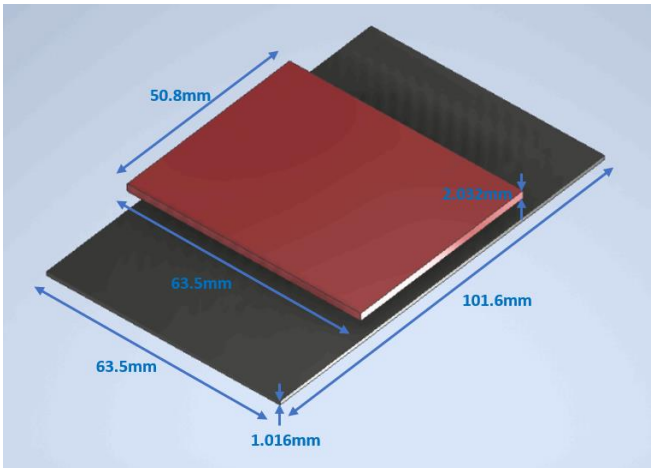

Figure 5.1 Dimension of the initial charge (red) and the final part (black)

The CAD models of the charge and the final part were imported into Moldflow.

5.2 3D Meshing

There are three types of meshes in Moldflow: midplane mesh, dual domain mesh and 3D mesh. A midplane mesh consists of a web of 3-noded triangular elements and forms a 2D representation of a solid model. The local thickness of the part is added to each element to simulate the part volume. The dual domain analysis works by simulating the flow of the melt on both the top and bottom parts of the mold cavity. A 3D mesh represents the CAD model by filling the volume of the model with four-node, tetrahedral elements (tetras). 3D meshes give a true 3D representation of the model and appears to be more accurate. However, 3D analyses often require additional computational time to complete since they do not make the assumptions that are made for midplane or dual domain analyses.

The dimensions of the charge and the final part are not big in this study, which makes them fast to be analyzed. Therefore, 3D meshes were chosen to be the mesh type since they could better represent the 3D models.

Tetrahedral elements with 12 layers along the thickness direction and estimated in-plane edge length of 1.63 mm were applied to mesh the charge and the part. Advancing front meshing algorithm built in Moldflow was utilized to generate the mesh. After the mesh was generated, a series of diagnostic checks were performed to ensure that the mesh is suitable for analysis. To obtain the best analysis results, the mesh must be free of errors and the element average aspect ratio ideally should be below 50:1 for tetrahedral elements in a 3D mesh. The mesh information in this study is shown in Figure 5.2. It can be seen that the average aspect ratio is 16.98, which is smaller than 50. Therefore, the generated mesh meets the requirement.

The meshed initial charge and part are shown in Figure 5.3.

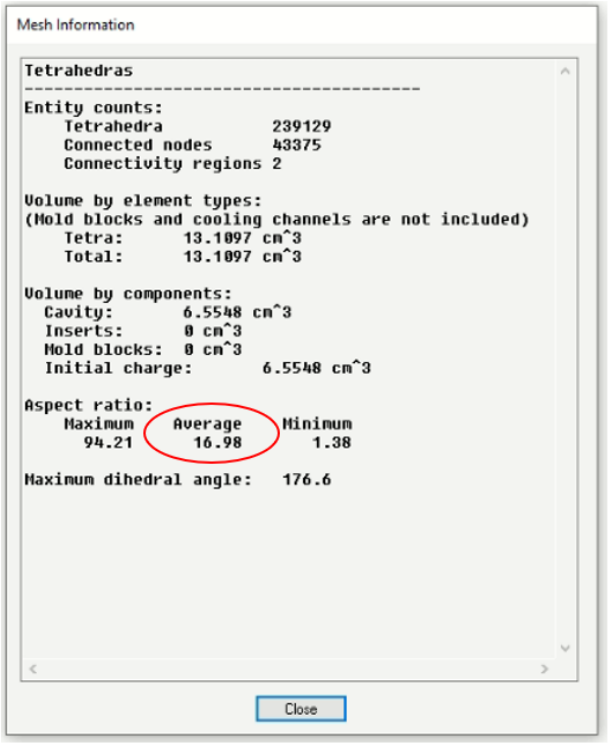

Figure 5.2 The 3D mesh information of this study

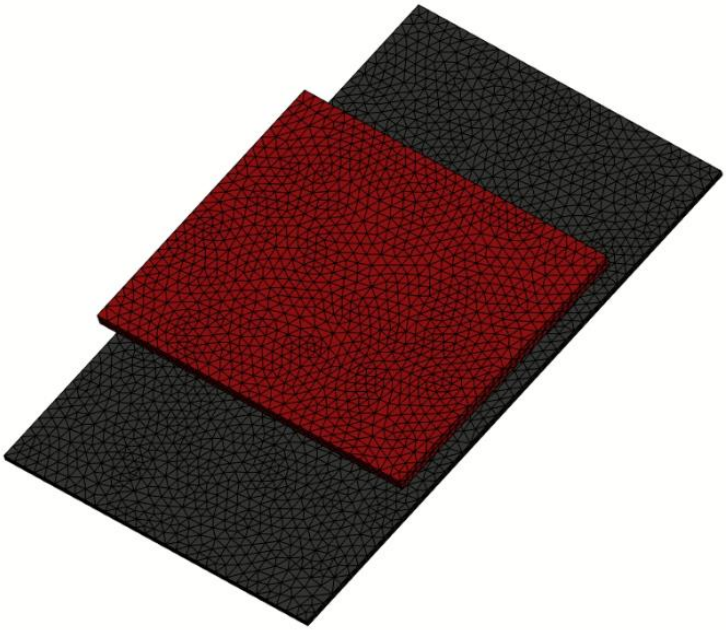

Figure 5.3 The meshed charge and part

5.3 Material Model Implementation Through API

Reliable material models which represent the real properties of the material are the fundamental building blocks for an accurate simulation. This section describes a way to implement self-developed models of CF-SMC into Moldflow through Moldflow Solver API.

Cure kinetics model and viscosity models were developed for the extracted resin in Chapter 3, which are used to represent the behaviors of the CF-SMC. The cure kinetics model and viscosity model supplied by Moldflow do not follow the same modeling method as the self-developed ones in this study. Therefore, the two material models need to be implemented into Moldflow to better represent the CF-SMC.

Moldflow provides a Solver API where own C++ functions can be created for a solver to call when it needs to calculate a property, such as the degree of cure and the melt viscosity during a Fill analysis in this study.

The cure kinetics model and the viscosity model were programmed in the API C++ source file through Microsoft Visual Studio 2017, following the calling syntaxes which are provided in the Solver API Reference documentation from the application help menu. The source file was then compiled into a native shared user library (DLL file). The user library was copied into the binary directory of the Moldflow Insight installation so that the solver can reach it during an analysis.

The detailed codes which were programmed in the user library can be found in APPENDIX B. The implementation of the two material models is validated from comparing the degree of cure data and the viscosity data of the simulation with the data generated from the material models in Chapter 3.

The other material properties, i.e., the thermal properties (specific heat, thermal conductivity and melt density), and pressure-volume-temperature properties were provided by Magna International Inc.. The data of those material properties was input in Moldflow directly.

The initial fiber orientations were set as 2D random in XY plane in the initial charge element. Since the fiber orientation distribution is not studied in this research, the fiber orientation is predicted using the built-in Folgar-Tucker model with the default interaction coefficient of 0.01. Further development regarding the fiber orientation can be studied in future work.

5.4 Process Settings

The mold surface temperature and the prepreg temperature were both set to 130°C.

The press speed and the press force profile were set up corresponding to one of the testing conditions of flow-compaction test so that the simulation results can be compared with the experimental data. The condition is compressing with a speed of 1 mm/s until a compression force of 55kN is reached and then the force is kept constant thereafter.

The mold material is set as aluminum, which is the same as the flow-compaction test jig.

5.5 Results and Comparison

5.5.1 Press Force

The press force data was generated from the Moldflow simulation and it is compared with the experimental data from the flow-compaction test, which is shown in Figure 5.4. Only the comparison of the first 10 seconds of the molding process was shown since the press force remained constant at pre-set peak force value for both the simulation and the experiment. The simulated press force data was generally well matched with the experimental results. However, at the beginning of the process (0-1 second), the simulated press force ramped up faster than the experimentally measured force. The root cause of this requires further study in the future.

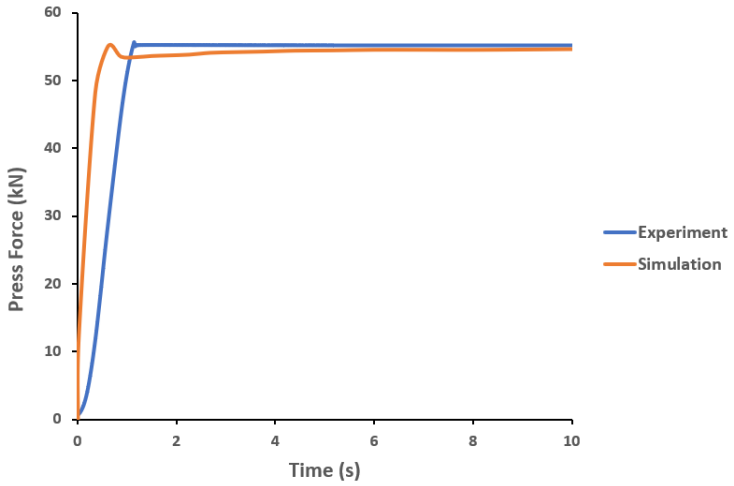

Figure 5.4 Comparison between the experimental press force and the simulated press force

5.5.2 Reaction Progress

After the implementation of the cure kinetics model, the solver calculates the reaction progress (degree of cure) at every timestep during the simulation. The simulated reaction progress data is plotted against the prediction of the cure kinetics model in order to validate the success of the implementation of the model. As can be seen from Figure 5.5, the simulation matches perfectly with the cure kinetics model, which means that the programming in the API is correct and the implementation method is successful.

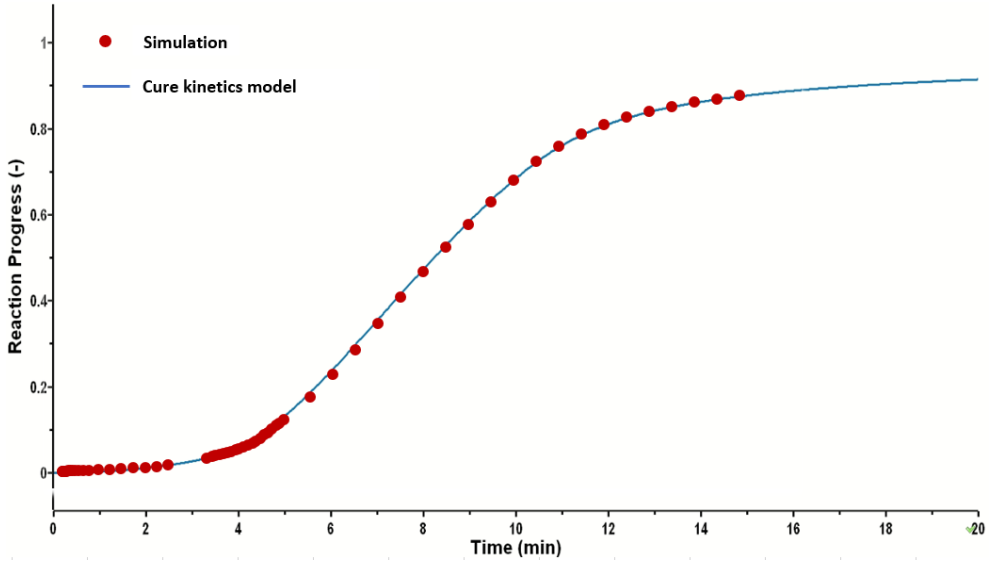

Figure 5.5 Comparison between the simulation in Moldflow and the cure kinetics model

5.5.3 Fill Time

As shown in Figure 5.6, it took 74.47 seconds for the material to completely fill the cavity. The majority of the cavity was filled within 18.62 seconds, however it took more than 37.23 seconds for the charge to fill the edges and corners. The viscosity builds up quickly at 130°C, causing slower flow velocity after a short period of time.

Fill time is also a good method to validate the accuracy of the simulation. However, it is very hard to capture this piece of information inside the mold during compression molding and it is beyond the capability of the experimental device in this study. Fill time validation could be done in future work.

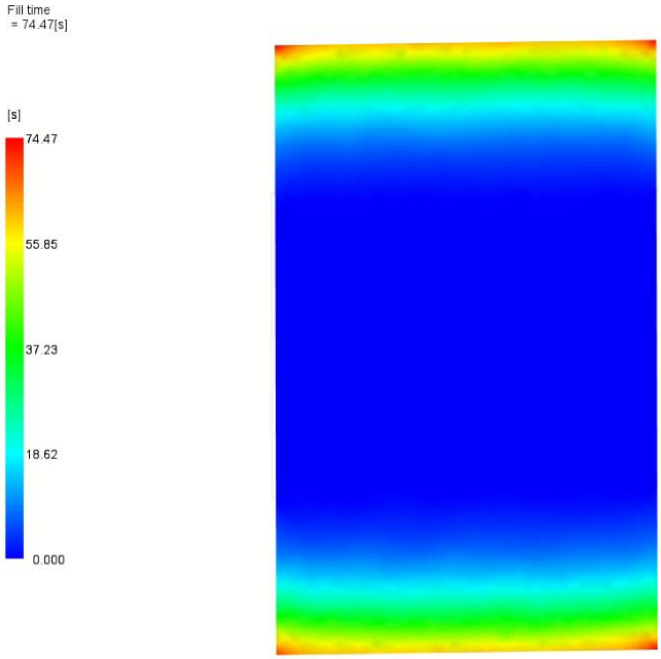

Figure 5.6 The fill time prediction in Moldflow simulation

5.6 Conclusion

A CF-SMC compression molding process is developed using Autodesk Moldflow 2021. Self-developed cure kinetics model and viscosity model are implemented successfully into the software through Solver API. From comparing the simulated data with experimental data, the simulation is validated to be adequate to predict the press force, reaction progress

and viscosity of the material. However, the simulation's ability to predict other variables, such as fill time and flow velocity, needs to be validated in the future.

Chapter 6. Conclusions and Future Work

6.1 Conclusions

The main theme of this work was to characterize a CF-SMC prepreg and to build a compression molding simulation for this material in order to facilitate the real-life compression molding process development. The main conclusions of this research are summarized as follows:

1. **Cure kinetics of the material was studied.**

The curing behaviors of the neat resin, extracted resin and CF-SMC were studied using DSC. Different fiber contents in the CF-SMC samples promote unpredictable variations in the measured heat of cure. No accurate model could be developed for the CF-SMC. A cure kinetics model was developed for the extracted resin to represent the curing behavior of the CF-SMC. Molding temperature around 140°C is recommended for this CF-SMC for automotive applications based on the model.

2. **Gelation and viscosity of the material was characterized.**

Gelation and viscosity of the neat resin, extracted resin and CF-SMC were studied using a rheometer. The inhibitor was found to delay the gelation to a great extent. Gel time model and viscosity model were developed and were validated to be accurate.

3. **Flow-compaction tests were performed to study the material flow.**

A flow-compaction test jig was successfully developed to study the CF-SMC flow under different strain rate and temperature conditions. A recommendation is given for CF-SMC compression molding, which is using a strain rate bigger than 0.7 1/s in order to have adequate material flow.

4. **A compression molding simulation was developed for CF-SMC.**

Two self-developed material models were successfully implemented into Autodesk Moldflow 2021 through Moldflow Solver API, which is instructive for other researchers

who wants to use a model which is not supplied in the software package. The simulation was validated to be accurate in terms of press force, reaction progress and viscosity.

6.2 Future Work

1. The author failed to determine the gel point of the CF-SMC under isothermal conditions despite a large number of attempts, which is unfortunate. It is hoped that an experimental method could be found out for the CF-SMC gel point determination at isothermal temperatures.
2. Fiber orientation models could be studied and implemented into the software to further improve the ability of the simulation.
3. Experiments could be designed to measure other variables during the compression molding, such as the fill time and flow velocity. The accuracy of the simulation could be further validated from comparing the simulated data with the experimental data.

Reference

[1] M. Hohberg, L. Kärger, F. Henning, and A. Hrymak, "Rheological measurements and rheological shell model considering the compressible behavior of long fiber reinforced sheet molding compound (SMC)," *Composites Part A: Applied Science and Manufacturing*, vol. 95, pp. 110-117, 2017/04/01/ 2017, doi: https://doi.org/10.1016/j.compositesa.2017.01.006.

[2] Y. Li *et al.*, "Modeling and Simulation of Compression Molding Process for Sheet Molding Compound (SMC) of Chopped Carbon Fiber Composites," *SAE International Journal of Materials and Manufacturing*, vol. 10, no. 2, pp. 130-137, 2017.

[3] H. L. Friedman, "Kinetics of thermal degradation of char-forming plastics from thermogravimetry. Application to a phenolic plastic," *Journal of Polymer Science Part C: Polymer Symposia*, vol. 6, no. 1, pp. 183-195, 1964, doi: https://doi.org/10.1002/polc.5070060121.

[4] A. W. Smith and P. Hubert, "Development of a versatile recycled compression moulding compound made from uncured aerospace prepreg offcuts," *ICCM22*, no. 102, pp. 4189-4202, 2019.

[5] "(2018). Canada's action on climate change: Our low carbon transportation. Available: https://www.canada.ca/en/services/environment/weather/climatechange/climate-action/low-carbon-transportation-future.html."

[6] "(2019). Where Canada's emissions come from and what are we doing to reduce them. Available: https://www.canada.ca/en/services/environment/weather/climatechange/climate-plan/reduce-emissions.html."

[7] A. Bandivadekar *et al.*, "Reducing the fuel use and greenhouse gas emissions of the US vehicle fleet," *Energy Policy*, vol. 36, pp. 2754-2760, 07/01 2008, doi: 10.1016/j.enpol.2008.03.029.

[8] H. G. Kia, *Sheet Molding Compounds: Science and Technology*. Hanser, 1993.

[9] P. K. Mallick, "6 - Thermoset–matrix composites for lightweight automotive structures," in *Materials, Design and Manufacturing for Lightweight Vehicles*, P. K. Mallick Ed.: Woodhead Publishing, 2010, pp. 208-231.

[10] "Mahajan, G. and V. Aher, Composite material: A review over current development and automotive application. International Journal of Scientific and Research Publications, 2012. 2(11): p. 1-5.."

[11] D. V. Rosato, D. V. Rosato, and M. V. Rosato, "15 - REINFORCED PLASTIC," in *Plastic Product Material and Process Selection Handbook*, D. V. Rosato, D. V. Rosato, and M. V. Rosato Eds. Oxford: Elsevier, 2004, pp. 455-496.

[12] L. R. A. Thomas, A.A.M. Groenendaal, J.R. Kolczynski, "The use of peroxyketals as initiators for curing unsaturated polyester sheet molding compound," *Journal of Elastomers & Plastics*, vol. 11, no. 2, pp. 117-132, 1979.

[13] M. Harsch, F. Herzog, and J. Karger-Kocsis, "Cure-induced Normal Force Development in Unfilled and Filled Epoxy Resins," *Journal of Composite Materials*, vol. 42, no. 21, pp. 2299-2309, 2008, doi: 10.1177/0021998308094969.

[14] O. R. Abolafia, "Application of differential scanning calorimetry to epoxy curing studies," in *Society of Plastics Engineers. Annual technical conference*, 1969, vol. 15, pp. 610-616.

[15] R. A. Fava, "Differential scanning calorimetry of epoxy resins," *Polymer*, vol. 9, pp. 137-151, 1968, doi: 10.1016/0032-3861(68)90024-4.

[16] L. T. Pappalardo, "DSC evaluation of epoxy and polyimide-impregnated laminates (prepregs)," *Journal of Applied Polymer Science*, vol. 21, no. 3, pp. 809-820, 1977, doi: 10.1002/app.1977.070210321.

[17] R. B. Prime, "Differential scanning calorimetry of the epoxy cure reaction," *Polymer Engineering & Science*, vol. 13, no. 5, pp. 365-371, 1973, doi: 10.1002/pen.760130508.

[18] S. Sourour and M. R. Kamal, "Differential scanning calorimetry of epoxy cure: isothermal cure kinetics," *Thermochimica Acta*, vol. 14, no. 1, pp. 41-59, 1976, doi: 10.1016/0040-6031(76)80056-1.

[19] L. Khoun, T. Centea, and P. Hubert, "Characterization Methodology of Thermoset Resins for the Processing of Composite Materials -- Case Study: CYCOM 890RTM

Epoxy Resin," *Journal of Composite Materials,* vol. 44, no. 11, pp. 1397-1415, 2010.

[20] L. Woo Il, A. C. Loos, and G. S. Springer, "Heat of Reaction, Degree of Cure, and Viscosity of Hercules 3501-6 Resin," *Journal of Composite Materials,* vol. 16, no. 6, pp. 510-520, 1982, doi: 10.1177/002199838201600605.

[21] K. E. J. Barrett, "Determination of rates of thermal decomposition of polymerization initiators with a differential scanning calorimeter," *Journal of Applied Polymer Science,* vol. 11, no. 9, pp. 1617-1626, 1967, doi: https://doi.org/10.1002/app.1967.070110901.

[22] R. Prime, "Analytical Calorimetry, Vol. 2, eds. RS Porter, JF Johnson," ed: Plenum Press, New York, 1970.

[23] W. L. Ng, "Thermal decomposition in the solid state," *Australian Journal of Chemistry,* Article vol. 28, no. 6, pp. 1169-1178, 1975, doi: 10.1071/CH9751169.

[24] M. R. Kamal and S. Sourour, "Kinetics and thermal characterization of thermoset cure," *Polymer Engineering & Science,* vol. 13, no. 1, pp. 59-64, 1973, doi: https://doi.org/10.1002/pen.760130110.

[25] L. J. Lee and C. W. Macosko, "Heat transfer in polymer reaction molding," *International Journal of Heat and Mass Transfer,* vol. 23, no. 11, pp. 1479-1492, 1980.

[26] A. J. Rojas, J. Borrajo, and R. J. J. Williams, "The curing of unsaturated polyester resins in adiabatic reactors and heated molds," *Polymer Engineering & Science,* vol. 21, no. 17, pp. 1122-1127, 1981, doi: https://doi.org/10.1002/pen.760211703.

[27] H. E. Adabbo, A. J. Rojas, and R. J. J. Williams, "Critical parameters for thermoset curing in heated molds," *Polymer Engineering & Science,* vol. 19, no. 12, pp. 835-840, 1979, doi: https://doi.org/10.1002/pen.760191204.

[28] M. Reboredo and A. Vazquez, "Curing of thermosetting polymers by an external fluid," *Polymer Engineering & Science,* vol. 35, no. 19, pp. 1521-1526, 1995.

[29] A. AG, "AKTS-Thermokinetics Software," 2021. [Online]. Available: https://akts.com/akts-thermokinetics-tga-dsc-dta-tma-ftir-ms/download-tga-dsc-dta-tma-ms-ftir-akts-thermokinetics-software.html.

[30] E. G. Prout and F. C. Tompkins, "The thermal decomposition of potassium permanganate," *Transactions of the Faraday Society*, Article vol. 40, pp. 488-498, 1944, doi: 10.1039/tf9444000488.

[31] M. R. Kamal, "Thermoset characterization for moldability analysis," *Polymer Engineering & Science*, vol. 14, no. 3, pp. 231-239, 1974, doi: https://doi.org/10.1002/pen.760140312.

[32] R. C. Progelhof and J. L. Throne, "Non-isothermal curing of reactive plastics," *Polymer Engineering & Science*, vol. 15, no. 9, pp. 690-695, 1975, doi: https://doi.org/10.1002/pen.760150910.

[33] A. Dutta and M. Ryan, "Effect of fillers on kinetics of epoxy cure," *Journal of Applied Polymer Science*, vol. 24, no. 3, pp. 635-649, 1979.

[34] S. Pusatcioglu, A. Fricke, and J. Hassler, "Heats of reaction and kinetics of a thermoset polyester," *Journal of Applied Polymer Science*, vol. 24, no. 4, pp. 937-946, 1979.

[35] R. Lin, L. Lee, and M. Liou, "Non-isothermal mold filling and curing simulation in thin cavities with preplaced fiber mats," *International Polymer Processing*, vol. 6, no. 4, pp. 356-369, 1991.

[36] B. R. Gebart, "Critical parameters for heat transfer and chemical reactions in thermosetting materials," *Journal of applied polymer science*, vol. 51, no. 1, pp. 153-168, 1994.

[37] S. Vyazovkin, A. K. Burnham, J. M. Criado, L. A. Pérez-Maqueda, C. Popescu, and N. Sbirrazzuoli, "ICTAC Kinetics Committee recommendations for performing kinetic computations on thermal analysis data," *Thermochimica Acta*, vol. 520, no. 1-2, pp. 1-19, 2011, doi: 10.1016/j.tca.2011.03.034.

[38] S. Vyazovkin and N. Sbirrazzuoli, "Isoconversional Kinetic Analysis of Thermally Stimulated Processes in Polymers," *Macromolecular Rapid Communications*, vol. 27, no. 18, pp. 1515-1532, 2006, doi: 10.1002/marc.200600404.

[39] G. Wuzella, A. R. Mahendran, C. Beuc, and H. Lammer, "Isoconversional cure kinetics of a novel thermosetting resin based on linseed oil," *Journal of Thermal Analysis and Calorimetry*, pp. 1-17, 2020.

[40] S. Vyazovkin and N. Sbirrazzuoli, "Mechanism and kinetics of epoxy− amine cure studied by differential scanning calorimetry," *Macromolecules*, vol. 29, no. 6, pp. 1867-1873, 1996.

[41] S. Vyazovkin, "A unified approach to kinetic processing of nonisothermal data," *International journal of chemical kinetics*, vol. 28, no. 2, pp. 95-101, 1996.

[42] V. P. Privalko, V. Y. Kramarenko, V. L. Sokol, and A. M. Karateev, "Kinetics of formation of heterocyclic polymer networks. 3. Catalyst effect," *Polymers & Polymer Composites*, vol. 6, no. 5, pp. 331-336, 1998. [Online]. Available: <Go to ISI>://WOS:000076997100010.

[43] J. W. Wang, M. P. G. Laborie, and M. P. Wolcott, "Comparison of model-free kinetic methods for modeling the cure kinetics of commercial phenol-formaldehyde resins," *Thermochimica Acta*, vol. 439, no. 1-2, pp. 68-73, Dec 2005, doi: 10.1016/j.tca.2005.09.001.

[44] J. M. Salla, A. Cadenato, X. Ramis, and J. M. Morancho, "Thermoset Cure Kinetics by Isoconversional Methods," *Journal of Thermal Analysis and Calorimetry*, vol. 56, no. 2, pp. 771-781, 1999/09/01 1999, doi: 10.1023/A:1010158223347.

[45] G. He, B. Riedl, and A. Aït-Kadi, "Model-free kinetics: Curing behavior of phenol formaldehyde resins by differential scanning calorimetry," *Journal of applied polymer science*, vol. 87, no. 3, pp. 433-440, 2003.

[46] S. Li, E. Vuorimaa, and H. Lemmetyinen, "Application of isothermal and model-free isoconversional modes in DSC measurement for the curing process of the PU system," *Journal of applied polymer science*, vol. 81, no. 6, pp. 1474-1480, 2001.

[47] G. Vázquez, F. López-Suevos, J. González-Alvarez, and G. Antorrena, "Curing process of phenol-urea-formaldehyde-tannin (PUFT) adhesives," *Journal of thermal analysis and calorimetry*, vol. 82, no. 1, pp. 143-149, 2005.

[48] Y.-S. Yang and L. Suspene, "Curing of unsaturated polyester resins: Viscosity studies and simulations in pre-gel state," *Polymer Engineering & Science*, vol. 31, no. 5, pp. 321-332, 1991, doi: https://doi.org/10.1002/pen.760310505.

[49] H. H. Winter, "Can the gel point of a cross-linking polymer be detected by the G′ – G″ crossover?," *Polymer Engineering & Science,* vol. 27, no. 22, pp. 1698-1702, 1987, doi: https://doi.org/10.1002/pen.760272209.

[50] J. Lange, N. Altmann, C. T. Kelly, and P. J. Halley, "Understanding vitrification during cure of epoxy resins using dynamic scanning calorimetry and rheological techniques," *Polymer,* vol. 41, no. 15, pp. 5949-5955, 2000/07/01/ 2000, doi: https://doi.org/10.1016/S0032-3861(99)00758-2.

[51] S. R. Raghavan, L. A. Chen, C. McDowell, S. A. Khan, R. Hwang, and S. White, "Rheological study of crosslinking and gelation in chlorobutyl elastomer systems," *Polymer,* vol. 37, no. 26, pp. 5869-5875, 1996/01/01/ 1996, doi: https://doi.org/10.1016/S0032-3861(96)00446-6.

[52] Y. M. Lee, Y. S. Yang, and L. J. Lee, "Rheological changes during the polymerization of polyurethane based interpenetrating polymer network(IPN)," *Polymer Engineering & Science,* vol. 27, no. 10, pp. 716-726, 1987, doi: https://doi.org/10.1002/pen.760271004.

[53] V. M. González‐Romero and C. W. Macosko, "Viscosity Rise during Free Radical Crosslinking Polymerization with Inhibition," *Journal of Rheology,* vol. 29, no. 3, pp. 259-272, 1985, doi: 10.1122/1.549790.

[54] C.-Y. M. Tung and P. J. Dynes, "Relationship between viscoelastic properties and gelation in thermosetting systems," *Journal of Applied Polymer Science,* vol. 27, no. 2, pp. 569-574, 1982, doi: https://doi.org/10.1002/app.1982.070270220.

[55] D. U. Shah and P. J. Schubel, "Evaluation of cure shrinkage measurement techniques for thermosetting resins," *Polymer Testing,* vol. 29, no. 6, pp. 629-639, 2010/09/01/ 2010, doi: https://doi.org/10.1016/j.polymertesting.2010.05.001.

[56] D. Harran and A. Laudouard, "Caractérisation de la gélification d'une résine thermodurcissable par méthode rhéologique," *Rheologica Acta,* Article vol. 24, no. 6, pp. 596-602, 1985, doi: 10.1007/BF01332593.

[57] L. Núñez-Regueira, C. A. Gracia-Fernández, and S. Gómez-Barreiro, "Use of rheology, dielectric analysis and differential scanning calorimetry for gel time determination of a thermoset," *Polymer,* vol. 46, no. 16, pp. 5979-5985, 2005/07/25/ 2005, doi: https://doi.org/10.1016/j.polymer.2005.05.060.

[58] S. C. Sequera, Y. Ruiz, F. L. Moreno, M. X. Quintanilla-Carvajal, and F. Salcedo, "Rheological evaluation of gelation during thermal treatments in block freeze concentration of coffee extract," *Journal of Food Engineering,* Article vol. 242, pp. 76-83, 2019, doi: 10.1016/j.jfoodeng.2018.07.030.

[59] A. Cadenato, J. M. Salla, X. Ramis, J. M. Morancho, L. M. Marroyo, and J. L. Martin, "Determination of gel and vitrification times of thermoset curing process by means of TMA, DMTA and DSC techniques: TTT diagram," *Journal of Thermal Analysis,* Article vol. 49, no. 1, pp. 269-279, 1997. [Online]. Available: https://www.scopus.com/inward/record.uri?eid=2-s2.0-0030646993&partnerID=40&md5=11d4bb7b0f141ff37b207dbacab1b4f6.

[60] M. Hayaty, M. H. Beheshty, and M. Esfandeh, "A new approach for determination of gel time of a glass/epoxy prepreg," *Journal of Applied Polymer Science,* vol. 120, no. 3, pp. 1483-1489, 2011, doi: https://doi.org/10.1002/app.33251.

[61] B. Bilyeu, W. Brostow, and K. P. Menard, "Separation of gelation from vitrification in curing of a fiber-reinforced epoxy composite," *Polymer Composites,* Article vol. 23, no. 6, pp. 1111-1119, 2002, doi: 10.1002/pc.10505.

[62] M. R. Martínez-Miranda, V. García-Martínez, and M. R. Gude, "Gel point determination of a thermoset prepreg by means of rheology," *Polymer Testing,* vol. 78, p. 105950, 2019/09/01/ 2019, doi: https://doi.org/10.1016/j.polymertesting.2019.105950.

APPENDIX A – MATLAB CODES OF PHOTO PROCESSING PROGRAM

```
clc;
close all;
imtool close all;
clear;
workspace;
format long g;
format compact;
fontSize = 22;

% Convert into grayscale image
grayImage = imread('140oC_1.jpg');
grayImage = grayImage(:, :, 2); % Take green channel.

% Display the original gray scale image.
subplot(2,2,1)
imshow(grayImage, []);
axis on;
title('Original Grayscale Image', 'FontSize', fontSize);
% Enlarge figure to full screen.
set(gcf, 'Units', 'Normalized', 'OuterPosition', [0 0 1 1]);
% Give a name to the title bar.
set(gcf, 'Name', 'Strain Measurement by Yining', 'NumberTitle', 'Off')

% Display the histogram.
[pixelCount, grayLevels] = imhist(grayImage);
subplot(2,2,2)
bar(grayLevels, pixelCount);
grid on;
title('Histogram of original image', 'FontSize', fontSize);
xlim([0 grayLevels(end)]); % Scale x axis manually.

% Convert into binary image
binaryImage = grayImage < 128;
% Display the binary image.
subplot(2,2,3)
imshow(binaryImage, []);
axis on;
title('Binary Image', 'FontSize', fontSize);

% Fill the binary image.
binaryImage = imfill(binaryImage, 'holes');

% Pick a column and calculate the distance
Col = 950;
distance_pixels = find(binaryImage(:,Col), 1, 'last')-find(binaryImage(:,Col), 1, 'first')
```

```
% Calculate the scale
realDistance = 50.8; % Unit: mm
distancePerPixel = realDistance/distance_pixels  % Unit: mm/pixel

% Display the binary image.
subplot(2,2,4)
imshow(binaryImage, []);
axis on;
title('Filled Binary Image', 'FontSize', fontSize);

% Calculate the area of SMC sample
measurements = regionprops(binaryImage, 'Area');
allAreas = [measurements.Area]
SMC_Area_Pixels = allAreas(2)

% Calculate the final length of the SMC sample
% Assume that the width is always 2.5inches, which is 63.5mm
Length_pixels = SMC_Area_Pixels/distance_pixels/1.25
Length_SMC_real = Length_pixels * distancePerPixel

% Print out the result
message = sprintf('One pixel = %.4f mm.\nThe SMC sample final length = %.3f mm',distancePerPixel, Length_SMC_real);
uiwait(helpdlg(message));
```

APPENDIX B – CODES (C++) FOR MATERIAL MODEL IMPLEMENTATION THROUGH MOLDFLOW SOLVER API

```
extern "C" int STDCALL SolverUserHb3dUserNodeFieldsDimensions()
{
  return 1;
}

//Initialize the degree of cure to zero
extern "C" void STDCALL SolverUserHb3dUserNodeFieldsInitialize(double* X, size_t nodeID,
size_t Lam) {
  int nDim = SolverUserHb3dUserNodeFieldsDimensions();
  for (int i = 0; i < nDim; i++)
    X[i] = 0;
}

extern "C" void STDCALL SolverUserHb3dInitializeTDegradation()
{
  // Write a message to the screen at the start of the analysis.
  std::wostringstream Message1;
  Message1 << L" Utilizing self-developed cure kinetics model and viscosity model. ";
  SolverUtilityHb3dInfo(Message1.str().c_str());
}

// Develop cure kinetics model
extern "C"  void STDCALL SolverUserHb3dUserNodeFieldsEvolution(double* dXdt, double
const* X, size_t nodeID, size_t Lam) {

  double T; //Temperature
  double A; //Pre-exponential Factor
  double Eact; //Activation Energy
  double t = SolverUtilityHb3dGetTime();

  double BPE0 = 0, BPE1 = 0.039552610391694, BPE2 = 0.11285734250251, BPE3 =
0.57630627832725, BPE4 = 0.9151202024778;
  double BPE5 = 0.93771508078744, BPE6 = 0.94160160303276, BPE7 = 1;
  double BPE1_a3 = 186525959.736352, BPE1_a2 = -20581396.4522829, BPE1_a1 =
632332.572900413, BPE1_a0 = 15328.9440668611;
  double BPE2_a3 = -7072004.27569553, BPE2_a2 = 1550250.23212511, BPE2_a1 = -
120360.876560411, BPE2_a0 = 19683.4330068031;
  double BPE3_a3 = 680.790225485036, BPE3_a2 = -4983.90462402625, BPE3_a1 = -
7085.54238308558, BPE3_a0 = 16405.0836879734;
  double BPE4_a3 = 219834.742592538, BPE4_a2 = -4037.37010746432, BPE4_a1 = -
11266.4425571771, BPE4_a0 = 12118.5961864316;
```

```
 double BPE5_a3 = 23919835.2157379, BPE5_a2 = 219411.845300067, BPE5_a1 = 61705.4285445897, BPE5_a0 = 16388.1741067454;
 double BPE6_a3 = -435962642.762125, BPE6_a2 = 1840809.14296317, BPE6_a1 = 108255.871065233, BPE6_a0 = 18170.3399524021;
 double BPE7_a3 = 12293145.9393862, BPE7_a2 = -3242326.38469889, BPE7_a1 = 102808.843128024, BPE7_a0 = 18593.2906462836;


 if (X[0] <= BPE1) {
        Eact = BPE1_a3*pow((X[0] - BPE0), 3) + BPE1_a2*pow((X[0] - BPE0), 2) + BPE1_a1*pow((X[0] - BPE0), 1) + BPE1_a0*pow((X[0] - BPE0), 0);
 }
 else if (X[0] <= BPE2) {
        Eact = BPE2_a3*pow((X[0] - BPE1), 3) + BPE2_a2*pow((X[0] - BPE1), 2) + BPE2_a1*pow((X[0] - BPE1), 1) + BPE2_a0*pow((X[0] - BPE1), 0);
 }
 else if (X[0] <= BPE3) {
        Eact = BPE3_a3*pow((X[0] - BPE2), 3) + BPE3_a2*pow((X[0] - BPE2), 2) + BPE3_a1*pow((X[0] - BPE2), 1) + BPE3_a0*pow((X[0] - BPE2), 0);
 }
 else if (X[0] <= BPE4) {
        Eact = BPE4_a3*pow((X[0] - BPE3), 3) + BPE4_a2*pow((X[0] - BPE3), 2) + BPE4_a1*pow((X[0] - BPE3), 1) + BPE4_a0*pow((X[0] - BPE3), 0);
 }
 else if (X[0] <= BPE5) {
        Eact = BPE5_a3*pow((X[0] - BPE4), 3) + BPE5_a2*pow((X[0] - BPE4), 2) + BPE5_a1*pow((X[0] - BPE4), 1) + BPE5_a0*pow((X[0] - BPE4), 0);
 }
 else if (X[0] <= BPE6) {
        Eact = BPE6_a3*pow((X[0] - BPE5), 3) + BPE6_a2*pow((X[0] - BPE5), 2) + BPE6_a1*pow((X[0] - BPE5), 1) + BPE6_a0*pow((X[0] - BPE5), 0);
 }
 else if (X[0] <= BPE7) {
        Eact = BPE7_a3*pow((X[0] - BPE6), 3) + BPE7_a2*pow((X[0] - BPE6), 2) + BPE7_a1*pow((X[0] - BPE6), 1) + BPE7_a0*pow((X[0] - BPE6), 0);
 }

 double BPA0 = 0, BPA1 = 0.045446029068767, BPA2 = 0.050202721854481, BPA3 = 0.12156985920965, BPA4 = 0.57960910763724, BPA5 = 0.92670951777491, BPA6 = 1;
 double BPA1_a3 = 469774.212692127, BPA1_a2 = -53304.7672628073, BPA1_a1 = 1703.06613019649, BPA1_a0 = 28.1007614955264;
 double BPA2_a3 = -597519.877394402, BPA2_a2 = 10740.5316692192, BPA2_a1 = -231.224229408978, BPA2_a0 = 39.5000120034413;
 double BPA3_a3 = -10463.6759335196, BPA3_a2 = 2213.8761988499, BPA3_a1 = -169.604090959748, BPA3_a0 = 38.5788576107421;
 double BPA4_a3 = 14.6718347952737, BPA4_a2 = -26.4115939124179, BPA4_a1 = -13.4910040396101, BPA4_a0 = 33.9471023446237;
 double BPA5_a3 = 475.388734596492, BPA5_a2 = -6.25076536437647, BPA5_a1 = -28.4516465346242, BPA5_a0 = 23.6364554576089;
 double BPA6_a3 = -53098.4056816709, BPA6_a2 = 488.772108895374, BPA6_a1 = 139.031709705192, BPA6_a0 = 32.8876964730107;
```

```
 if (X[0] <= BPA1) {
        A = BPA1_a3*pow((X[0] - BPA0), 3) + BPA1_a2*pow((X[0] - BPA0), 2) +
BPA1_a1*pow((X[0] - BPA0), 1) + BPA1_a0*pow((X[0] - BPA0), 0);
 }
 else if (X[0] <= BPA2) {
        A = BPA2_a3*pow((X[0] - BPA1), 3) + BPA2_a2*pow((X[0] - BPA1), 2) +
BPA2_a1*pow((X[0] - BPA1), 1) + BPA2_a0*pow((X[0] - BPA1), 0);
 }
 else if (X[0] <= BPA3) {
        A = BPA3_a3*pow((X[0] - BPA2), 3) + BPA3_a2*pow((X[0] - BPA2), 2) +
BPA3_a1*pow((X[0] - BPA2), 1) + BPA3_a0*pow((X[0] - BPA2), 0);
 }
 else if (X[0] <= BPA4) {
        A = BPA4_a3*pow((X[0] - BPA3), 3) + BPA4_a2*pow((X[0] - BPA3), 2) +
BPA4_a1*pow((X[0] - BPA3), 1) + BPA4_a0*pow((X[0] - BPA3), 0);
 }
 else if (X[0] <= BPA5) {
        A = BPA5_a3*pow((X[0] - BPA4), 3) + BPA5_a2*pow((X[0] - BPA4), 2) +
BPA5_a1*pow((X[0] - BPA4), 1) + BPA5_a0*pow((X[0] - BPA4), 0);
 }
 else if (X[0] <= BPA6) {
        A = BPA6_a3*pow((X[0] - BPA5), 3) + BPA6_a2*pow((X[0] - BPA5), 2) +
BPA6_a1*pow((X[0] - BPA5), 1) + BPA6_a0*pow((X[0] - BPA5), 0);
 }

 if (t <= 0.019) {
        T = 135 + 273.15;
        dXdt[0] = exp(A - Eact / T);
 }

 else {
        if (SolverUtilityHb3dGetNodeScalarResult(nodeID, "Temperature", &T) > 0) {
                T += 273.15;
                dXdt[0] = exp(A - Eact / T);
        }

        else {
                //Report error
                std::wostringstream Message1;
                Message1 << L"Cannot find node with ID " << nodeID;
                SolverUtilityHb3dFail(Message1.str().c_str());
        }
 }
}

extern "C"  void STDCALL SolverUserHb3dUserNodeFieldsCheckAndFix(double* X, size_t
nodeID, size_t Lam) {
 //if injection node then the residence time is zero
 if (SolverUtilityHb3dIsInjNode(nodeID))
 {
```

```
   //X[0] = 0.0;
  }
  if (X[0] > 1.0)
  {
            X[0] = 1.0;
  }
}

extern "C" double STDCALL SolverUserHb3dTemperatureIncrementAtNode(double aTimeInc, size_t aNodeID, double aCurrentTime, double aDensity, double aSpecificHeat)
{
          double TotalEnthalpy = 280000;  //J/kg
          double TempInc;
          double X = SolverUtilityHb3dGetUserNodeField(aNodeID, 0, 0);
          double dXdt;
          double T; //Temperature
          double A; //Pre-exponential Factor
          double Eact; //Activation Energy

          double BPE0 = 0, BPE1 = 0.039552610391694, BPE2 = 0.11285734250251, BPE3 = 0.57630627832725, BPE4 = 0.9151202024778;
          double BPE5 = 0.93771508078744, BPE6 = 0.94160160303276, BPE7 = 1;
          double BPE1_a3 = 186525959.736352, BPE1_a2 = -20581396.4522829, BPE1_a1 = 632332.572900413, BPE1_a0 = 15328.9440668611;
          double BPE2_a3 = -7072004.27569553, BPE2_a2 = 1550250.23212511, BPE2_a1 = -120360.876560411, BPE2_a0 = 19683.4330068031;
          double BPE3_a3 = 680.790225485036, BPE3_a2 = -4983.90462402625, BPE3_a1 = -7085.54238308558, BPE3_a0 = 16405.0836879734;
          double BPE4_a3 = 219834.742592538, BPE4_a2 = -4037.37010746432, BPE4_a1 = -11266.4425571771, BPE4_a0 = 12118.5961864316;
          double BPE5_a3 = 23919835.2157379, BPE5_a2 = 219411.845300067, BPE5_a1 = 61705.4285445897, BPE5_a0 = 16388.1741067454;
          double BPE6_a3 = -435962642.762125, BPE6_a2 = 1840809.14296317, BPE6_a1 = 108255.871065233, BPE6_a0 = 18170.3399524021;
          double BPE7_a3 = 12293145.9393862, BPE7_a2 = -3242326.38469889, BPE7_a1 = 102808.843128024, BPE7_a0 = 18593.2906462836;

          if (X <= BPE1) {
                    Eact = BPE1_a3*pow((X - BPE0), 3) + BPE1_a2*pow((X - BPE0), 2) + BPE1_a1*pow((X - BPE0), 1) + BPE1_a0*pow((X - BPE0), 0);
          }
          else if (X <= BPE2) {
                    Eact = BPE2_a3*pow((X - BPE1), 3) + BPE2_a2*pow((X - BPE1), 2) + BPE2_a1*pow((X - BPE1), 1) + BPE2_a0*pow((X - BPE1), 0);
          }
          else if (X <= BPE3) {
                    Eact = BPE3_a3*pow((X - BPE2), 3) + BPE3_a2*pow((X - BPE2), 2) + BPE3_a1*pow((X - BPE2), 1) + BPE3_a0*pow((X - BPE2), 0);
          }
          else if (X <= BPE4) {
```

```
		Eact = BPE4_a3*pow((X - BPE3), 3) + BPE4_a2*pow((X - BPE3), 2) + BPE4_a1*pow((X - BPE3), 1) + BPE4_a0*pow((X - BPE3), 0);
	}
	else if (X <= BPE5) {
		Eact = BPE5_a3*pow((X - BPE4), 3) + BPE5_a2*pow((X - BPE4), 2) + BPE5_a1*pow((X - BPE4), 1) + BPE5_a0*pow((X - BPE4), 0);
	}
	else if (X <= BPE6) {
		Eact = BPE6_a3*pow((X - BPE5), 3) + BPE6_a2*pow((X - BPE5), 2) + BPE6_a1*pow((X - BPE5), 1) + BPE6_a0*pow((X - BPE5), 0);
	}
	else if (X <= BPE7) {
		Eact = BPE7_a3*pow((X - BPE6), 3) + BPE7_a2*pow((X - BPE6), 2) + BPE7_a1*pow((X - BPE6), 1) + BPE7_a0*pow((X - BPE6), 0);
	}

	double BPA0 = 0, BPA1 = 0.045446029068767, BPA2 = 0.050202721854481, BPA3 = 0.12156985920965, BPA4 = 0.57960910763724, BPA5 = 0.92670951777491, BPA6 = 1;
	double BPA1_a3 = 469774.212692127, BPA1_a2 = -53304.7672628073, BPA1_a1 = 1703.06613019649, BPA1_a0 = 28.1007614955264;
	double BPA2_a3 = -597519.877394402, BPA2_a2 = 10740.5316692192, BPA2_a1 = -231.224229408978, BPA2_a0 = 39.5000120034413;
	double BPA3_a3 = -10463.6759335196, BPA3_a2 = 2213.8761988499, BPA3_a1 = -169.604090959748, BPA3_a0 = 38.5788576107421;
	double BPA4_a3 = 14.6718347952737, BPA4_a2 = -26.4115939124179, BPA4_a1 = -13.4910040396101, BPA4_a0 = 33.9471023446237;
	double BPA5_a3 = 475.388734596492, BPA5_a2 = -6.25076536437647, BPA5_a1 = -28.4516465346242, BPA5_a0 = 23.6364554576089;
	double BPA6_a3 = -53098.4056816709, BPA6_a2 = 488.772108895374, BPA6_a1 = 139.031709705192, BPA6_a0 = 32.8876964730107;

	if (X <= BPA1) {
		A = BPA1_a3*pow((X - BPA0), 3) + BPA1_a2*pow((X - BPA0), 2) + BPA1_a1*pow((X - BPA0), 1) + BPA1_a0*pow((X - BPA0), 0);
	}
	else if (X <= BPA2) {
		A = BPA2_a3*pow((X - BPA1), 3) + BPA2_a2*pow((X - BPA1), 2) + BPA2_a1*pow((X - BPA1), 1) + BPA2_a0*pow((X - BPA1), 0);
	}
	else if (X <= BPA3) {
		A = BPA3_a3*pow((X - BPA2), 3) + BPA3_a2*pow((X - BPA2), 2) + BPA3_a1*pow((X - BPA2), 1) + BPA3_a0*pow((X - BPA2), 0);
	}
	else if (X <= BPA4) {
		A = BPA4_a3*pow((X - BPA3), 3) + BPA4_a2*pow((X - BPA3), 2) + BPA4_a1*pow((X - BPA3), 1) + BPA4_a0*pow((X - BPA3), 0);
	}
	else if (X <= BPA5) {
		A = BPA5_a3*pow((X - BPA4), 3) + BPA5_a2*pow((X - BPA4), 2) + BPA5_a1*pow((X - BPA4), 1) + BPA5_a0*pow((X - BPA4), 0);
	}
```

```
	else if (X <= BPA6) {
		A = BPA6_a3*pow((X - BPA5), 3) + BPA6_a2*pow((X - BPA5), 2) +
BPA6_a1*pow((X - BPA5), 1) + BPA6_a0*pow((X - BPA5), 0);
	}


	if (SolverUtilityHb3dGetNodeScalarResult(aNodeID, "Temperature", &T) > 0) {
		T += 273.15;
		dXdt = exp(A - Eact / T);
		}

	else {
			//Report error
			std::wostringstream Message1;
			Message1 << L"Cannot find node with ID " << aNodeID;
			SolverUtilityHb3dFail(Message1.str().c_str());
		}
	TempInc = TotalEnthalpy * aTimeInc * dXdt / aSpecificHeat;
	return TempInc;
}

//Develop viscosity model
extern "C" double STDCALL SolverUserHb3dViscosity (double temperature, double shearRate,
double pressure) {
	// Compute viscosity at given temperature and time.
	// Shear rate and pressure are not used in this model
	// * Note that temperatures are passed to the user viscosity functions in degrees C.

	double T_K; //Temperature in kalvin
	double T_relative;
	double tgel; //Gelation time
	double t = SolverUtilityHb3dGetTime() / 60; //universal time in the analysis; unit: minute
	double viscosity_ref; // Reference viscosity
	double viscosity;

	T_K = temperature + 273.15;
	T_relative = 363.15 / T_K - 1;
	tgel = exp(42.419 * T_relative + 4.0163); // Gelation time model
	viscosity_ref = exp(6125720.061*pow((1 / T_K), 2) - 31451.23*(1 / T_K) + 40.441); //
Reference viscosity

	// Viscosity equations in three stages
	if (t / tgel <= 0.85) {
		viscosity = 200000 * viscosity_ref * exp(1.3735 * (t / tgel) + 0.0523);
	}

	else if (t / tgel <= 1) {
		viscosity = 200000 * viscosity_ref * exp(4.798 * (t / tgel) - 2.8594);
	}

	else if (t / tgel > 1) {
```

```
		viscosity = 200000 * viscosity_ref * exp(7.6648 * (t / tgel) - 5.75);
	}

	if (viscosity >= 10000000) {
		viscosity = 10000000;
	}

	return viscosity;
}

// Develop viscosity model
extern "C" double STDCALL SolverUserHb3dViscosityAtNode(double temperature, double shearRate, double pressure, size_t nodeId) {
	// Compute viscosity at given temperature and time.
	// Shear rate and pressure are not used in this model
	// * Note that temperatures are passed to the user viscosity functions in degrees C.

	double T_K; //Temperature in kalvin
	double T_relative;
	double tgel; //Gelation time
	double t = SolverUtilityHb3dGetTime() / 60; //universal time in the analysis
	double viscosity_ref; // Reference viscosity
	double viscosity;

   T_K = temperature + 273.15;
	T_relative = 363.15 / T_K - 1;
	tgel = exp(42.419 * T_relative + 4.0163); // Gelation time model

	viscosity_ref = exp(6125720.061*pow((1 / T_K), 2) - 31451.23*(1 / T_K) + 40.441); // Reference viscosity

	// Viscosity equations in three stages
	if (t / tgel <= 0.85) {
		viscosity = 200000 * viscosity_ref * exp(1.3735 * (t / tgel) + 0.0523);
	}

	else if (t / tgel <= 1) {
		viscosity = 200000 * viscosity_ref * exp(4.798 * (t / tgel) - 2.8594);
	}

	else if (t / tgel > 1) {
		viscosity = 200000 * viscosity_ref * exp(7.6648 * (t / tgel) - 5.75);
	}

	if (viscosity >= 10000000) {
		viscosity = 10000000;
	}
	return viscosity;
}
```

```
extern "C" double STDCALL SolverUserHb3dViscosityAtElement(double temperature, double shearRate, double pressure, size_t elementId) {
	// Compute viscosity at given temperature and time.
	// Shear rate and pressure are not used in this model
	// * Note that temperatures are passed to the user viscosity functions in degrees C.

	double T_K; //Temperature in kalvin
	double T_relative;
	double tgel; //Gelation time
	double t = SolverUtilityHb3dGetTime() / 60; //universal time in the analysis
	double viscosity_ref; // Reference viscosity
	double viscosity;

	T_K = temperature + 273.15;

	T_relative = 363.15 / T_K - 1;
	tgel = exp(42.419 * T_relative + 4.0163); // Gelation time model

	viscosity_ref = exp(6125720.061*pow((1 / T_K), 2) - 31451.23*(1 / T_K) + 40.441); // Reference viscosity

	// Viscosity equations in three stages
	if (t / tgel <= 0.85) {
		viscosity = 200000 * viscosity_ref * exp(1.3735 * (t / tgel) + 0.0523);
	}

	else if (t / tgel <= 1) {
		viscosity = 200000 * viscosity_ref * exp(4.798 * (t / tgel) - 2.8594);
	}
	else if (t / tgel > 1) {
		viscosity = 200000 * viscosity_ref * exp(7.6648 * (t / tgel) - 5.75);
	}

	if (viscosity >= 10000000) {
		viscosity = 10000000;
	}
	return viscosity;
}
```